UNCLASSIFIED
SECURITY CLASSIFICATION OF THIS PAGE

AD-A224539

(4)

REPORT DOCUMENTATION PAGE

1a. REPORT SECURITY CLASSIFICATION: Unclassified	1b. RESTRICTIVE MARKINGS
2a. SECURITY CLASSIFICATION AUTHORITY	3. DISTRIBUTION/AVAILABILITY OF REPORT: Approved for public release; distribution unlimited.
2b. DECLASSIFICATION/DOWNGRADING SCHEDULE	
4. PERFORMING ORGANIZATION REPORT NUMBER(S)	5. MONITORING ORGANIZATION REPORT NUMBER(S): ARO 24626.146-PH-UIR
6a. NAME OF PERFORMING ORGANIZATION: University of Rochester; 6b. OFFICE SYMBOL (If applicable)	7a. NAME OF MONITORING ORGANIZATION: U. S. Army Research Office
6c. ADDRESS (City, State, and ZIP Code): The Institute of Optics, Rochester, New York 14627	7b. ADDRESS (City, State, and ZIP Code): P. O. Box 12211, Research Triangle Park, NC 27709-2211
8a. NAME OF FUNDING/SPONSORING ORGANIZATION: U. S. Army Research Office; 8b. OFFICE SYMBOL (If applicable)	9. PROCUREMENT INSTRUMENT IDENTIFICATION NUMBER: DAAL03-86-K-0173
8c. ADDRESS (City, State, and ZIP Code): P. O. Box 12211, Research Triangle Park, NC 27709-2211	10. SOURCE OF FUNDING NUMBERS: PROGRAM ELEMENT NO. / PROJECT NO. / TASK NO. / WORK UNIT ACCESSION NO.

11. TITLE (Include Security Classification)

Effects and control of the correlation properties of light sources

12. PERSONAL AUTHOR(S)

Dean Faklis

13a. TYPE OF REPORT	13b. TIME COVERED	14. DATE OF REPORT (Year, Month, Day)	15. PAGE COUNT
Technical	FROM _____ TO _____	May 1990	127

16. SUPPLEMENTARY NOTATION

The view, opinions and/or findings contained in this report are those of the author(s) and should not be construed as an official Department of the Army position, policy, or decision, unless so designated by other documentation.

17. COSATI CODES			18. SUBJECT TERMS (Continue on reverse if necessary and identify by block number)
FIELD	GROUP	SUB-GROUP	Coherence; statistical optics; physical optics

19. ABSTRACT (Continue on reverse if necessary and identify by block number)

Please see pages iv - v.

20. DISTRIBUTION/AVAILABILITY OF ABSTRACT	21. ABSTRACT SECURITY CLASSIFICATION
☐ UNCLASSIFIED/UNLIMITED ☐ SAME AS RPT. ☐ DTIC USERS	Unclassified
22a. NAME OF RESPONSIBLE INDIVIDUAL: G. Michael Morris	22b. TELEPHONE (Include Area Code) / 22c. OFFICE SYMBOL

DD FORM 1473, 84 MAR — 83 APR edition may be used until exhausted. All other editions are obsolete.

SECURITY CLASSIFICATION OF THIS PAGE
UNCLASSIFIED

Effects and Control of the Correlation Properties of Light Sources

by

Dean Faklis

Submitted in Partial Fulfillment

of the

Requirements for the Degree

DOCTOR OF PHILOSOPHY

Supervised by Professor G. Michael Morris

The Institute of Optics

University of Rochester

Rochester, New York

1990

Curriculum Vitae

Dean Faklis was born on March 24, 1962 in Chicago, Illinois. He graduated in 1984 from Loyola University of Chicago with a Bachelor of Science degree in Physics.

The author began graduate studies at the University of Rochester's Institute of Optics in the fall of 1984.

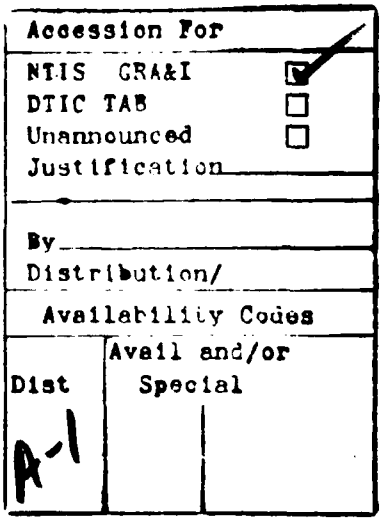

Acknowledgements

I would sincerely like to thank my advisor, Professor G. Michael Morris, for his guidance and support throughout my studies at the Institute of Optics. Professor Morris provided an outstanding research environment including excellent facilities.

In addition, I am grateful to other members of the faculty as well, especially Professor Emil Wolf, for providing a valued education and many stimulating discussions.

Extra special thanks to my wife, Julie, for her everlasting love, understanding, and laughter during these many years of study. My feet will rest firmly on the ground next to hers forever.

Thanks to my parents for their encouragement (i.e., sense of humor).

I also want to thank the graduate students and staff at the Institute, particularly Tom Isberg, Len Saaf, Dale Buralli, Doo Jin Cho, Tony Martino, W. A. Turner, and Gayle Thompson for their advice and support. Special thanks to John Ragazzo and the Triad.

The financial assistance by the University of Rochester, The Institute of Optics, and the U. S. Army Research Office/University Research Initiative is gratefully acknowledged. Partial support of this research was provided by the New York State Center for Advanced Optical Technology.

Abstract

Several topics associated with the influence and control of the statistical properties of light are investigated. One topic that is considered is the modification of the observed spectrum by the correlation properties of a partially coherent secondary source. It is demonstrated experimentally that source correlations that violate a certain scaling condition give rise to a normalized spectrum in the far zone that is different from the normalized spectrum of the light at the source.

Statistical correlations can also give rise to frequency shifts in the spectrum observed in the far field if the correlation function of the emitted radiation does not satisfy the scaling condition. A Fourier achromat is used to generate a secondary source in which the degree of spatial coherence is independent of wavelength; i.e., it violates the scaling condition. The spectrum detected in the far zone of the secondary source is found to be displaced in frequency and distorted relative to the spectrum measured at the secondary source. The displacement is found to be toward the higher frequencies or the lower frequencies depending on the direction of observation.

The use of a new method to generate partially coherent sources with controllable correlation is also investigated. Experiments are described in which the feasibility of synthesizing source correlations for use in spectral modulation applications is tested. The secondary source with controlled correlation is generated using an interferometric optical system that is designed and constructed around a general spectral filter. The degree of spectral coherence is shown to be directly related to the passband of the filter.

The final topic that is considered is the calculation of the correlation properties of synchrotron radiation. The second-order statistical properties of synchrotron radiation resulting from a three-dimensional relativistic electron bunch in a storage ring

are calculated. The theory is extended, using a formalism in the space-frequency domain, to allow for electrons in a 3-D bunch to have a distribution of velocities.

Table of Contents

List of Figures

Chapter 1

1. Introduction

1.1 Effects of Optical Coherence

Experimental evidence strongly suggests that the physical processes of light emission and the interaction of light and matter are *fundamentally* random. Optical coherence theory provides a framework in which statistical methods are used to describe these phenomena. The effects of optical coherence are generally regarded to be manifestations of the underlying statistical correlations. Interference is the basic example of a phenomenon that reveals correlations in optical fields. The historical evolution of the concepts of modern coherence theory can be traced with the aid of two volumes of reprinted works and an extensive bibliography edited by Mandel and Wolf.[1] There is also a number of excellent general references available for complete descriptions of the theory.[2-7]

In this Thesis, we restrict our attention to the discussion of the statistical properties of sources and fields. The effects of correlations that result from propagation through random media and the statistical description of light detection are not treated. Although, a general statistical description of the field which is based on the concepts of the theory of stochastic processes exists,[8] we are primarily concerned with the theory of second-order coherence.[4]

In the classical formulation of the theory of second-order coherence, the correlation in the optical field generated by a stationary source (at least in the wide sense) is described by the mutual coherence function, which is defined by

$$\Gamma(\mathbf{r}_1,\mathbf{r}_2;\tau) = \langle u^*(\mathbf{r}_1;t)\, u(\mathbf{r}_2;t+\tau)\rangle \quad . \tag{1.1.1}$$

In Eq. (1.1.1), the random field at the space-time point $(\mathbf{r};t)$ is represented by its complex analytic signal, $u(\mathbf{r};t)$, and the angled brackets denote an average over an ensemble. Traditionally, these correlations are characterized by the normalized value of the mutual coherence function which is called the complex degree of coherence and is defined by

$$\gamma(\mathbf{r}_1,\mathbf{r}_2;\tau) = \frac{\Gamma(\mathbf{r}_1,\mathbf{r}_2;\tau)}{[\Gamma(\mathbf{r}_1,\mathbf{r}_1;0)\Gamma(\mathbf{r}_2,\mathbf{r}_2;0)]^{1/2}} \quad . \tag{1.1.2}$$

Equation (1.1.2) describes the correlations in the *space-time* domain.

Many problems in statistical optics are most naturally described in the *space-frequency* domain. These problems include scattering from random media and propagation through general optical systems. The space-frequency description provides information about the process at each frequency of interest.

The mutual coherence function is related by a linear transform to the cross-spectral density function which describes the correlations in the space-frequency domain. The cross-spectral density of the process (defined in Eq. 2.2.3) is related to the mutual coherence by the Wiener-Khintchine theorem

$$W(\mathbf{r}_1,\mathbf{r}_2;\omega) = \frac{1}{2\pi}\int_{-\infty}^{\infty} \Gamma(\mathbf{r}_1,\mathbf{r}_2;\tau)\exp[i\omega\tau]\, d\tau \quad , \tag{1.1.3}$$

where ω represents the temporal frequency. It is also possible to define a normalized quantity, μ, which is called the degree of spatial (or spectral) coherence; this is given by

$$\mu(\mathbf{r}_1,\mathbf{r}_2;\omega) = \frac{W(\mathbf{r}_1,\mathbf{r}_2;\omega)}{[W(\mathbf{r}_1,\mathbf{r}_1;\omega)W(\mathbf{r}_2,\mathbf{r}_2;\omega)]^{1/2}} \quad , \tag{1.1.4}$$

where the spectral intensity of the light at the point r is expressed as

$$S(\mathbf{r};\omega) = W(\mathbf{r},\mathbf{r};\omega) \quad . \tag{1.1.5}$$

It is important to understand that the frequency description is introduced here with the (un-normalized) cross-spectral density as the Fourier transform of the mutual coherence function [see Eq. (1.1.3)]. The frequency characteristics are not introduced by a simple Fourier transformation of the space-time field representation. This is a direct result of the fact that a stationary random process does not possess a Fourier transform in the context of ordinary functions. Another important note here is that although there exists a simple relationship between the mutual coherence function and the cross-spectral density function, the complex degree of coherence, γ, and the complex degree of spatial coherence, μ, are related in a more complicated fashion. The formal relationship can be calculated using Eqs. (1.1.2)-(1.1.4).[9]

Wolf has shown[10-14] that under very general conditions the cross-spectral density of a statistically stationary source of any state of coherence can be represented directly as a correlation function in the space-frequency domain. The theory deals with ensembles of frequency-dependent realizations rather than time-dependent ones within the context of ordinary function theory. These ensembles are not connected with any (problematic) Fourier components of the random variable but rather with the eigenfunctions and the eigenvalues of an integral operator whose kernal is the cross-spectral density. This representation has found useful applications in studies of the

coherence properties of laser modes, investigations of radiometry, and some inverse problems involving partially coherent sources.

It is well known that both the cross-spectral density and the mutual coherence obey certain propagation laws. In regions of space where there are no primary sources, the propagation relation for the cross-spectral density can be written (using Maxwell's equations) as[15]

$$(\nabla_i^2 + k^2)W(\mathbf{r}_1,\mathbf{r}_2;\omega) = 0 \quad (i = 1,2) \qquad , \qquad (1.1.6)$$

in which $k=\omega/c$ where c is the speed of light in free space and the Laplacian operator is governed by $\mathbf{r}_i$. The existence of the relation in Eq. (1.1.6) indicates that the cross-spectral density (and similarly, the mutual coherence) is modified on propagation an amount that depends on the location of the observation region. The effect of coherence on the output intensity of linear optical systems is well known however the effect of coherence on the spectrum of light is a relatively new area of study.

Many of the fundamental properties of the theory of second-order coherence are used repeatedly in the following chapters. For this reason, an introduction to quasihomogeneous sources and the Van Cittert-Zernike theorem is given in the following sections of this chapter. Other discussions of this theory can be found in Refs. 2-7 and 16.

1.2 Concept of a Quasi-homogeneous Planar Source

A statistically stationary, homogeneous, planar, secondary source can be characterized by a cross-spectral density function given by[16]

$$W(\mathbf{r}_1,\mathbf{r}_2;\omega) = G(\mathbf{r}_1 - \mathbf{r}_2;\omega) \quad , \tag{1.2.1}$$

where the source is located in the plane defined by z=0. In Eq. (1.2.1), $\mathbf{r}_1$ and $\mathbf{r}_2$ are vectors in the source plane, $G(\mathbf{r}_2\text{-}\mathbf{r}_1{:}\omega)$ is a non-negative definite function, and ω is the spectral frequency. The spectral intensity is represented by the diagonal components of the cross-spectral density, i.e. $G(0;\omega)$. It is evident from Eq. (1.2.1) that the spectral intensity is independent of position in the source plane. The degree of spatial coherence in the source plane is simply the normalized cross-spectral density and is given by

$$\mu(\mathbf{r}_1,\mathbf{r}_2;\omega) = \frac{W(\mathbf{r}_1,\mathbf{r}_2;\omega)}{[W(\mathbf{r}_1,\mathbf{r}_1;\omega)W(\mathbf{r}_2,\mathbf{r}_2;\omega)]^{1/2}} \quad , \tag{1.2.2}$$

and substituting Eq. (1.2.1) into Eq. (1.2.2) gives

$$\mu(\mathbf{r}_1 - \mathbf{r}_2;\omega) = \frac{G(\mathbf{r}_1 - \mathbf{r}_2;\omega)}{G(0;\omega)} \quad . \tag{1.2.3}$$

Using Eqs. (1.2.1) and (1.2.3), the cross-spectral density of our source can now be written as

$$W(\mathbf{r}_1,\mathbf{r}_2;\omega) = G(0;\omega)\,\mu(\mathbf{r}_1-\mathbf{r}_2;\omega) \quad . \tag{1.2.4}$$

Note that because this form of the cross-spectral density must hold for all source points, the statistically homogeneous source must exist over an infinite domain.

In order to model sources of finite extent, we can place some restrictions on the behavior of the source intensity and the degree of spatial coherence of the statistically homogeneous source. We again assume that the degree of spatial coherence depends only on the difference of the position vectors in the source plane. An additional assumption requires that the spectral intensity of the source is a slowly varying function of the source coordinate and that the degree of spatial coherence is a fast function of the difference coordinate. Specifically, the intensity must remain sensibly constant over distances of the order of the correlation interval. Of course, the source domain must also be large compared with the effective correlation length (at each frequency) across the source. As a matter of terminology, sources of this type are said to be spatially incoherent in the global sense. When the coherence interval is of the order of a wavelength of light, the source is said to be locally incoherent. When the coherence interval is much greater than the wavelength, the source is said to be locally coherent. From these assumptions, the cross-spectral density of a *quasi-homogeneous* source can be approximated by the formula[16-17]

$$W(\mathbf{r}_1,\mathbf{r}_2;\omega) = G[(\mathbf{r}_1+\mathbf{r}_2)/2;\omega)]\,\mu(\mathbf{r}_1-\mathbf{r}_2;\omega) \quad . \tag{1.2.5}$$

The experiments in Chapter 2 make use of the concept of a quasi-homogeneous source. Specific propagation properties of quasi-homogeneous sources are described in the following section.

1.3 A Generalized Form of the Van Cittert-Zernike Theorem

In Section 1.1, the existence of precise propagation laws for the mutual coherence function and the cross-spectral density was discussed. These propagation formulas illustrate how the functions that describe the correlations will, in general, change on propagation. These changes can include modifications of the spectral intensity observed at points distant from the source region.[18]

For the experiments presented in Chapter 2, a generalized form of the Van Cittert-Zernike theorem is used to propagate the cross-spectral density. For this reason the theory is developed to illustrate the relationship between the correlations at the source and the cross-spectral density in a plane distant from the source. For a complete description of the theory the reader is referred to the paper by Wolf and Carter.[16]

Consider a stationary, quasi-homogeneous, planar, secondary source characterized by the cross-spectral density function given in Eq. (1.2.5). For sources of this type and near-axis observation points, the general propagation formula can be written as[19]

$$W(\mathbf{x}_1,\mathbf{x}_2;\lambda) = \frac{1}{(\lambda z)^2}\iint W(\xi_1,\xi_2;\lambda)\exp[ik|\mathbf{r}_1 - \mathbf{r}_2|]\, d^2\xi_1 d^2\xi_2 \quad , \qquad (1.3.1)$$

where λ represents the wavelength, $k=2\pi/\lambda$, and the distance to the observation plane, z, is assumed to be larger than the maximum extent of the source. The vectors $\mathbf{r}_1$ and $\mathbf{r}_2$ couple the source and observation regions and $\xi_1 = (\xi_1,\eta_1,0)$ and $\xi_2 = (\xi_2,\eta_2,0)$ represent the source plane. The vectors $\mathbf{x}_1 = (x_1,y_1,z)$ and $\mathbf{x}_2 = (x_2,y_2,z)$ denote the observation plane. In order to simplify Eq. (1.3.1), the magnitude r_1-r_2 is written as

$$r_1 - r_2 = z\left\{\left[1 + \frac{(x_1 - \xi_1)^2}{z^2} + \frac{(y_1 - \eta_1)^2}{z^2}\right]^{1/2} - \left[1 + \frac{(x_2 - \xi_2)^2}{z^2} + \frac{(y_2 - \eta_2)^2}{z^2}\right]^{1/2}\right\} \quad . \quad (1.3.2)$$

Making use of the binomial expansion theorem and assuming that the phase is accurately described by the first two terms, the difference can be written as

$$r_1 - r_2 \equiv \frac{1}{2z}\{(x_1 - x_2)(x_1 + x_2) + (y_1 - y_2)(y_1 + y_2) + (\xi_1 - \xi_2)(\xi_1 + \xi_2) + (\eta_1 - \eta_2)(\eta_1 + \eta_2) - 2x_1\xi_1 + 2x_2\xi_2 - 2y_1\eta_1 + 2y_2\eta_2\} \quad . \quad (1.3.3)$$

We now find it convenient to define a change of notation to the average and difference variables given by

$$\bar{\rho} = \frac{\rho_1 + \rho_2}{2} \ , \ \Delta\rho = \rho_1 - \rho_2 \ ; \ \rho = (x, y, \xi, \eta) \quad . \quad (1.3.4)$$

Equation (1.3.3) can now be simplified to give

$$r_1 - r_2 \equiv \frac{1}{z}\left\{\bar{x}\Delta x + \bar{y}\Delta y + \bar{\xi}\Delta\xi + \bar{\eta}\Delta\eta - (\bar{x} - \frac{\Delta x}{2})(\bar{\xi} - \frac{\Delta\xi}{2}) - (\bar{y} - \frac{\Delta y}{2})(\bar{\eta} - \frac{\Delta\eta}{2}) + (\bar{x} + \frac{\Delta x}{2})(\bar{\xi} + \frac{\Delta\xi}{2}) + (\bar{y} + \frac{\Delta y}{2})(\bar{\eta} + \frac{\Delta\eta}{2})\right\} \quad . \quad (1.3.5)$$

Regrouping terms in Eq. (1.3.5) gives

$$r_1 - r_2 \equiv \frac{1}{z}(\bar{x}\Delta x + \bar{y}\Delta y) + \frac{1}{z}(\bar{\xi}\Delta\xi + \bar{\eta}\Delta\eta) + \frac{1}{z}(\bar{\xi}\Delta x + \bar{\eta}\Delta y) + \frac{1}{z}(\bar{x}\Delta\xi + \bar{y}\Delta\eta) \quad . \quad (1.3.6)$$

Equation (1.3.6) contains four distinct terms. The first term on the right-hand side represents the familiar term that is proportional to the square of the output plane coordinates. The third and fourth terms give rise to information regarding the degree of spatial coherence and the spectral intensity, respectively in the plane z. The second term holds information about the square of the source coordinates. It is instructive to point out the circumstances when the second term can be neglected. As a sufficient condition for accuracy, we might require that the maximum phase change contributed by the second term be less than π. This condition will be met if the distance z satisfies

$$z > \frac{4}{\lambda}\bar{\xi}\Delta\xi \quad \text{and} \quad z > \frac{4}{\lambda}\bar{\eta}\Delta\eta \quad . \tag{1.3.7}$$

If we assume that the magnitude of the degree of spatial coherence across the source plane is negligible for source points separated by more than the coherence interval, l_c, and we assume that the spectral intensity of the source drops to zero for source points outside the source region of diameter D, Eq. (1.3.7) simplifies to

$$z > \frac{2}{\lambda} D\, l_c \quad . \tag{1.3.8}$$

In order to neglect the second term on the right-hand side of Eq. (1.3.6), we now assume that Eq. (1.3.8) holds. Note that when the correlations extend over just a few wavelengths, the distance z must only be greater than the maximum dimension of the source. Note also that in the far field of the source or in the rear focal plane of a positive lens that is appropriately placed between the source and the observation region that the term can always be neglected.

Using Eqs. (1.2.5), (1.3.1), (1.3.6), and (1.3.8), the cross-spectral density in the plane z can be written as

$$W(x_1,x_2;\lambda) = \frac{\kappa(\bar{x};\lambda)e^{i\psi}}{(\lambda z)^2}\iint S(\bar{\xi};\lambda)\exp[i\frac{k}{z}\bar{\xi}\bullet\Delta x]\,d^2\bar{\xi} \quad , \tag{1.3.9}$$

where

$$\kappa(\bar{x};\lambda) = \iint \mu(\Delta\xi;\lambda)\exp[i\frac{k}{z}\bar{x}\bullet\Delta\xi]\,d^2\Delta\xi \quad , \tag{1.3.10}$$

and

$$\psi = \frac{k}{z}(\bar{x}\bullet\Delta x) \quad . \tag{1.3.11}$$

In Eq. (1.3.9), S represents the spectral intensity in the source plane and in Eq. (1.3.10), μ represents the complex degree of spatial coherence across the source plane. Equation (1.3.9) represents a generalized form of the Van Cittert-Zernike theorem in terms of the cross-spectral density function. Equation (1.3.9) illustrates the Fourier-transform relationship between the intensity across the source and the field correlations in the observation region. While in the classic formulation the source is assumed to be spatially incoherent, it has been shown[7,16] that the theorem holds much more generally, namely for radiation from any quasihomogeneous source. Note that in general, the cross-spectral density will also be a function of the average variables in the observation plane. As a consequence, the complex degree of spatial coherence no longer is a function of the difference variables only. Note also that as for the case of a spatially incoherent source, it is the source size that determines the coherence area of the observed field, and in addition the source coherence area influences the distribution of spectral intensity across the observation plane.

1.4 Overview of Thesis

Each chapter of this Thesis contains an investigation of a topic associated with the influence and control of optical coherence in the space-frequency domain. In Chapter 2, the first experiments that illustrate the effects of source correlations on the spectrum of light are described. Sources with invariant spectra and sources with spectra that change on propagation are generated and compared with theory. In agreement with Wolf's theoretical predictions, the spectrum observed in the far field of the secondary source was found to depend on the spectrum at the source, the degree of spatial coherence of the source, and the location of the observation point.

In Section 2.3, the first experiments in which frequency shifts of the optical spectrum detected in the far zone of a partially coherent, planar secondary source are reported. Through application of the generalized Van Cittert-Zernike theorem, a Fourier achromat is used to generate a secondary source with a Gaussian correlation that is independent of wavelength. Fluorescence from a laser-illuminated dye jet is used as the primary source. In general, the spectrum detected in the far zone of the secondary source is found to be displaced in frequency and distorted relative to the spectrum measured at the secondary source. The displacement of the spectral peak is toward both the higher frequencies and the lower frequencies depending on the direction of the observation.

The generation of sources with controlled degree of coherence is important for the verification of new concepts in optical coherence theory. In Chapter 3, experiments are described in which a new method is employed to generate an optical secondary source with a controlled degree of spatial coherence. The technique consists of mixing controllable amounts of two uncorrelated sources in an interferometer. A spectral filter

is used to produce the desired source correlations. The spectral filter employs dispersive optics that are used to spatially separate (and recombine) the wavelength components of a broadband primary source, and an amplitude mask that is used to filter the dispersed light. The degree of coherence is shown to be related to the passband of the filter. A desirable feature of this new method of source synthesis is that the spectral filter is designed to be programmable and easily modified.

As explained earlier, the cross-spectral density function obeys a specific propagation formula [e.g., see Eq. 1.1.6]. In general, the correlations across the source will have a profound influence on the measured spectral intensity. With the increased use of unconventional light sources (i.e., non-thermal and non-laser) for a variety of applications in spectroscopy and imaging, models describing their source correlations should be investigated so that experiments that utilize these sources can be correctly explained.

The so-called unconventional sources include, among others, synchrotron radiation, undulator radiation, and Cerenkov radiation. The correlation properties of these sources do not appear to have been studied in detail either theoretically or experimentally. Because of the present importance of synchrotron radiation in industry, medicine, and research and its potential applications in astrophysics, Chapter 4 contains an investigation into the statistical properties of synchrotron radiation produced by a bunch of circulating charges.

The basic properties of synchrotron radiation such as source intensity, spectrum and polarization have been studied extensively. However, there have been very few investigations into the understanding of the statistical properties of the synchrotron source and the emitted radiation. Since the effects of coherence are very important in many synchrotron applications (e.g., propagation through optical systems and X-ray

holography), the correlation properties of the field should be studied. In Chapter 4, the second-order statistical properties of synchrotron radiation resulting from a three-dimensional relativistic electron bunch (N-electrons) in a storage ring are calculated. The new theory in the space frequency domain extends previous work to allow the electrons in a 3-D bunch to have an appropriate distribution of velocities (e.g., variance in the energy of the charges).

In Section 4.3, a model for the statistical behavior of the N-electron bunch and its associated classical field is investigated. Using a Gaussian distribution for the spatial characteristics of the bunch and a Gaussian velocity distribution, the mean value of the field and the second-order coherence are calculated. The present research will generate a framework that will permit future work on systems that utilize wigglers and undulators (e.g., the free-electron laser).

Much of the original work presented in this Thesis has been published or submitted for publication. The work in Chapter 2 concerning the effects of source correlations on the spectrum of light also appears in Refs. 20 and 21. The research described in Chapter 3 on source synthesis has been presented and submitted for publication [Refs. 22 and 23]. The work in Chapter 4 on the statistical properties of synchrotron radiation is currently being prepared for publication.

1.5 References: Chapter 1

1. *Selected Papers on Coherence and Fluctuations of Light*, Vols. 1 and 2 (L. Mandel and E. Wolf, editors), Dover Publications, New York (1970).

2. M. Born and E. Wolf, *Principles of Optics*, 6th ed., Pergamon, Oxford and New York, (1980).

3. M. J. Beran and G. B. Parrent, *Theory of Partial Coherence*, Prentice-Hall, Englewood Cliffs, New Jersey (1964).

4. L. Mandel and E. Wolf, "Coherence properties of optical fields," Rev. Mod. Phys. **37**, 231-287 (1965).

5. G. O. Reynolds, J. B. DeVelis, B. J. Thompson and G. B. Parrent, *The New Physical Optics Notebook: Tutorials in Fourier Optics*, SPIE Publishing, Washington, (1989).

6. J. Perina, *Coherence of Light*, 2nd ed., D. Reidel Publishing Company, Boston (1985).

7. J. W. Goodman, *Statistical Optics*, Wiley, New York, (1985).

8. See Ref. 4.

9. L. Mandel and E. Wolf, "Spectral coherence and the concept of cross-spectral purity," J. Opt. Soc. Am. **66**, 529 (1976).

10. E. Wolf, "New spectral representation of random sources and of the partially coherent fields that they generate," Opt. Commun. **38**, 3 (1981).

11. E. Wolf, "New theory of partial coherence in the space-frequency domain. Part I: Spectra and cross spectra of steady-state sources," J. Opt. Soc. Am. **72**, 343 (1982).

12. A. Starikov and E. Wolf, "Coherent-mode representation of Gaussian Schell-model sources and of their radiation fields," J. Opt. Soc. Am. **72**, 923 (1982).

13. E. Wolf, "New theory of partial coherence in the space-frequency domain. Part II: Steady-state fields and higher-order correlations," J. Opt. Soc. Am. A **3**, 76 (1986).

14. E. Wolf, "Coherent-mode propagation in spatially band-limited wave fields," J. Opt. Soc. Am. A **3**, 1920 (1986).

15. E. Wolf, "Coherence and radiometry," J. Opt. Soc. Am. **68**, 6 (1978).

16. W. H. Carter and E. Wolf, "Coherence and radiometry with quasihomogeneous planar sources," J. Opt. Soc. Am. **67**, 785 (1977).

17. E. Wolf and W. H. Carter, "Fields generated by homogeneous and by quasihomogeneous planar secondary sources," Opt. Commun. **50**, 131 (1984).

18. E. Wolf, "Invariance of the spectrum of light on propagation," Phys. Rev. Lett. **56**, 1370 (1986).

19. For example, see Ref. 2

20. G. M. Morris and D. Faklis, "Effects of source correlations on the spectrum of light," Opt. Commun. **62**, 5 (1987).

21. D. Faklis and G. M. Morris, "Spectral shifts produced by source correlations, J. Opt. Soc. Am. A P44, (OSA Annual Meeting) (1987); D. Faklis and G. M. Morris, "Spectral shifts produced by source correlations," Opt. Lett. **13**, 4 (1988).

22. D. Faklis and G. M. Morris, "Generation of sources with controlled correlation," ThR2, OSA Annual Meeting, Orlando, Technical Digest **18**, 181 (1989).

23. D. Faklis and G. Michael Morris, "Generation of partially coherent sources with controlled correlations," submitted for publication to Opt. Commun., March 1990.

Chapter 2

2. Effects of Source Correlations on the Spectrum of Light

2.1 Introduction

It has been shown in recent years that the statistical properties of a source can influence the spectrum of the emitted radiation.[1-23] It is well known that both the mutual coherence function and the cross-spectral density function obey precise propagation laws. Consequently, both the mutual coherence and the cross-spectral density will, in general, change on propagation. The Van Cittert-Zernike theorem illustrates an interesting example of how the statistical properties of the light change on propagation. By the same mechanisms, the spectrum of the light will also, in general, be modified on propagation.

Wolf[1] reported the first work that questioned under what conditions the normalized spectrum of light actually remains unchanged on propagation through free space. Shortly thereafter, the first experiments that illustrated the influence of source correlations on the spectrum of light were reported by Morris and Faklis.[2] In their experiments, they applied the generalized Van Cittert-Zernike theorem to generate a secondary source with specified degree of spatial coherence. In agreement with Wolf's theoretical predictions, the spectrum observed in the far field of the secondary source was found to depend on the spectrum at the source, the degree of spatial coherence of the source, and the location of the observation point.

It was later reported by Wolf[3-4] that the spectrum of the emitted light from a three-dimensional, quasi-homogeneous source with an appropriately chosen source

spectrum and degree of spatial coherence will be displaced relative to the source spectrum. It was shown that, independent of any source motion, the displacement could be either toward the lower or toward the higher frequencies.

A simple system was proposed[5] to facilitate the experimental verification of the frequency shifts. The first experiments illustrating the effect were reported by Bocko, Douglass, and Knox[6] on the observation of frequency shifts of spectral lines due to source correlations with acoustical sources. Faklis and Morris[7] described experiments in which frequency shifts of the optical spectrum were observed. Investigations by Knox and Knox[8] and Gori et. al.[9] presented results describing frequency shifts with optical sources using white-light interferometry. In all cases, there was excellent agreement with the theoretical predictions.

It has also been shown that scattering of polychromatic radiation by fluctuating media can affect the spectrum of the scattered radiation. Wolf, Foley, and Gori[18] have investigated the effect of random media whose physical properties do not change in time on the spectrum of the light scattered by it. They reported a spatial redistribution of the spectral components due to the correlation properties of the scatterer. Foley and Wolf[20] have shown theoretically some frequency shifts resulting from scattering from a model media whose dielectric susceptibility fluctuates both in space and in time. Wolf[22-23] presented results that reveal that scattering from some media whose macroscopic properties fluctuate randomly both in space and in time may generate frequency shifts of spectral lines which closely resemble Doppler shifts in the absence of any motion. Interestingly, his results predict relative frequency shifts that are essentially the same for all the lines in the source spectrum.

In this Section 2.2, the first experiments illustrating the effects of source correlations on the spectrum of light are described. Sources with invariant spectra and

sources with spectra that change on propagation are generated and compared with the theoretical predictions. The specific techniques that are used to generate these appropriately correlated secondary sources are described. In Section 2.3, we report the first experiments in which frequency shifts of the optical spectrum detected in the far field of a planar secondary source are observed. In these experiments we use a Fourier achromat to generate a secondary source with a degree of spatial coherence that is independent of wavelength. The spectral peak was found to be displaced in frequency in the absense of any motion of the source. The spectrum detected in the far field of the source depends on the spectrum at the source, the degree of spectral coherence at the source, and the location of the observation point.

Much of the analysis presented in this Chapter has been published previously (Faklis and Morris[2,7]). References 2 and 7 are expanded in Sections 2.2 and 2.3 of this Chapter, respectively.

2.2 Spectral Modification due to Source Correlations

2.2.1 Introduction

In a recent letter by Wolf[1], it was shown that the normalized spectrum of light is the same throughout the far zone and is equal to the normalized spectrum of light at the source provided that the complex degree of spectral coherence is a function of the variable $k(\rho_2 - \rho_1)$ only, where $(\rho_2 - \rho_1)$ denotes the (vectorial) distance between two points on the source, $k = \omega/c$, ω represents the angular frequency and c is the speed of the light. If the complex degree of spectral coherence depends on frequency only through the variable $k(\rho_2 - \rho_1)$, the source is said to satisfy the *scaling law*.

It is well known that the correlation properties of light can be controlled by application of the Van Cittert-Zernike theorem.[24-28] To date, using conventional sources and optical systems, the secondary sources with controlled correlation that have been produced all satisfy the scaling law.

In this Section, an experimental arrangement that provides a secondary source with a complex degree of coherence that is independent of the wavenumber k (i.e. violates the scaling law) is described. In accord with theoretical predictions, when the scaling law is violated the spectrum in the far zone is not equal to the spectrum of light at the secondary source and it also depends on the observation point. The experimental measurements of the spectrum in the far zone are found to be in good agreement with theory.

2.2.2 Coherence in Linear Optical Systems

Consider a general linear system with an impulse-response function given by $h(x,y;\xi,\eta;\omega)$, as illustrated in Fig. 2.2.1. With a given transverse component of the electric field, we associate a complex analytic signal $u(\xi,\eta;t)$ and define the spectral amplitude $U(\xi,\eta;\omega)$ to be the time-truncated Fourier transform of $u(\xi,\eta;t)$ [see Born and Wolf, Ref. 29, Chap. 10.],

$$U(\xi,\eta;\omega) = \int_{-T}^{T} u(\xi,\eta;t)\exp(i\omega t)\,dt \quad . \tag{2.2.1}$$

Using this definition one can express the spectral amplitude of the system output $U_{II}(x,y;\omega)$ in terms of the input spectral amplitude $U_I(\xi,\eta;\omega)$ as follows:

$$U_{II}(x,y;\omega) = \iint U_I(\xi,\eta;\omega)\,h(x,y;\xi,\eta;\omega)\,d\xi\,d\eta \quad . \tag{2.2.2}$$

In Eq. (2.2.2) the spatial coordinates in the input and output planes are denoted by (ξ,η) and (x,y), respectively, and $\omega = 2\pi c/\lambda$, where λ is the wavelength.

When one considers the operation of an optical system with broadband illumination, by far the most convenient quantity to calculate is the cross-spectral density function defined[29] as

$$W(x_1,y_1;x_2,y_2;\omega) = \lim_{T\to\infty} \frac{< U(x_1,y_1;\omega)\,U^*(x_2,y_2;\omega) >_s}{2T} \quad , \tag{2.2.3}$$

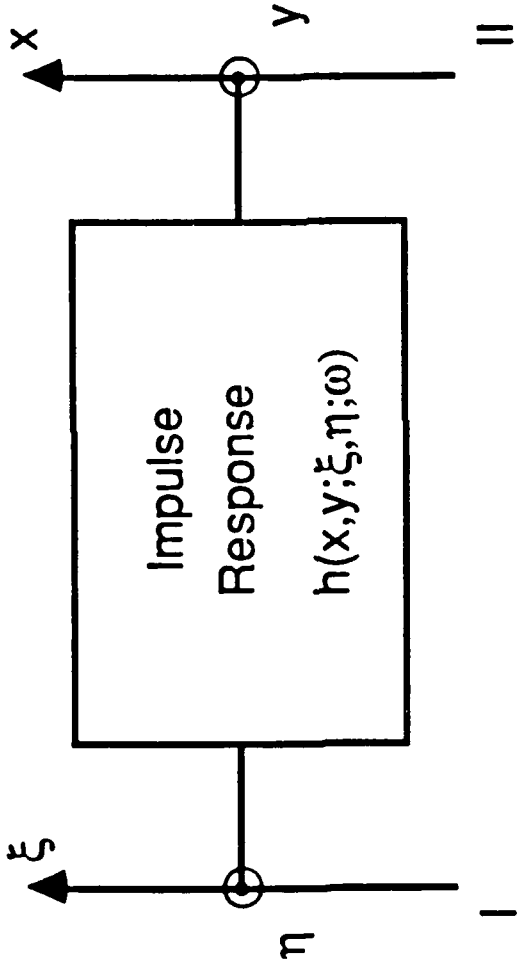

Fig. 2.2.1 Linear system with frequency-dependent impulse response $h(x,y;\xi,\eta;\omega)$.

in which $\langle ... \rangle_s$ denotes an average over an ensemble of sources. Note that the time-truncated field is used since, in general, the noiselike field u(x,y;t) is not mean-square integrable.

A quantity of particular interest here is the spectral intensity

$$S(x,y;\omega) \equiv W(x,y;x,y;\omega) \quad , \tag{2.2.4}$$

which represents the intensity at point (x,y) and frequency ω. Note that the total intensity at point (x,y) is obtained simply by integrating $S(x,y;\omega)$ over all temporal frequencies.

If an input object $t_I(\xi,\eta;\omega)$ is inserted at plane I and illuminated by a field with spectral amplitude $U_{in}(\xi,\eta;\omega)$, then the spectral amplitude $U_I(\xi,\eta;\omega)$ leaving plane I is given approximately by

$$U_I(\xi,\eta;\omega) = U_{in}(\xi,\eta;\omega)\, t_I(\xi,\eta;\omega) \quad . \tag{2.2.5}$$

Using Eqs. (2.2.2), (2.2.3) and (2.2.5), the cross-spectral density function $W_{II}(x_1,y_1;x_2,y_2;\omega)$ in plane II is written

$$\begin{aligned} W_{II}(x_1,y_1;x_2,y_2;\omega) = & \iint\iint t_I(\xi,\eta;\omega)\, t_I^*(\xi',\eta';\omega)\, W_{in}(\xi,\eta;\xi',\eta';\omega) \\ & \times \quad h(x_1,y_1;\xi,\eta;\omega)\, h^*(x_2,y_2;\xi',\eta';\omega)\, d\xi d\eta d\xi' d\eta' \quad . \end{aligned} \tag{2.2.6}$$

Equation (2.2.6) is a general expression relating the cross-spectral densities in planes I and II.

It is useful to define a normalized form of the cross-spectral density function given as follows:

$$\mu_{12}(\omega) = \frac{W(x_1,y_1;x_2,y_2;\omega)}{[S(x_1,y_1;\omega)\, S(x_2,y_2;\omega)]^{1/2}} \quad , \tag{2.2.7}$$

in which $|\mu_{12}(\omega)|$ can assume values in the range $0 \le |\mu_{12}(\omega)| \le 1$. $\mu_{12}(\omega)$ is known as the *complex degree of spectral coherence.*[30]

2.2.3 Control of Spatial Coherence

Diagrams of the optical systems used in the experiments are shown in Fig. 2.2.2. In both system configurations, a primary source illuminates a circular aperture of radius a_1 in plane I. It is assumed that illumination is provided by a quasi-homogeneous thermal source[28] located directly behind the aperture in plane I. The impulse-response function connecting planes I and II is used to produce a secondary source with controlled spatial coherence at plane II. The spectrum of light is measured at the secondary source, plane II, and in the far field of the secondary source, plane III.

A theoretical expression for the complex degree of spectral coherence in the secondary source plane II can be calculated using Eqs. (2.2.6) and (2.2.7). For the system shown in Fig. 2.2.2(a), plane I is located in the front focal plane of an achromatic telescope objective of focal length F. Plane II is located in the back focal plane of the objective. For this case the impulse-response function connecting planes I and II is given by

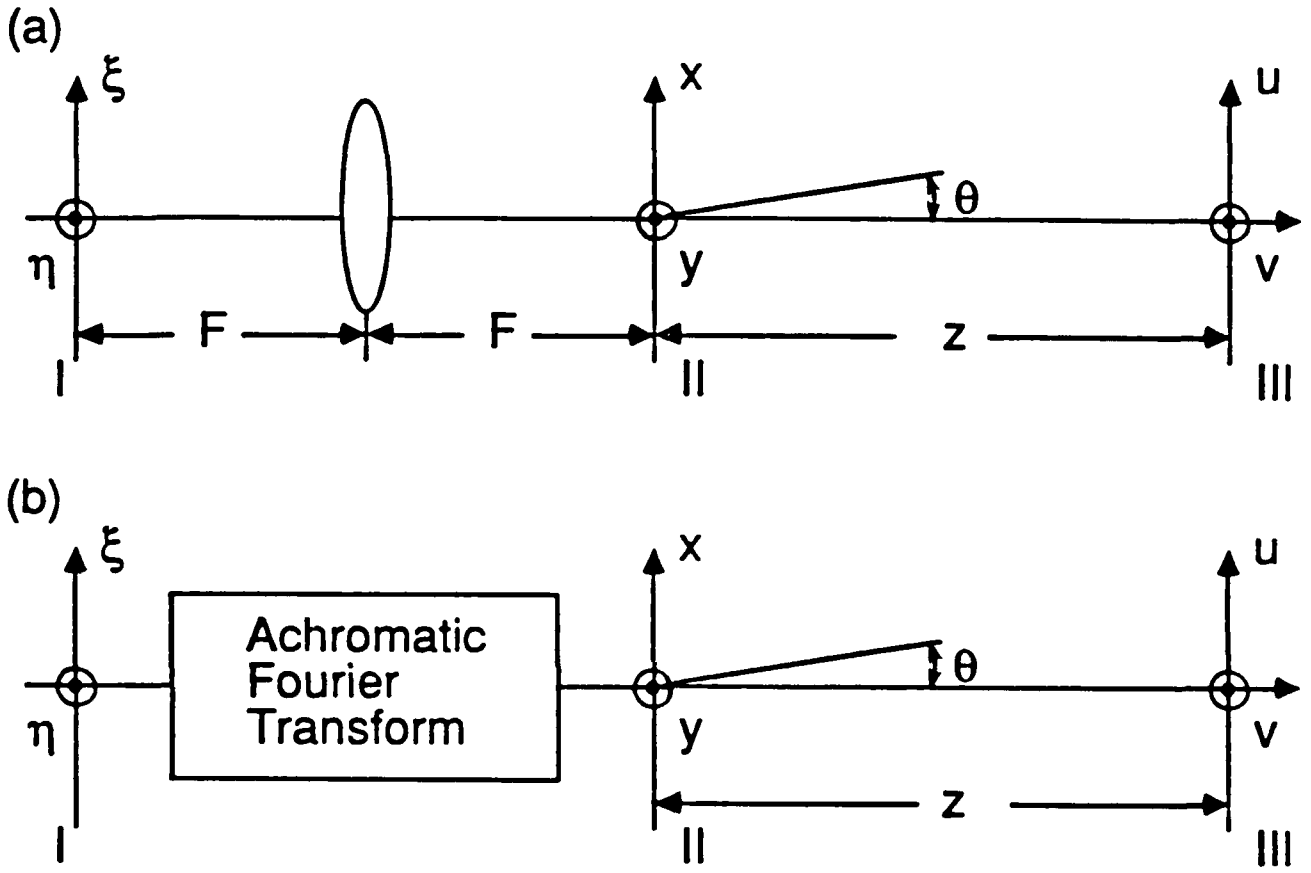

Fig. 2.2.2 Experimental configurations for realization of secondary sources with controlled spatial coherence that (a) satisfy the scaling law, and (b) violate the scaling law. An aperture function in plane I is illuminated using a broadband, spatially incoherent source. A secondary source with a specified complex degree of spectral coherence is formed in plane II through application of the Van Cittert-Zernike theorem. Measurements of the spectral intensity are made in the secondary source plane II and in the far field of the secondary source, plane III.

$$h^{conv}(x,y;\xi,\eta;\omega) = \left(\frac{-i\omega}{2\pi cF}\right) \exp\left[\left(\frac{-i\omega}{cF}\right)(x\xi + y\eta)\right] \quad ; \qquad (2.2.8)$$

this is the conventional impulse response for a F-to-F Fourier-transform system.[31]

In the system arrangement shown in Fig. 2.2.2(b), an achromatic-Fourier-transform lens[32-34] is inserted between planes I and II. With spatially coherent light the effect of this *Fourier achromat* is to produce an optical Fourier transform in plane II in which the transform size is independent of wavelength. The impulse response of the Fourier achromat is given by

$$h^{aft}(x,y;\xi,\eta;\omega) = \left(\frac{-i\omega_0}{2\pi cF}\right) \exp\left[\left(\frac{-i\omega_0}{cF}\right)(x\xi + y\eta)\right] \quad , \qquad (2.2.9)$$

in which ω_0 is a constant and corresponds to a particular design frequency.

The effect of the impulse-response functions given by Eqs. (2.2.8) and (2.2.9) is illustrated in Fig. 2.2.3; these photographs are optical transform patterns recorded in plane II of the systems in Figs. 2.2.2(a) and 2.2.2(b), respectively. In each case, a 400-μm-diameter, circular aperture is inserted in plane I and illuminated with spatially coherent, broadband light. The spectral bandwidth of the light is 200 nm. In Fig. 2.2.3(a) one notes that the size of the transform pattern scales linearly with the wavelength of illumination. The scaling of the pattern with wavelength can be traced directly to the frequency dependence of $h^{CONV}(x,y;\xi,\eta;\omega)$ in Eq. (2.2.8). The system in Fig. 2.2.2(a) produces a secondary source in plane II that obeys the scaling law. In Fig. 2.2.3(b) it is seen that the scale size of the optical transform pattern produced by the Fourier achromat is independent of the illumination wavelength. The Fourier achromat of Fig. 2.2.2(b) produces a secondary source in plane II such that the

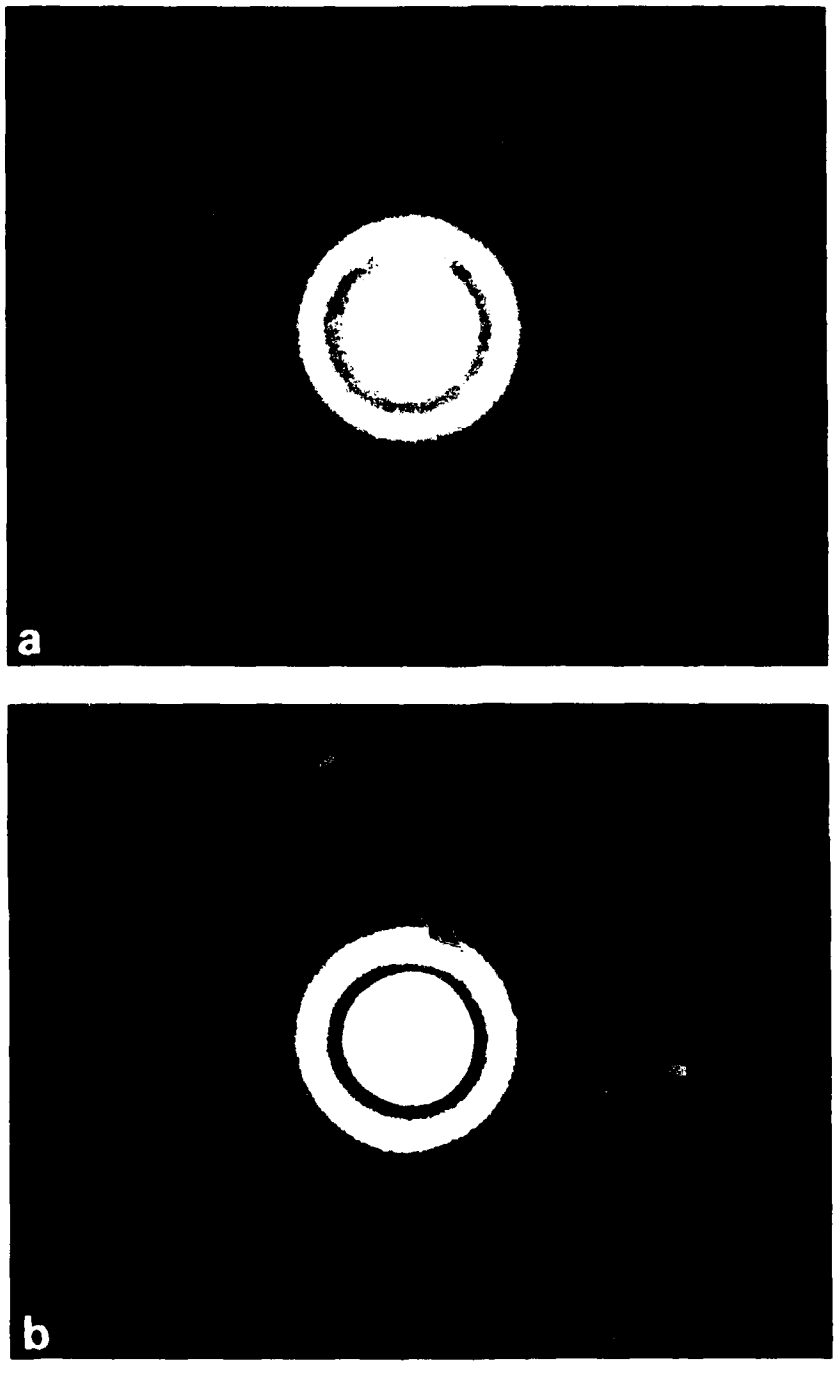

Fig. 2.2.3 Airy-disk diffraction pattern recorded in the back focal plane, plane II of (a) an achromatic telescope objective lens, and (b) an achromatic-Fourier-transform lens. These photographs were produced by illuminating a circular aperture located in plane I with broadband, spatially coherent light. In (a) the diffraction pattern scales linearly with wavelength, and in (b) the size of the diffraction pattern is independent of the wavelength.

complex degree of spectral coherence is independent of the illumination wavelength, and therefore, does not satisfy the scaling law.

Using Eqs. (2.2.6) - (2.2.8) gives the following expressions for the spectral intensity and complex degree of spectral coherence in plane II for the system in Fig. 2.2.2(a):

$$S_{II}^{conv}(\omega) = \kappa_0 S^{(0)}(\omega) \quad , \tag{2.2.10}$$

$$\mu_{12}^{conv}(\omega) = \frac{2\,J_1(\chi)}{\chi} \quad , \tag{2.2.11}$$

where $S^{(0)}(\omega)$ denotes the spectrum at the primary source, $J_1(\chi)$ is the Bessel function of order one, $\chi = [\omega a_1/(cF)]\left[(x_2 - x_1)^2 + (y_2 - y_1)^2\right]^{1/2}$, and κ_0 is a constant. We will refer to sources that have a complex degree of spectral coherence with the functional form of Eq. (2.2.11) as *Bessel-correlated* sources.

By using Eqs. (2.2.6), (2.2.7) and (2.2.9) one can calculate expressions for spectral intensity and complex degree of spectral coherence in plane II of Fig. 2.2.2(b) as follows:

$$S_{II}^{aft}(\omega) = \kappa_1 \left(\frac{\omega_0}{\omega}\right)^2 T(\omega)\, S^{(0)}(\omega) \quad , \tag{2.2.12}$$

$$\mu_{12}^{aft}(\omega) = \frac{2\,J_1(\chi')}{\chi'} \quad , \tag{2.2.13}$$

where $T(\omega)$ is introduced to account for transmission losses through the Fourier achromat, $\chi' = [\omega_0 a_1/(cF)]\left[(x_2 - x_1)^2 + (y_2 - y_1)^2\right]^{1/2}$, and κ_1 is a constant. Note that

the only difference in the expressions for the complex degree of spectral coherence in Eqs. (2.2.11) and (2.2.13) is that ω in Eq. (2.2.11) has been replaced by ω_0 in Eq. (2.2.13). A detailed calculation for the spectral intensity shows that $S_{II}^{AFT}(r;\omega)$ is independent of the spatial location r only in a region whose size depends on the spectral bandwidth. In the experiments reported below, a circular aperture is inserted in plane II to ensure that $S_{II}^{AFT}(r;\omega) = S_{II}^{AFT}(\omega)$ for all points within the aperture.

2.2.4 Spectrum of Light in the Far Zone

The spectrum of light in the far field of the secondary source located in plane II can be calculated using the above linear system formalism to describe the propagation between planes II and III of Fig. 2.2.2. The spectral intensity in plane III is readily found to be given by the following formula:

$$S_{III}(u,v;\omega) = \iiint\!\!\iint t_{II}(x_1,y_1;\omega)\, t_{II}^{*}(x_2,y_2;\omega)\, W_{II}(x_1,y_1;x_2,y_2;\omega) \times h^{(\infty)}(u,v;x_1,y_1;\omega)\, h^{(\infty)*}(u,v;x_2,y_2;\omega)\, dx_1dy_1dx_2dy_2 \quad , \qquad (2.2.14)$$

where $t_{II}(x,y;\omega)$ represents a transmission function in plane II, and

$$h^{(\infty)}(u,v;x,y;\omega) = \left(\frac{-i\omega}{2\pi cz}\right) \exp\left[\left(\frac{i\omega}{2cz}\right)(u^2+v^2)\right] \exp\left[\left(\frac{-i\omega}{cz}\right)(ux+vy)\right]. \qquad (2.2.15)$$

Taking $t_{II}(x,y;\omega)=1$ and using Eqs. (2.2.7), (2.2.10), (2.2.11) and (2.2.14), one finds that

$$\begin{aligned} S_{III}^{conv}(r;\omega) &= \kappa_2\, S_{II}^{conv}(\omega) && , r \le a_1 z/F \\ &= 0 && , r > a_1 z/F \quad , \end{aligned} \qquad (2.2.16)$$

where $r = [u^2 + v^2]^{1/2}$ and κ_2 is a constant. The circular aperture of radius a_2 is used to ensure that the observation plane, plane III, is in the far field of the secondary source.

Using Eqs. (2.2.7) and (2.2.12) - (2.2.14) one obtains the following expression for the spectrum of the field in the far zone of the achromatized secondary source of Fig. 2.2.2(b):

$$S_{III}^{aft}(r;\omega) = \kappa_3 \left(\frac{\omega}{\omega_0}\right)^4 S_{II}^{aft}(\omega) \ , \ r \le a_1 z\omega_0 / \omega F$$
$$= 0 \qquad\qquad\qquad\qquad , \ r > a_1 z\omega_0 / \omega F \ , \qquad (2.2.17)$$

where κ_3 is a constant.

2.2.5 Experimental Results

In the experiments a 100-watt tungsten-halogen lamp is used as the primary source and is located in close proximity behind a circular aperture of radius $a_1 = 2.5$ mm in plane I [see Fig. 2.2.2]. The focal length F is 180 mm. Using these values the coherence interval at the secondary source plane II is 24 μm at $\lambda = \lambda_0 = 550$ nm.

A circular aperture of radius $a_2 = 0.5$ mm is located in plane II. The far-field condition is satisfied when $z >> a_2^2/\lambda = 0.5$ m at $\lambda = 500$ nm. To obtain an acceptable SNR in our detection system, the distance z is taken to be one meter. The aperture in plane II is also used to ensure that the spectrum of the secondary source in the experimental arrangement of Fig. 2.2.2(b) is independent of the spatial location within the aperture [see Eq. (2.2.12)].

The spectral intensity of the light at the various observations points is measured using a grating monochromator.

Figure 2.2.4(a) shows curves for the spectral intensity measured at the source plane II and at various locations in the far field, plane III, for the system configuration of Fig. 2.2.2(a). As expected, since this source obeys the scaling law, the normalized spectrum is invariant on propagation.

In the experiments involving the system configuration of Fig. 2.2.2(b), an all-glass Fourier achromat[33] is used. The lens consists of three widely spaced lens groups. The lens is capable of forming 250 adjacent, achromatized Airy disks across a 7-mm diameter in the optical transform plane. The system is well corrected for wavelengths ranging from approximately 470 nm to 590 nm [$4.0 \times 10^{15} > \omega > 3.2 \times 10^{15}$ sec^{-1}].

The spectral intensity measured on-axis at planes II and III for the Fourier-achromat-system configuration is shown in Fig. 2.2.4(b) -- the solid curves are plotted from laboratory measurements and the dashed curve is the theoretical prediction for the spectral intensity as given in Eq. (2.2.17).

In Fig. 2.2.5, measurements of the spectral intensity at various off-axis points in plane III of Fig. 2.2.2(b) are given. Note that the width of the spectral intensity vs. ω narrows as the angle of observation increases. For the off-axis points, the measured values of the spectral intensity are somewhat lower than that predicted by Eq. (2.2.17). This can be explained by the fact that the far-field condition is only approximately satisfied. For the calculation of the spectral intensity at off-axis points in plane III, one should actually use the impulse response that corresponds to a Fresnel-diffraction geometry. However, for the sake of brevity, this calculation is omitted in the present treatment.[10]

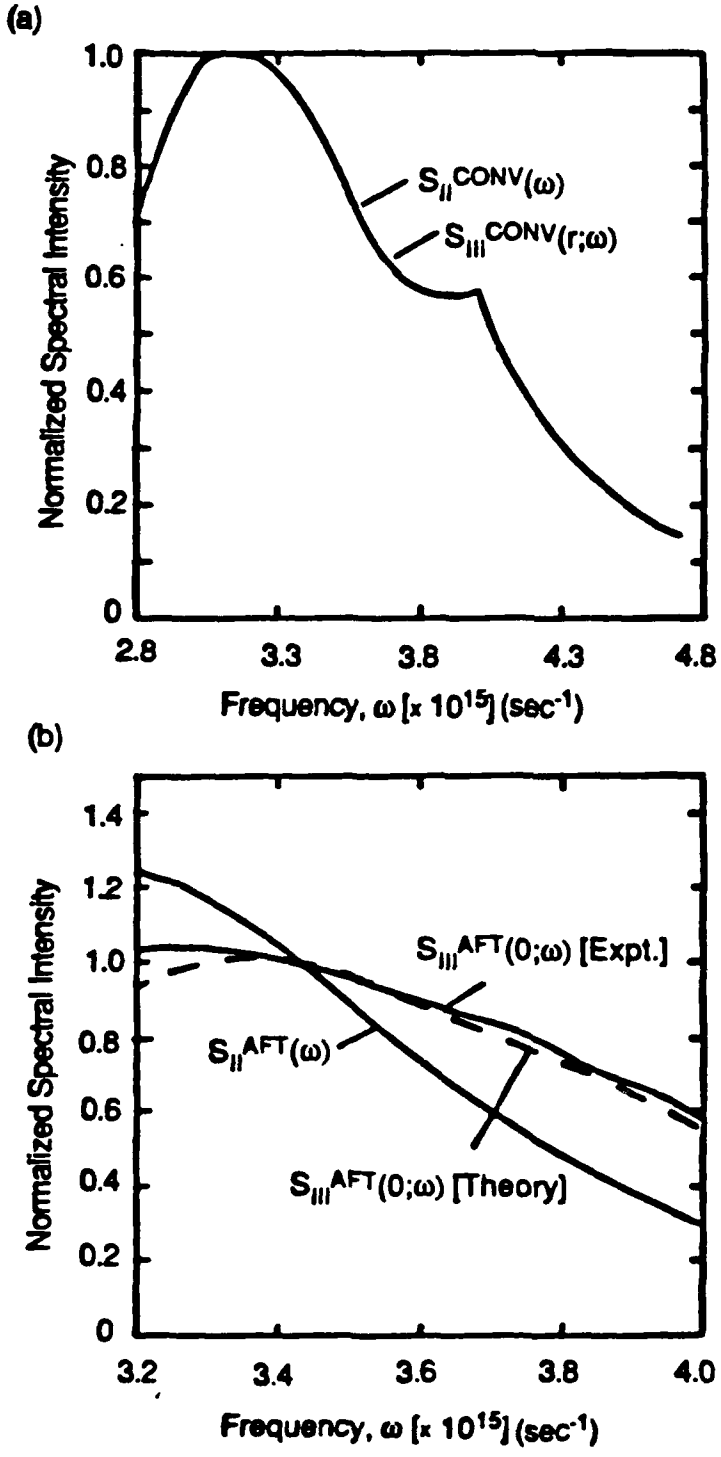

Fig. 2.2.4 Normalized spectral intensity at the secondary source plane II and in the far field of the secondary source, plane III, for (a) a source that obeys the scaling law, and (b) a source in which the complex degree of spectral coherence is independent of the illumination frequency (i.e., violates the scaling law). In (a) the spectral intensity is normalized to the peak value of the spectral intensity in the respective planes. In (b) the spectral intensity in planes II and III are scaled such that $S_{II}^{AFT}(\omega_0)=S_{III}^{AFT}(0;\omega_0)=1$.

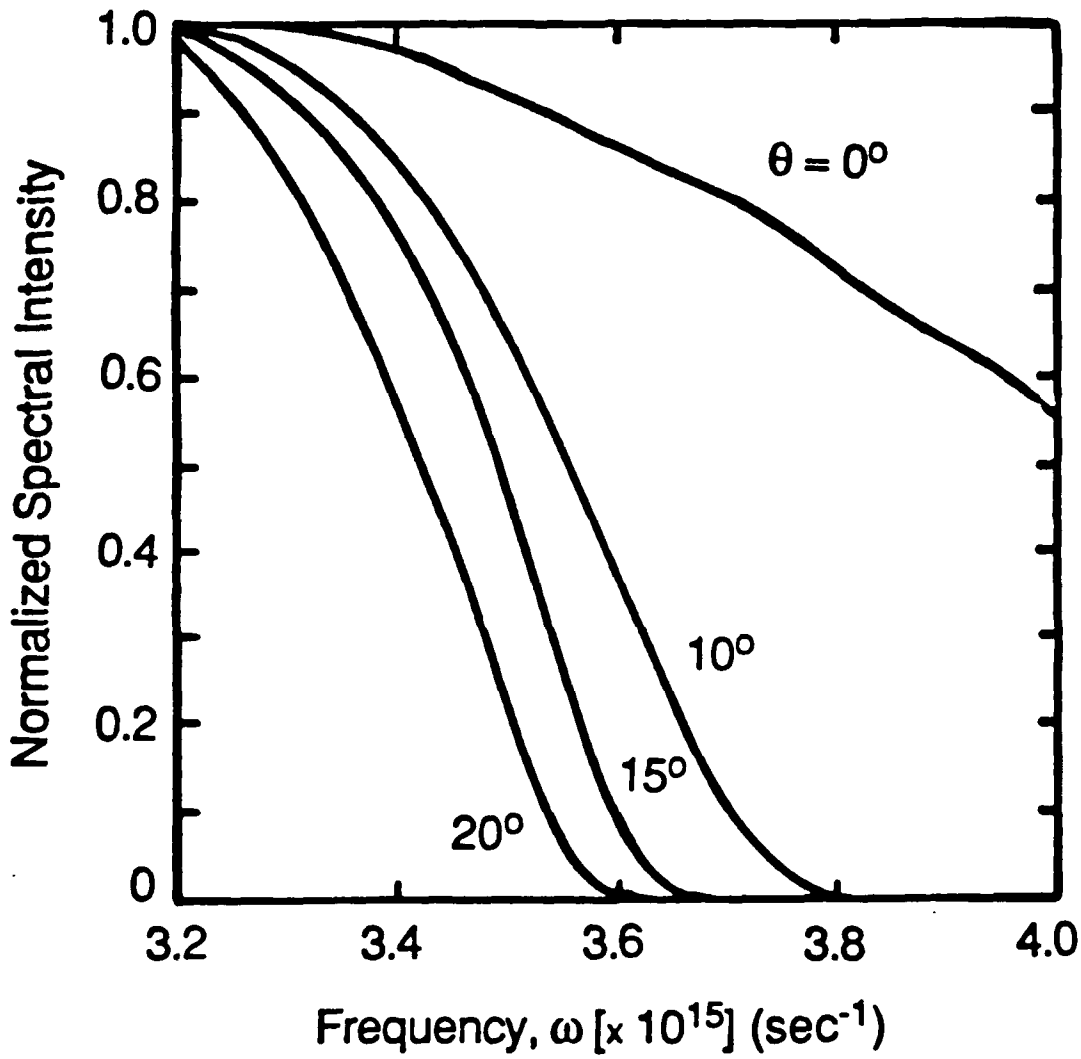

Fig. 2.2.5 Measured values of the normalized spectral intensity in the far field, plane III, for case (b) (i.e., when the source does not obey the scaling law). The spectral intensity is measured at off-axis angle $\theta = 0^0, 10^0, 15^0, 20^0$. Note that the spectral intensity vs. frequency narrows as the off-axis angle θ increases. The intensity data are normalized with respect to $S_{III}(0;\omega_1)$, where $\omega_1 = 3.2 \times 10^{15}$ sec^{-1}.

2.2.6 Discussion

We have experimentally demonstrated that the statistical properties of the light emitted by a partially coherent source can affect the spectrum detected at a distant point. In our experiments a circular aperture is inserted in plane I of Fig. 2.2.2 to produce a secondary source at plane II that is Bessel-correlated [see Eqs. (2.2.11) and (2.2.13)]. A Fourier achromat [see Fig. 2.2.2(b)] is used to produce a field correlation in plane II that is independent of the illumination frequency (a departure from the scaling law). In this case the spectrum in the far field is different from the spectrum measured at the source and changes for different observation points in the far field [see Eq. (2.2.17) and Figs. 2.2.4 and 2.2.5]. While a Bessel-correlated source was used in these experiments, it is noted that virtually any allowed functional form for the complex degree of spectral coherence can be produced through application of the Van Cittert-Zernike theorem. For example, a Gaussian-correlated source can be produced by inserting a Gaussian transmission function in plane I. A Fourier achromat inserted between planes I and II eliminates the wavelength dependence in the complex degree of spectral coherence in plane II. A different frequency dependence for the complex degree of spectral coherence could be produced by a modification of the design rules used for the Fourier achromat.

The effects of source correlation on the spectrum is to be distinguished from changes in the spectrum due to diffraction of fully or partially coherent light by an aperture function located in the source plane. Although both effects can modify the spectrum of light on propagation, their physical origin is different. For example, suppose that one placed a diffraction grating in the secondary-source plane II. Using

Eq. (2.2.14) and the appropriate expression for the transmission function $t_{II}(x,y;\omega)$ of a diffraction grating, one can write an expression for the spectrum $S_{III}(u,v;\omega)$ in the far field. The transmission function $t_{II}(x,y;\omega)$ will affect $S_{III}(u,v;\omega)$ only if the coherence interval, associated with the cross-spectral density $W_{II}(x_1,y_1;x_2,y_2;\omega)$, is on the order of or greater than the grating period, i.e. the light is spatially coherent over at least a portion of the grating structure. Similar reasoning can be used for the case in which a refractive element, such as a prism, is placed in the secondary-source plane.

In our experiments, a 1-mm-diameter circular aperture is inserted in plane II. The purpose of this aperture is to ensure that the far-field condition is satisfied (approximately) in the measurements of $S_{III}(u,v;\omega)$. As stated above, the coherence interval at plane II is 24 μm. Since the coherence interval is much less than the object structure (aperture diameter), the illumination in plane II is essentially incoherent and the aperture does not modify the spectrum of light in the far field. In our experiments changes in the spectrum on propagation are due to the correlation properties of the secondary source.

2.3 Spectral Shifts Produced by Source Correlations

Wolf[3-5] has shown that under certain conditions, source correlations can produce frequency shifts in the observed spectrum. Recently Bocko et. al.[6] have observed frequency shifts of the field spectrum generated by two appropriately correlated acoustical sources.

In this Section, we describe experiments in which frequency shifts of the optical spectrum detected in the far field of a planar secondary source are observed. In the experiments we use a Fourier achromat to generate a secondary source with a degree of spectral coherence that is independent of wavelength, and therefore, does not satisfy the scaling law. The spectrum detected in the far field of the source depends on the spectrum at the source, the degree of spectral coherence at the source, and the location of the observation point.

2.3.1 Synthesis of the Secondary Source

Consider a general linear optical system with an impulse-response function given by $h(\mathbf{x},\xi;\nu)$ in which the vectors ξ and $\mathbf{x}$ represent points in the input and output planes, respectively, and ν denotes the illumination frequency, $\nu=c/\lambda$, where λ is the wavelength. The spectral amplitude of the system output $U_{II}(\mathbf{x};\nu)$ may be expressed as a superposition of the input spectral amplitude $U_I(\xi;\nu)$ and the system impulse response as follows:

$$U_{II}(\mathbf{x};\nu) = \int U_I(\xi;\nu)\, h(x,\xi;\nu)\, d^2\xi \quad . \tag{2.3.1}$$

The cross-spectral density function may be shown to be expressible in the form[29]

$$W(\mathbf{x}_1,\mathbf{x}_2;\nu) = \langle U(\mathbf{x}_1;\nu)\, U^*(\mathbf{x}_2;\nu)\rangle \quad , \tag{2.3.2}$$

in which $\langle\ldots\rangle_S$ denotes an average over an ensemble of sources. The spectral intensity is given by

$$S(\mathbf{x};\nu) = W(\mathbf{x},\mathbf{x};\nu) \quad , \tag{2.3.3}$$

and the normalized cross-spectral density function (the complex degree of spectral coherence) is written as

$$\mu(\mathbf{x}_1,\mathbf{x}_2;\nu) = \frac{W(\mathbf{x}_1,\mathbf{x}_2;\nu)}{\left[S(\mathbf{x}_1;\nu)\, S(\mathbf{x}_2;\nu)\right]^{1/2}} \quad . \tag{2.3.4}$$

A diagram of the optical system used in the experiments is shown in Fig. 2.3.1. The illumination is provided by a quasi-homogeneous thermal source[35] that is imaged onto plane I. The two-lens imaging system between the primary source and plane I is characterized by a pupil function $P(\mathbf{r})$ and a magnification $M=F_2/F_1$, where F_1 and F_2 are the focal lengths of the two lenses. The primary source is located at a distance F_1 in front of the first lens with the pupil $P(\mathbf{r})$ located at a distance F_1 behind the first lens and at a distance F_2 in front of the second lens. The image of the primary source is located at a distance F_2 behind the second lens in plane I.

The impulse-response function relating the field in planes I and II is used to produce a secondary source with specified spatial coherence at plane II. The spectrum

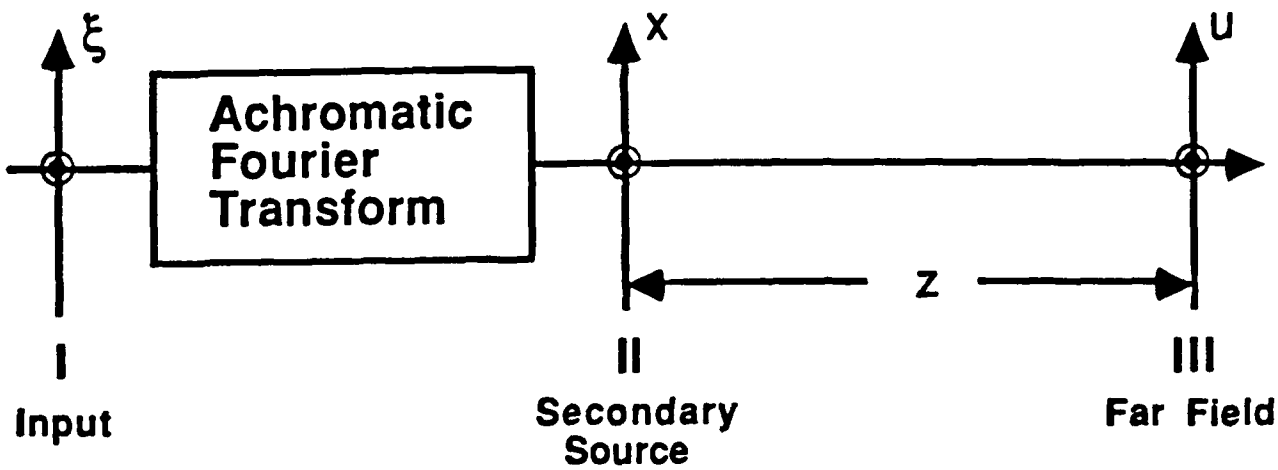

Fig. 2.3.1 Experimental configuration for realization of a secondary source with controlled degree of spatial coherence. An object located in plane I is illuminated using a broadband, partially-coherent source that obeys the scaling law. A secondary source with wavelength-independent spatial coherence is formed in plane II through application of the generalized Van Cittert-Zernike theorem. The spectral intensity is measured at the secondary source, plane II, and in the far field of the secondary source, plane III.

of the light is measured at the secondary source, plane II, and in the far field of the secondary source, plane III.

The impulse response of the achromatic Fourier transform system[32-34] is given by

$$h_{AFT}(\mathbf{x},\xi;\nu) = \frac{-i}{\lambda_0 F_0} \exp\left[\frac{-i2\pi}{\lambda_0 F_0}\mathbf{x}\bullet\xi\right] \quad , \tag{2.3.5}$$

where F_0 is the focal length of the lens system when $\lambda=\lambda_0$ and λ_0 is a constant that corresponds to a particular design wavelength. The cross-spectral density function in plane II of Fig. 2.3.1 is then given by

$$W_{II}(\mathbf{x}_1,\mathbf{x}_2;\nu) = \iint g(\xi';\nu)\, g^*(\xi'';\nu)\, W_{in}(\xi',\xi'';\nu) \times h_{AFT}(\mathbf{x}_1,\xi';\nu)\, h_{AFT}{}^*(\mathbf{x}_2,\xi'';\nu)\, d^2\xi'\, d^2\xi'' \quad , \tag{2.3.6}$$

where $g(\xi;\nu)$ is the amplitude transmittance of the aperture in plane I and $W_{in}(\xi',\xi'';\nu)$ is the cross-spectral density of the incident illumination. The illumination incident on plane I is assumed to satisfy the scaling law and to have a spectrum $S^{(0)}(\nu)$, which is the same at all spatial locations. The amplitude transmittance of the aperture in plane I is assumed to be independent of the illumination frequency, i.e. $g(\xi;\nu)=g(\xi)$. With these assumptions, Eqs. (2.3.3) - (2.3.6) lead to the following expressions for the spectral intensity and complex degree of spectral coherence in plane II for the system shown in Fig. 2.3.1:

$$S_{II}(\mathbf{x};\nu) = \frac{S^{(0)}(\nu)T(\nu)}{\pi F_0^2}\left(\frac{\nu_0}{\nu}\right)^2 \left|P\left(\frac{-\nu_0 F_2}{\nu F_0}\mathbf{x}\right)\right|^2 \times \int \left|f\left(\frac{-\xi}{M}\right)\right|^2 |g(\xi)|^2 \, d^2\xi \quad , \tag{2.3.7}$$

$$\mu_{II}(\Delta\mathbf{x};\nu) = \mu_{II}(\Delta\mathbf{x};\nu_0) = \frac{\int \left|f\left(\frac{-\xi}{M}\right)\right|^2 |g(\xi)|^2 \exp\left[\frac{i2\pi}{\lambda_0 F_0}\Delta\mathbf{x}\bullet\xi\right] d^2\xi}{\int \left|f\left(\frac{-\xi}{M}\right)\right|^2 |g(\xi)|^2 \, d^2\xi} \quad , \tag{2.3.8}$$

where $T(\nu)$ is introduced to account for transmission losses through the Fourier achromat, $|f(\xi)|^2$ represents the intensity of the primary source, and $\Delta\mathbf{x}=\mathbf{x}_2-\mathbf{x}_1$. Note that the degree of spectral coherence in plane II is independent of wavelength so the secondary source indeed violates the scaling law. Consequently, the spectrum observed at different field points away from the source will, in general, be different from that measured in plane II. The spectrum throughout the near zone of plane II can be determined using the impulse-response function corresponding to Fresnel propagation between planes II and III. However, in the present work it is assumed that plane III is located in the far field of plane II.

2.3.2 Spectrum in the Far Zone

The impulse-response function that represents propagation to the far zone is given by

$$h(\mathbf{u},\mathbf{x};\nu) = \frac{-i}{\lambda z}\exp\left[\frac{i\pi}{\lambda z}\mathbf{u}\bullet\mathbf{u}\right]\exp\left[\frac{-i2\pi}{\lambda z}\mathbf{u}\bullet\mathbf{x}\right] \quad , \tag{2.3.9}$$

in which the vector **u** denotes a point in plane III and z is the distance between planes II and III. The spectral intensity in the far field plane III is

$$S_{III}(\mathbf{u};\nu) = \iint Q(\mathbf{x}_1)\, Q^*(\mathbf{x}_2)\, W(\mathbf{x}_1,\mathbf{x}_2;\nu) \times h(\mathbf{u},\mathbf{x}_1;\nu) h^*(\mathbf{u},\mathbf{x}_2;\nu)\, d^2x_1 d^2x_2 \quad , \tag{2.3.10}$$

where $Q(\mathbf{x})$ represents the amplitude transmission function of an aperture located in plane II. Using Eqs. (2.3.6), (2.3.9), and (2.3.10), one finds that

$$S_{III}(\mathbf{u};\nu) = \frac{S^{(0)}(\nu)T(\nu)}{\pi z^2} \left|f\left(\frac{\nu F_0}{M\nu_0 z}\mathbf{u}\right)\right|^2 \left|g\left(\frac{-\nu F_0}{\nu_0 z}\mathbf{u}\right)\right|^2 \times \int \left|P\left(\frac{-\nu_0 F_2}{\nu F_0}\mathbf{x}\right)\right|^2 |Q(\mathbf{x})|^2\, d^2x \quad . \tag{2.3.11}$$

In the experiments, $P(\mathbf{r})$ and $Q(\mathbf{x})$ represent circular apertures where the diameter of the image of $P(\mathbf{r})$ in plane II is chosen to be larger than the aperture $Q(\mathbf{x})$ over the entire source bandwidth. Under these circumstances, $|P[-\nu_0 F_2 \mathbf{x}/(\nu F_0)]|^2 = 1$ in Eq. (2.3.11) and the integral is evaluated to give

$$S_{III}(\mathbf{u};\nu) = \frac{AS^{(0)}(\nu)T(\nu)}{\pi z^2} \left|f\left(\frac{\nu F_0}{M\nu_0 z}\mathbf{u}\right)\right|^2 \left|g\left(\frac{-\nu F_0}{\nu_0 z}\mathbf{u}\right)\right|^2 \quad , \tag{2.3.12}$$

where A is the area of the aperture $Q(\mathbf{x})$. Comparison of Eqs. (2.3.7) and (2.3.12) indicates that the spectrum measured in the far zone will be different than the spectrum measured at the secondary source. From Eqs. (2.3.7) and (2.3.12) we readily find that

$$S_{III}(\mathbf{u};\nu) = KS_{II}(\nu) \left(\frac{\nu}{\nu_0}\right)^2 \left|f\left(\frac{\nu F_0}{M\nu_0 z}\mathbf{u}\right)\right|^2 \left|g\left(\frac{-\nu F_0}{\nu_0 z}\mathbf{u}\right)\right|^2 \quad , \tag{2.3.13}$$

where K is a constant. In our experiments we choose $g(\xi)$ to be a circular-Gaussian function with a $1/e^2$ half-width $2\sigma_1$ and we assume that the primary source has a Gaussian shape with a $1/e^2$ half-width $2\sigma_2$. Under these conditions, it follows that

$$S_{III}(\mathbf{u};\nu) = KS_{II}(\nu)\left(\frac{\nu}{\nu_0}\right)^2 \exp\left[-\left(\frac{\nu F_0}{\nu_0 z}\right)^2 \left(\frac{1}{\sigma_1^2}+\frac{1}{M^2\sigma_2^2}\right)\mathbf{u}\bullet\mathbf{u}\right] . \quad (2.3.14)$$

Notice that the spatial extent of the Gaussian term in Eq. (2.3.14) increases with decreasing frequency so that at a given off-axis point in plane III the contribution to the spectrum by the Gaussian term is greater for lower frequencies. However, the contribution of the ν^2 term in Eq. (2.3.14) is weighted toward the higher frequencies. Consequently, the peak of the spectrum measured far enough off axis in plane III is expected to shift towards the red relative to the spectrum in plane II while the spectrum measured near the axis will be shifted toward the blue relative to $S_{II}(\nu)$.

2.3.3 Experimental Results

In the experiments fluorescence from a Rhodamine-6G dye jet is used as the primary source; this source is produced by focusing four watts of 514.5-nm radiation from an argon ion laser into the 100 μm-thick jet. The focal lengths F_1 and F_2 of the two-lens imaging system between the primary source and plane I are 4 mm and 80 mm respectively. The spectrum of the incident illumination measured in plane I is found to be the same at all points within the aperture of the Fourier achromat. The computer-generated transmission mask, $g(\xi)$, is circular-Gaussian with σ_1=1.2 mm; it was recorded on Kodak Linagraph Shellburst film using an Optronics P-1700 Photomation

read/write microdensitometer. A calibration procedure was implemented to determine the relation between gray-level values (integers 0 to 255) input to the plotting system of the Optronics scanning/plotting unit, and the transmittance (or the density) of the resulting developed film. The film was written with a 12.5 μm pixel size and negative polarity, and was developed in freshly mixed Kodak D-19 for five minutes at 20 degrees C.

The spectral coherence interval at wavelength λ of light at plane I is given by $t_1=1.22\lambda F_2/d$, where d is the diameter of the pupil P(r). For these experiments t_1 is equal to 10 μm at λ = 550 nm. Since $g(\xi)$ is slowly varying over a coherence interval the illumination is essentially incoherent at plane I.

The all-glass Fourier achromat[33] used in the experiments consists of three widely spaced lens groups. The lens is capable of forming 250 adjacent, achromatized Airy disks across a 7-mm diameter in the optical transform plane. Achromatization is achieved for wavelengths ranging between 450 nm and 620 nm [$6.7\times10^{14} > \nu > 4.8\times10^{14}$ (sec^{-1})] for the aperture diameter used in these experiments. The focal length F_0 of the Fourier achromat is 180 mm and the design wavelength λ_0 = 550 nm.

A circular aperture Q(x) of radius a = 0.5 mm is placed in plane II so that the far-field condition can be approximately satisfied with the distance z equal to one meter. The coherence interval in plane II is given by $t_2 \approx \lambda_0 F_0/\pi\sigma_1$ = 26 μm, which is small compared to the aperture radius a. Since the coherence interval is much smaller than the aperture radius, the illumination in plane II is essentially incoherent and aperture diffraction effects do not modify the spectrum.

The spectral intensity of the light is measured using a grating monochromator with 0.1-nm resolution and photomultiplier detection system. Measurements of the spectral intensity in planes II and III are given in Fig. 2.3.2. The peak of the spectral

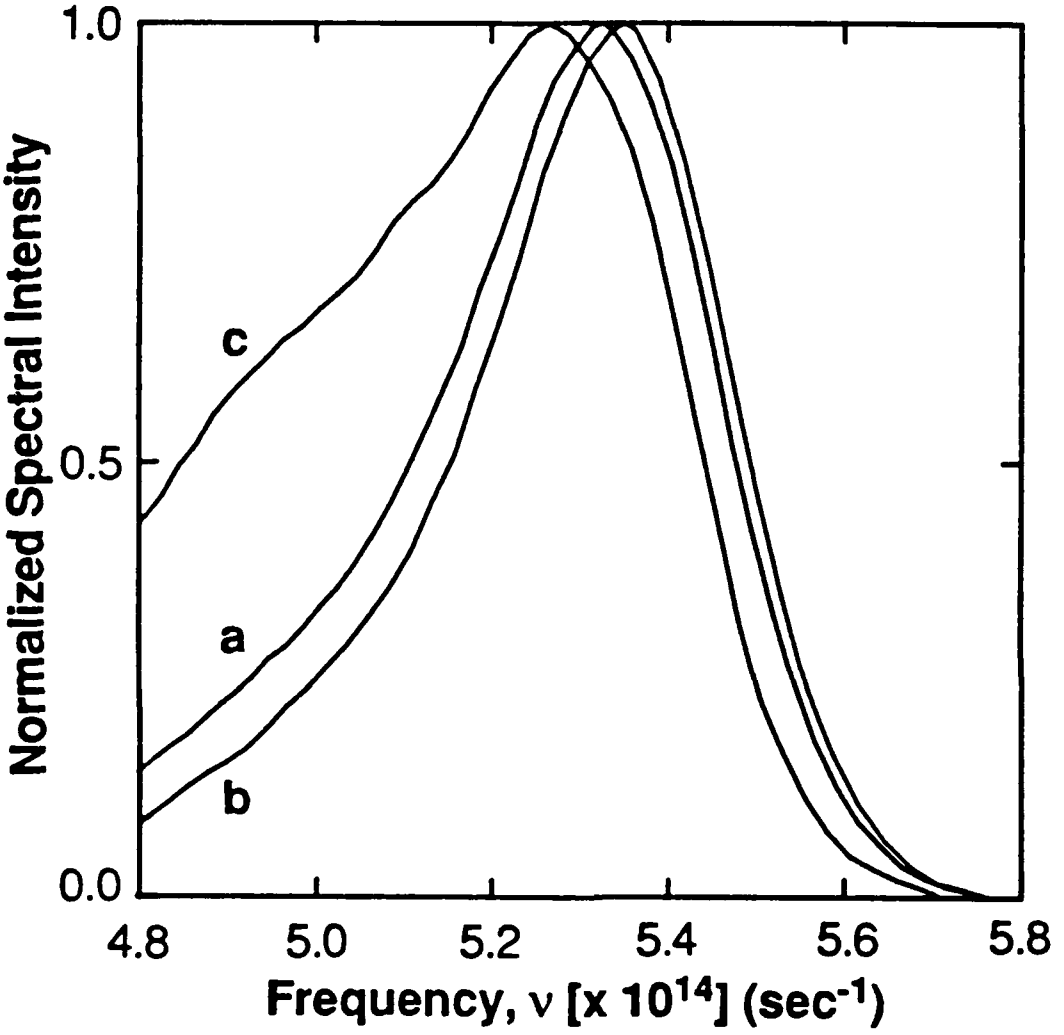

Fig. 2.3.2 Spectral shifts produced by a Gaussian-correlated planar source. The spectral intensity is measured at (a) the secondary source; and in the far field of the secondary source (b) on-axis and (c) **u**=20 mm off-axis. The peak spectral intensity measured at the off-axis point exhibits a redshift while that measured on axis exhibits a blueshift. The peak of each curve has been normalized to unity.

intensity measured 20 mm off-axis is found to be redshifted with respect to the peak of the spectrum measured at the secondary source. The peak of the spectrum measured on-axis is found to be blueshifted; this effect occurs because of the domination of the ν^2 term in Eq. (2.3.14), as was explained earlier.

In summary, frequency shifts of the spectrum of light detected in the far zone of a planar, secondary source that violates the scaling law are observed. A Fourier achromat [see Fig. 2.3.1] is used to produce a secondary source with a Gaussian field correlation that is independent of wavelength. Correlations having different wavelength dependence can be produced by an appropriate choice of the impulse-response function relating planes I and II. In fact, any dispersive medium placed between planes I and II will give rise to a secondary source in plane II that violates the scaling law.

2.4 Summary of Chapter 2

As observed in the experiments and consistent with Wolf's theoretical predictions, the spectrum of light in the far field is dependent on the correlation properties of the light at the source. If the optical field at the source obeys the scaling law, the spectrum of light on propagation is invariant. Departures from the scaling law produce changes in the spectrum that depend on the spectrum at the source, the degree of spectral coherence at the source, and the location of the observation point.

In our first set of experiments a circular aperture was inserted in plane I of Fig. 2.2.2 to produce a secondary source at plane II that was Bessel-correlated [see Eqs. (2.2.11) and (2.2.13)]. A Fourier achromat [see Fig. 2.2.2(b)] was used to produce a field correlation in plane II that is independent of the illumination frequency (a departure from the scaling law). In this case, the spectrum *in* the far field is different from the spectrum measured at the source and changes for different observation points in the far field [see Eq. (2.2.17) and Figs. 2.2.4 and 2.2.5].

We have also demonstrated experimentally that source correlations can produce frequency shifts in the spectrum observed in the far field of an optical source if the correlation function of the emitted radiation does not obey Wolf's scaling condition. A Fourier achromat [see Fig. 2.3.1] was again used to generate the non-scaling-law secondary source. The spectrum detected in the far zone of the secondary source was found to be displaced in frequency and distorted relative to the spectrum measured at the secondary source [see Fig. 2.3.2]. The displacement was toward both the higher frequencies and the lower frequencies depending on the direction of observation [see Eq. (2.3.14)]. For planar secondary sources that violate the scaling law, source

correlations have the effect of spatially redistributing the spectral components of the light in the far zone; this effect is to be distinguished from changes in the spectrum due to diffraction of fully or partially coherent light by an aperture.

2.5 References: Chapter 2

1. E. Wolf, "Invariance of spectrum of light on propagation," Phys. Rev. Lett. **56**, 1370 (1986).

2. G.M. Morris and D. Faklis, "Effects of source correlations on the spectrum of light," Opt. Commun. **62**, 5 (1987).

3. E. Wolf, "Non-cosmological redshifts of spectral lines," Nature **326**, 363 (1987).

4. E. Wolf, "Redshifts and blueshifts of spectral lines caused by source correlations," Opt. Commun. **62**, 12 (1987).

5. E. Wolf, "Redshifts and blueshifts of spectral lines emitted by two correlated sources," Phys. Rev. Lett. **58**, 2646 (1987).

6. M. F. Bocko, D.H. Douglass and R. S. Knox, "Observation of frequency shifts of spectral lines due to source correlations," Phys. Rev. Lett. **58**, 2649 (1987).

7. D. Faklis and G.M. Morris, "Spectral shifts produced by source correlations", Opt. Lett. **13**, 4 (1988).

8. W.H. Knox and R.S. Knox, "Direct observation of the optical Wolf shift using white-light interferometry," abstract of postdeadline paper PD21, Annual Meeting of the Optical Society of America (Rochester, NY), October 1987. J. Opt. Soc. Amer. **A 4**, P131 (1987).

9. F. Gori, G. Guattari, C. Palma and G. Padovani, "Observation of optical redshifts and blueshifts produced by source correlations," Opt. Commun. **67**, 1 (1988).

10. Z. Dacic and E. Wolf, "Changes in the spectrum of a partially coherent light beam propagating in free space," J. Opt. Soc. Amer. **A 5**, 1118 (1988).

11. A. Gamliel and E. Wolf, "Spectral modulation by control of source correlations," Opt. Commun. **65**, 91 (1988).

12. J.T. Foley and E. Wolf, "Partially coherent sources which generate the same far field spectra as completely incoherent sources," J. Opt. Soc. Amer. **A 5**, 1683 (1988).

13. D.F.V. James and E. Wolf, "A spectral equivalence theorem", Opt. Commun, 72, 1 (1989).

14. A. Gamliel, "New method for spectral modulation," SPIE Vol **976**, Statistical Optics, 137 (1988).

15. A. Gamliel, "Spectral changes in light propagation from a class of partially coherent sources," Proc. 6th Rochester Conference on Coherence and Quantum Optics (1989), ed. J.H. Eberly, L. Mandel and E. Wolf (Plenum, New York), in press.

16. G. Indebetouw, "Synthesis of polychromatic light sources with arbitrary degrees of coherence: Some experiments," J. Mod. Opt. **36**, 251 (1989).

17. J. T. Foley, "The effect of an aperture on the spectrum of partially coherent light," Submitted to Opt. Commun. (October, 1989).

18. E. Wolf, J.T. Foley and F. Gori, "Frequency shifts of spectral lines produced by scattering from spatially random media," J. Opt. Soc. Amer. **A 6**, 1142 (1989).

19. E. Wolf and J.T. Foley, "Scattering of electromagnetic fields of any state of coherence from space-time fluctuations," Phys. Rev. A, **40**, 579 (1989).

20. J.T. Foley and E. Wolf, "Frequency shifts of spectral lines generated by scattering from space-time fluctuations," Phys. Rev. A., **40**, 588 (1989).

21. J.T. Foley and E. Wolf, "Scattering of electromagnetic fields of any state of coherence from fluctuating media," Proc. 6th Rochester Conference on Coherence and Quantum Optics (1989), ed. J.H. Eberly, L. Mandel and E. Wolf (Plenum, New York), in press.

22. E. Wolf, "Correlation-induced Doppler-like frequency shifts of spectral lines," submitted to Phys. Rev. Lett. (October 1989).

23. E. Wolf, "On the possibility of generating Doppler-like frequency shifts of spectral lines scattering from space-time fluctuations," Proc. 6th Rochester Conference on Coherence and Quantum Optics (1989), ed. J.H. Eberly, L. Mandel and E. Wolf (Plenum, New York), in press.

24. B. J. Thompson, "Multiple-beam interference with partially coherent light," J. Opt. Soc. Am. **56**, 1157 (1963).

25. B. J. Thompson, in *Optical Data Processing -- Applications*, D. Casasent (ed.), Topics In Appl. Phys. Vol. 23 (Springer-Verlag, Berlin, 1978).

26. M. Born and E. Wolf, *Principles of Optics, 6-th ed.* (Pergamon Press, Oxford, 1980), Ch. 10.

27. F. T. S. Yu, *Optical Information Processing* (Wiley, New York, 1983).

28. J. W. Goodman, *Statistical Optics*, (Wiley, New York, 1985), Ch. 5.

29. See for example E. Wolf, "New theory of partial coherence in the space-frequency domain. Part I: spectra and cross spectra of steady-state sources," J. Opt. Soc. Am. **72**, 343 (1982); J.W. Goodman, *Statistical Optics* (Wiley, New York, 1985), p. 80; M. Born and E. Wolf, *Principles of Optics*, 6-th ed. (Pergamon Press, Oxford, 1980), p. 503.

30. L. Mandel and E. Wolf, "Spectral coherence and the concept of cross-spectral purity," J. Opt. Soc. Am. **66**, 529 (1976).

31. J. W. Goodman, *Introduction to Fourier Optics* (McGraw-Hill, San Francisco, 1968).

32. G. M. Morris, "Diffraction theory for an achromatic Fourier transformation," Appl. Opt. **20**, 2017 (1981).

33. C. Brophy, "Design of an all-glass achromatic Fourier transform lens," Opt. Commun. **47**, 364 (1983).

34. G. M. Morris and D. L. Zweig, in *Optical Signal Processing*, J. L. Horner, ed., (Academic Press, New York, 1989).

35. W. H. Carter and E. Wolf, "Coherence and radiometry with quasihomogenous planar sources," J. Opt. Soc. Am. **67**, 785 (1977).

Chapter 3

3. Synthesis of a Source with Controlled Coherence

3.1 Introduction

As we have seen in the previous chapter, the coherence properties of the light emanating from the source have a profound influence on the outcome of optical experiments that make use of the source. The statistical properties of the light emitted by a partially coherent source can affect the spectrum detected at a distant point. Also, the statistical fluctuations of the light at the source play a central role in determining the character of the light distribution in the image plane of the optical system. It is therefore essential to understand the coherence properties of the source in addition to those describing propagation and detection.

Most experiments on coherence theory involve the production of optical fields with prescribed coherence properties. Several methods exist for controlling the correlation properties of a secondary light source by means of modifying the coherence properties of the light emitted by some primary source.[1-13] The techniques include the application of the Van Cittert-Zernike theorem,[1-2] scattering by moving diffusers[3-5] and liquid crystals,[6] acoustooptic interactions,[7-11] optical feedback devices,[12] and holographic optics.[13]

An interesting example underlining the importance of the need to generate sources with controlled coherence is the recent research by Wolf[21] [also see Chapter 2 of this thesis]. He proved that an appropriately correlated source can give rise to redshifts or blueshifts of the emitted light with respect to an uncorrelated source. In

order to facilitate experiments on these effects, Wolf offered a simple model of a source exhibiting redshifts and blueshifts due to source correlations. His model consists of two small correlated sources with identical spectra consisting of a single line of Gaussian profile. Wolf showed that with an appropriate choice of the correlation, the spectrum of the emitted radiation also consisted of a single line with a Gaussian profile; however, the measured spectrum was shifted in frequency with respect to the spectrum that would be produced if the sources were uncorrelated. The nature of the shift was shown to depend on the choice of one of the parameters that specifies the exact form of the correlation. Bocko, Douglass, and Knox[22] succeeded in synthesizing an acoustic source of this type and found a complete agreement with the theoretical predictions. Knox and Knox[23] performed experiments based on Wolf's model in the optical region and also showed excellent agreement with the theory. Gori et. al.[24] provided additional experimental verification of Wolf's model in the optical region.

In this Chapter, experiments are described in which a new method is employed to generate an optical secondary source with a controlled degree of spectral coherence. Our intention is to generalize the synthesis process regarding the two-source model to further facilitate experiments on the effects of source correlations. Gamliel and Wolf[25] have examined the possibility of using source correlations to modulate spectra in a controllable manner for possible application in secure communications systems. The experiments described in this Chapter illustrate the feasibility of synthesizing source correlations for use in spectral modulation applications.

The technique consists of mixing controllable amounts of two uncorrelated sources in an interferometer. In the experiments, a spectral filtering device is used to produce the desired source correlations. The spectral filter consists of dispersive optics that are used to spatially separate (and recombine) the wavelength components of a

broadband primary source, and an amplitude mask that is used to filter the dispersed light. The complex degree of spectral coherence is shown to be directly related to the passband of the filter.

The secondary source with controlled correlation is generated using an interferometric optical system that was designed and constructed around the spectral filter. The degree of coherence is measured using an additional interferometric system in which the secondary source is allowed to form fringes. To demonstrate the system performance, the degree of spectral coherence of a specific source generated using this scheme was measured as a function of the wavelength and was compared to the theoretical predictions. The experimental measurements of the degree of coherence are found to be in good agreement with theory.

In Section 3.2, a theoretical analysis is presented that describes the synthesis of source correlations for a source consisting of two radiators. In Section 3.3, the design of a spectral filtering system to facilitate the source synthesis is reported. The results of experimental measurements and a comparison with the theory are given in Section 3.4.

Much of the analysis presented in this Chapter has been previously presented and submitted for publication (Faklis and Morris[29-30]).

3.2 Theoretical Treatment of Source Synthesis

Using this method of source generation, two mutually incoherent primary sources are mixed in proportionate amounts to result in a partially coherent secondary source. Consider the bivariate linear process given by,

$$U_1(\nu) = H_{11}(\nu)\, V_1(\nu) + H_{12}(\nu)\, V_2(\nu) \quad , \tag{3.2.1}$$

$$U_2(\nu) = H_{21}(\nu)\, V_1(\nu) + H_{22}(\nu)\, V_2(\nu) \quad , \tag{3.2.2}$$

where $V_1(\nu)$ and $V_2(\nu)$ are the uncorrelated primary sources and the functions $H_{ij}(\nu)$ $(i,j = 1,2)$ represent arbitrary deterministic functions of the spectral frequency, ν. The cross-spectral density of the secondary source is given by

$$W(\nu) = \langle U_1(\nu)\, U_2{}^*(\nu) \rangle \quad , \tag{3.2.3}$$

in which <...> denotes an average over an ensemble of sources. Two other quantities of interest here in the theoretical treatment are the spectral intensity (of each of the primary sources)

$$S(\nu) = \langle |V(\nu)|^2 \rangle \quad , \tag{3.2.4}$$

and the normalized cross-spectral density function

$$\mu(\nu) = \frac{W(\nu)}{[S_1(\nu)\, S_2(\nu)]^{1/2}} \quad , \tag{3.2.5}$$

known as the complex degree of spectral coherence.

In order to visualize the effects of the mixing process we can calculate the cross-spectral density function. The cross-spectral density of the secondary source defined by Eqs. (3.2.1) and (3.2.2) is given by

$$W(\nu) = H_{11}(\nu)\, H_{21}{}^*(\nu)\, S_1(\nu) + H_{12}(\nu)\, H_{22}{}^*(\nu)\, S_2(\nu) \quad , \tag{3.2.6}$$

where for these experiments, the spectrum of each of the uncorrelated sources $V_1(\nu)$ and $V_2(\nu)$ is assumed to be the same at all spatial locations. The complex degree of spectral coherence is given by

$$\mu(\nu) = \frac{H_{11}(\nu)\, H_{21}{}^*(\nu)\, S_1(\nu) + H_{12}(\nu)\, H_{22}{}^*(\nu)\, S_2(\nu)}{\{[|H_{11}|^2 S_1(\nu)+|H_{12}|^2 S_2(\nu)][|H_{21}|^2 S_1(\nu)+|H_{22}|^2 S_2(\nu)]\}^{1/2}} \quad . \tag{3.2.7}$$

Equation (3.2.7) represents a general method to control the frequency dependence of the degree of spatial coherence. Note that using Eqs. (3.2.1) and (3.2.2), the degree of spatial coherence is represented by a complex function of the frequency variable. The denominator of Eq. (3.2.7) is, by definition, a real function of the frequency. The numerator is, in general, complex-valued and can be designed to synthesize complex correlation functions. The spectra, $S_1(\nu)$ and $S_2(\nu)$, and the filter functions $[H_{ij}(\nu)\ (i,j = 1,2)]$ are used as parameters for the source synthesis. It is evident from Eq. (3.2.7) that at least one complex-valued filter is needed to realize a complex degree of coherence.

As an important special case of the general result, we allow the spectrum of both sources to be the same in Eq. (3.2.7), i.e., $S_1(\nu) = S_2(\nu)$,

$$\mu(\nu) = \frac{H_{11}(\nu)\,H_{21}^{*}(\nu) + H_{12}(\nu)\,H_{22}^{*}(\nu)}{\{[|H_{11}(\nu)|^2 + |H_{12}(\nu)|^2][|H_{21}(\nu)|^2 + |H_{22}(\nu)|^2]\}^{1/2}} \quad . \qquad (3.2.8)$$

Equation (3.2.8) can also be used to control the degree of spectral coherence by appropriately controlling the mixing of the two uncorrelated sources through the functions, $H_{ij}(\nu)$. To illustrate our technique for source synthesis and to obtain a particularly simple result for the degree of coherence, we next assume the following:

$$H_{11}(\nu) = H_{22}(\nu) = 1 \quad , \quad H_{12}(\nu) = H_{21}(\nu) = G(\nu) \quad . \qquad (3.2.9)$$

The function $G(\nu)$ represents a general spectral filter. Note that since we chose the spectra of the two sources to be the same and that we use Eq. (3.2.9) as a constraint, the degree of coherence is a real function. For the experiments we will assume Eq. (3.2.9) holds and that the spectral filter is a real function of frequency. Using the assumption of a real-valued spectral filter along with Eq. (3.2.9) in Eq. (3.2.8), the degree of coherence is then given by

$$\mu(\nu) = \frac{2\,G(\nu)}{1 + G^2(\nu)} \quad . \qquad (3.2.10)$$

Equation (3.2.10) illustrates the special case where the degree of coherence is controlled using a single spectral filter. Given a desired degree of coherence, Eq. (3.2.10) can be solved for the spectral filter needed for the synthesis problem. The

uncorrelated primary sources (with the same arbitrary spectra) are mixed [see Eqs. (3.2.1) and (3.2.2)] using the spectral filter to give rise to a controllable partially coherent source. Note that Eq. (3.2.10) has two possible solutions. The choice of a particular solution may depend on the actual fabrication constraints.

3.3 Spectral Filter Design

The role of the real spectral filter in the experiments is to selectively attenuate certain wavelength components relative to some specified component [see Eq. (3.2.10)]. The filter used in the experiments was designed with the intent that it be programmable and easily modified. In fact, some applications may require a real-time filter so that the degree of correlation can be modified continuously by a computer program. For these applications, the synthesis procedure would be to specify a degree of coherence; calculate the required spectral filter; and display the filter function on a spatial light modulator that is appropriately placed in the image plane of a spectrometer. For the synthesis of complex source correlations, it may be possible to modulate the phase of each wavelength component using another electrically-addressable spatial light modulator. Complex synthesis may be accomplished using two light modulators and non-equal source spectra [see Eq. (3.2.7)].

A schematic of the optical system used in the experiments to realize the spectral filter is shown in Fig. 3.3.1. The optical system needed to generate the filter was designed to be symmetric and on-axis so that it could be easily aligned and maintained. The spectral filter was designed around a direct-vision spectroscope, commonly known as an Amici prism. The Amici prism disperses the broadband, collimated input light leaving the central component undeviated. A unit magnification (mag = -1) imaging system is used to focus the wavelength components on a filter plane and to recollimate the light. The spectral components are located at well defined locations on the filter plane so that selective filtering is possible using a programmable amplitude mask. The back half of the imaging system sends the light through another Amici prism to spatially

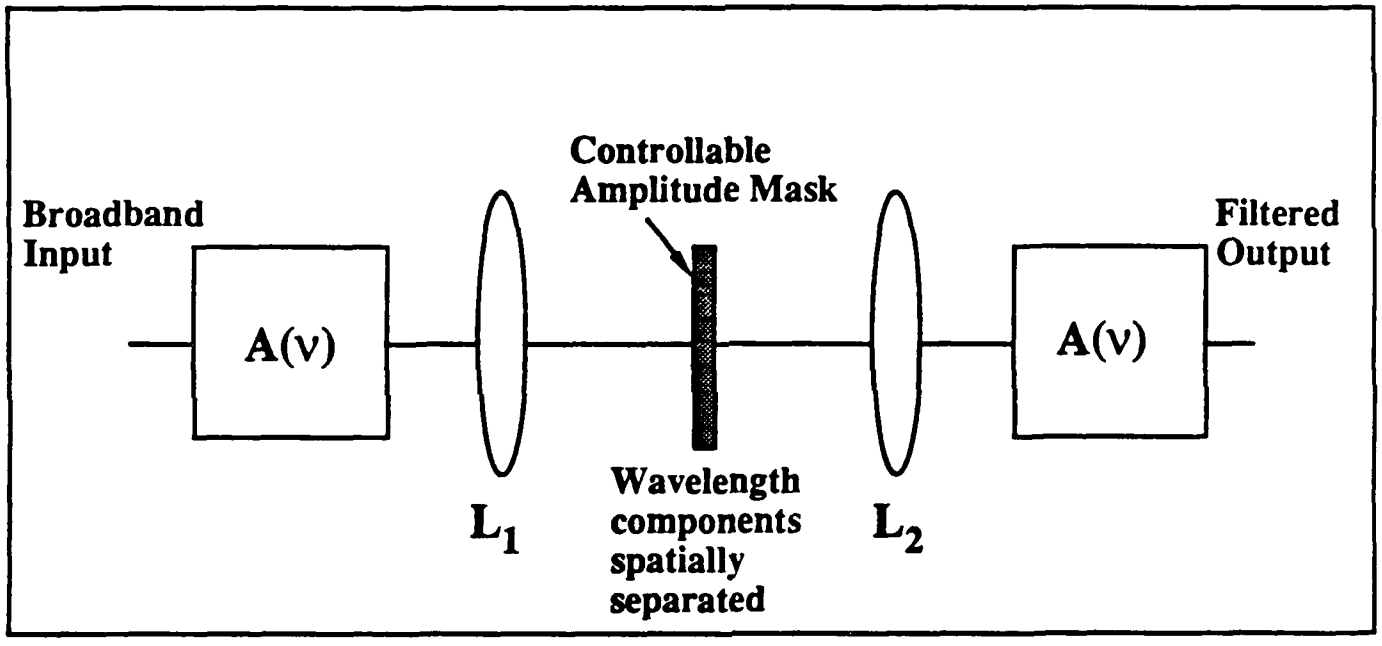

Fig. 3.3.1 Schematic of the spectral filter design.

recombine the spectral components. The filtered image has a magnification of minus one; this fact makes the design of the mixing interferometer less complex.

In order to generate the appropriate amplitude mask in the filter plane, the dispersion of the Amici prism must be known. The three-element direct-vision spectroscopes that were used in the experiments were Spindler & Hoyer 33 1120. The component glasses were BK7 (elements 1 and 3) and SF14 (element 2). The manufacturer quoted the dispersion for the cemented prism (between F' and C' light) to be approximately 4.5 degrees.

The relationship between the output angle of refraction and the wavelength is certainly not linear. The output angle as a function of the wavelength was calculated using ray-tracing techniques. The derivation was completed by keeping track of the angle of refraction at each interface starting with a collimated input. A plot of the dispersion is shown in Fig. 3.3.2. Although this result must be used to predict the location of the wavelength components in the rear focal plane of the first lens, the actual dispersion must be measured experimentally. In practice, a photographic recording is used to calibrate the spectrometer. In the experiments, the achromatic doublets have a focal length of F = 140 mm and they operate at approximately f/40.

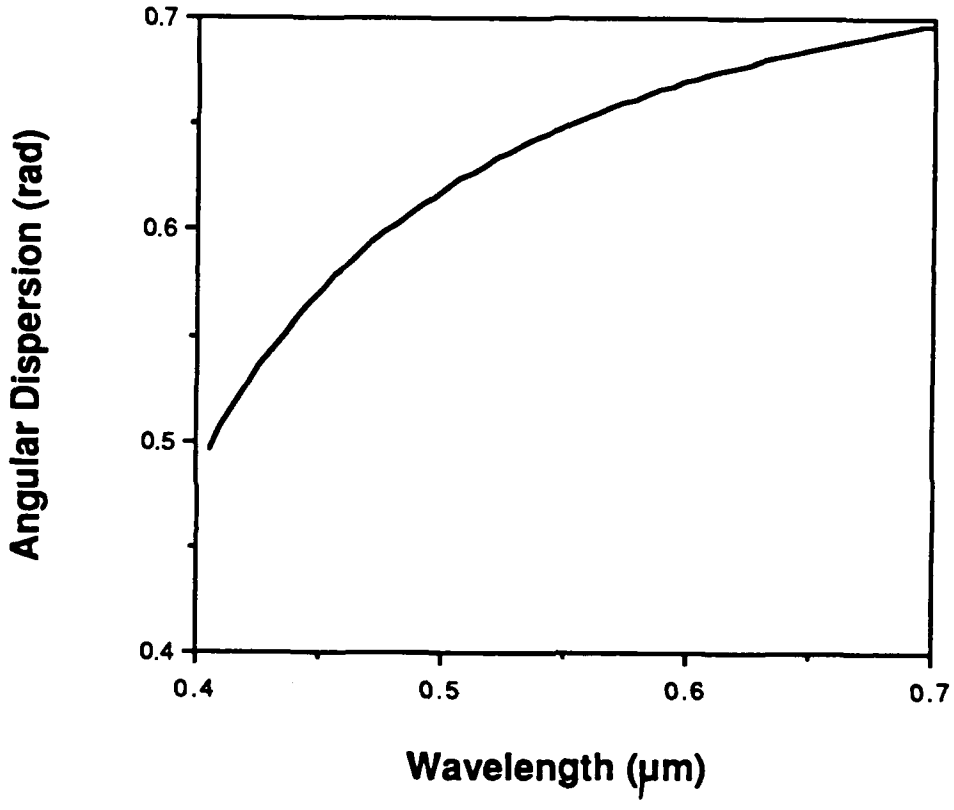

Fig. 3.3.2 Dispersion characterics of the direct-vision spectroscope. The three-element prisms used in the experiments were Spindler & Hoyer 33 1120. The component glasses were BK7 (elements 1 and 3) and SF14 (element 2).

3.4 Experimental Demonstrations

3.4.1 Source Characteristics

In the experiments, illumination from a Rhodamine-6G dye jet was used as the primary source; this source is produced by focussing seven watts from a Coherent I-90 argon-ion laser operating on all lines into a 100 μm-thick dye jet. To facilitate the coherence measurements, the dye spectrum was scanned using a laser cavity and wavelength tuning element. In fact, a Coherent 699-01 dye laser (without the Faraday rotator and etalon assembly) was used to scan the dye spectrum with a relatively broad linewidth of approximately 2.5 GHz at a maximum power of 800 mW. The wavelength tuning element consists of an stack of birefringent plates that narrows the linewidth from about 350 GHz to 2.5 GHz.

Two virtually uncorrelated sources were derived from the single multi-longitudinal-mode laser source subject to the following considerations. A value for the coherence length of the primary source can be calculated using a model for the laser's longitudinal mode structure. An idealized model of the (normalized) power spectral density of the laser oscillating in N equal-intensity axial modes is written as a sum of equally spaced Dirac delta functions. Based on such a model , it is well-known that the degree of coherence of the source has a periodic component that depends on the number of modes. However, as the number of modes, N, gets large, only the principal maxima of the periodic term contribute significantly. It is therefore possible to generate two nearly uncorrelated sources with the same spectrum from a single primary source. The primary source (laser beam) was divided into two equally-intense beams and one of the beams was allowed to propagate through an optical delay line. The length of the

delay line was set so that the degree of coherence is not at one of the principal maxima. The two derived sources were then mixed together. The optical delay line was adjusted for an absense of interference fringes. The optical delay used in the experiments consisted of about 75 cm of airspace.

It is very important to mention that in the experiments all measurements were performed on a time scale of the order of seconds. The presence of any transient correlation effects (such as the Alford-Gold effect[26-28]) is completely masked out on this time scale.

The region of the dye spectrum under investigation extended from 570 nm to 610 nm. The actual spectral profile is known however it is unimportant here since it conveniently cancels out in the calculation of the degree of coherence (both sources were generated from the same primary) [see Eq. (3.2.10)]. The illumination wavelength was continuously monitored using an Oriel 0.25-meter grating spectrometer and detection system. The resolution of the grating spectrometer is approximately 0.1 nm. The power fluctuations in the dye laser output are of the order of 5% of the total light power (at that frequency). Because of the symmetric design of the optical system, power fluctuations do not significantly effect the visibility measurements.

A schematic of the optical system used in the experiments is shown in Fig. 3.4.1. The dye laser beam is used to generate two uncorrelated beams. The two beams enter the interferometer where the are mixed through the use of the spectral filter. The spectral filter system utilized a variable optical density mask in the back focal plane of the first lens [see Fig. 3.3.1]. Specifically, the mask was a Newport variable attenuator that was calibrated for each wavelength. A plot of the transmission calibration curve for the variable mask is shown in Fig. 3.4.2. This curve represents the function G(v). The appropriately correlated source is then available at the output of the interferometer.

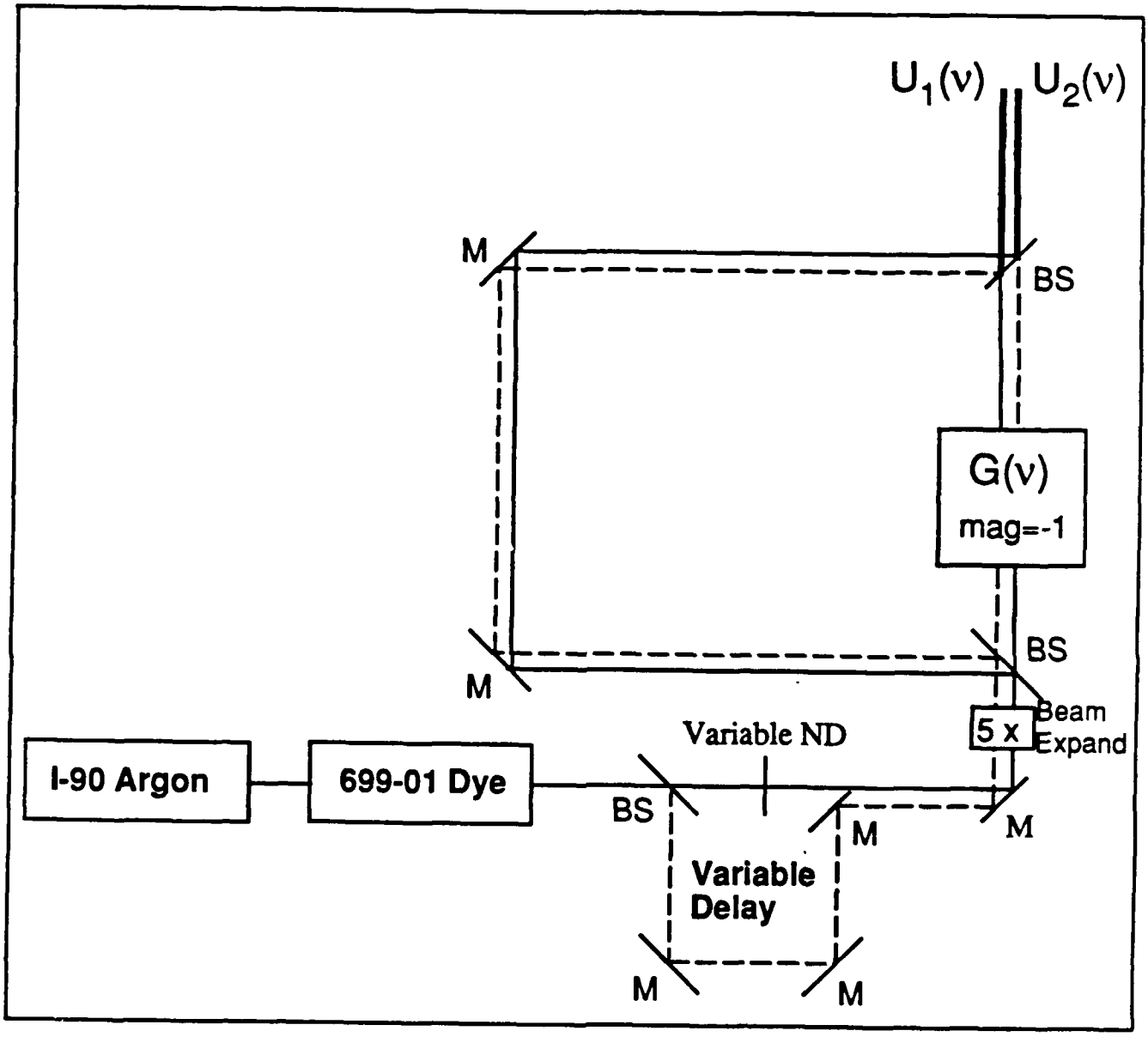

Fig. 3.4.1 Interferometric system to generate sources with controlled correlation.

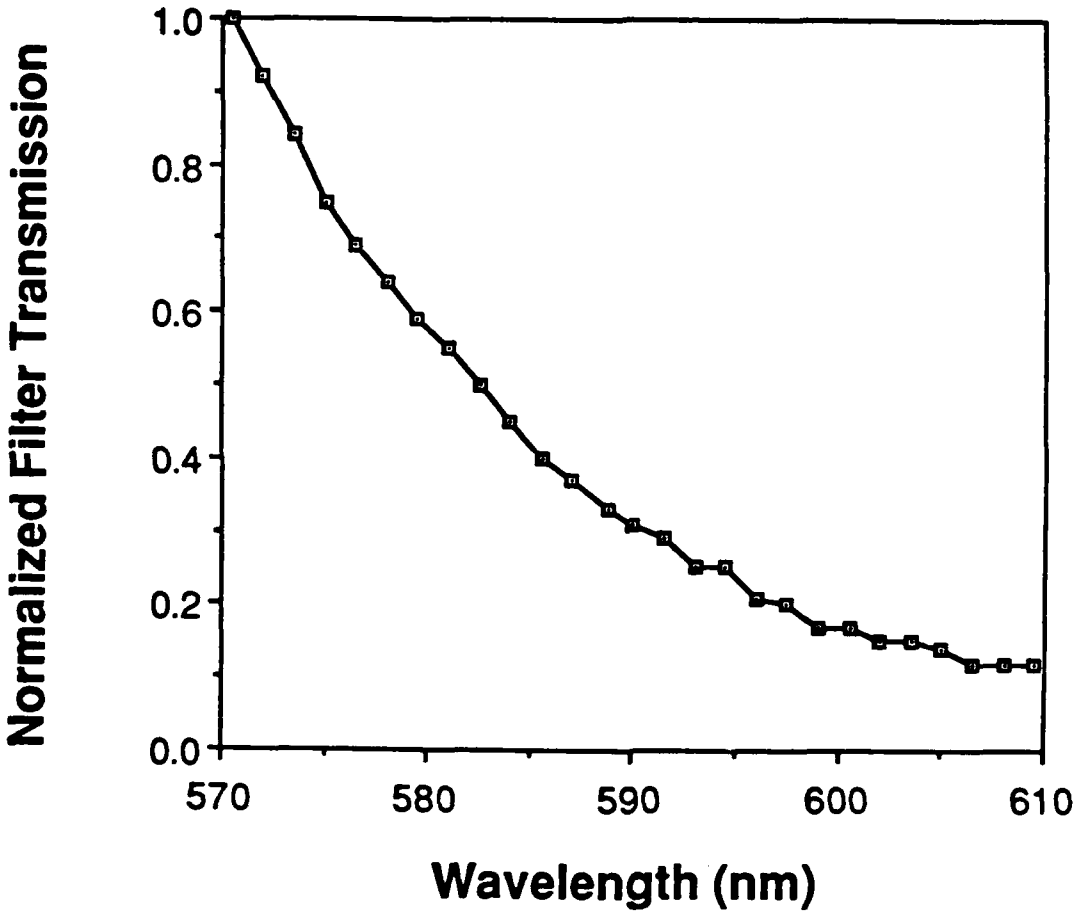

Fig. 3.4.2 Transmission characteristics for calibration of the spectral filter. The data presented here represents the basis for the theoretical model.

3.4.2 Coherence Measurements

In order to verify the synthesis procedure, the secondary source, $U_1(\nu)$ and $U_2(\nu)$, was allowed to interfere with itself and the resultant interference fringes were projected onto a linear detector array. The visibility of the fringes was measured for each wavelength component of a discrete sample set (i.e., from the tunable dye laser). Approximately thirty sample points were investigated over the wavelength range 570 nm to 610 nm. It is important to note that both arms of the source-synthesis interferometer were balanced.

For the visibility measurements, a Fairchild ISCAN linear CCD array containing 256 detector elements was utilized. The output of the detector array was input to a Tektronix 2445 oscilloscope for display of the interference fringes. The fringe visibility was computed from the oscilloscope trace. The experimental results along with the theoretical predictions [see Eq. (3.2.10)] are shown in Fig. 3.5.1. The experimental measurements of the visibility are in good agreement with theory.

In order to facilitate the coherence measurements, the spectrum of the primary source was sampled frequency-by-frequency using the laser cavity and frequency tuning element. However, the interferometric system was designed specifically to operate on a broadband input spectrum with all of the frequency components present all at once. In true operation, a source with controlled correlation is synthesized with a broadband input to the system. The partially-coherent broadband output is available at the output of the source interferometer.

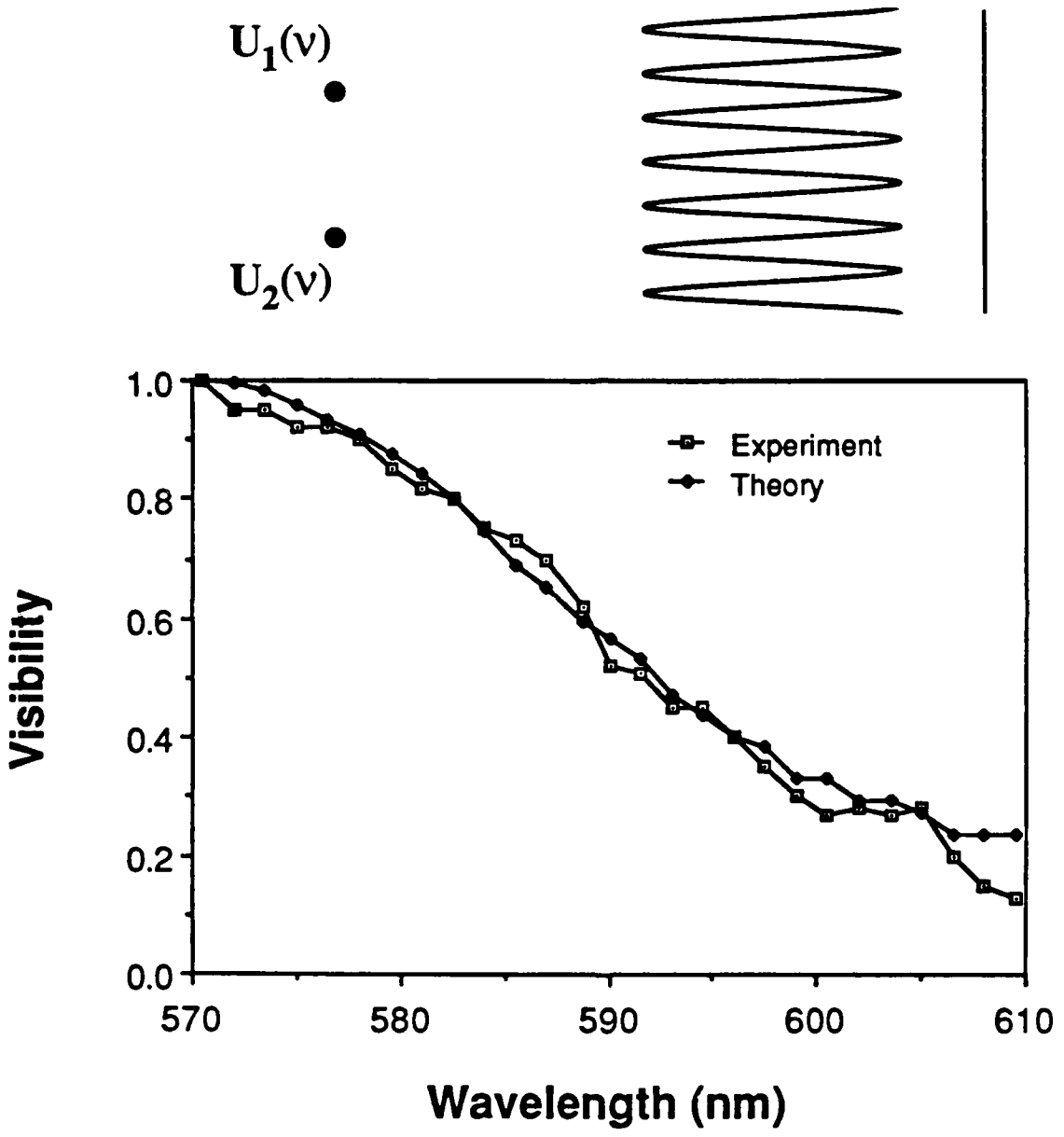

Fig. 3.5.1 Illustrating the comparison between theory and experiment for source synthesis. To test the theory, the source was produced and the visibility of interference fringes was measured as a function of the wavelength and plotted against the theoretical predictions.

3.5 Summary of Chapter 3

Experiments were described in which a new method is employed to generate an optical secondary source with a controlled degree of spectral coherence. The technique consists of mixing controllable amounts of two uncorrelated sources [see Eqs. (3.2.1) and (3.2.2)]. For a special case of the general formalism, the complex degree of coherence was shown to be directly related to the passband of a spectral filter [see Eq. (3.2.10)].

In the experiments, a novel spectral filtering device was employed to produce the desired source correlations. The spectral filter consists of dispersive optics that were used to spatially separate (and recombine) the broadband primary source, and an amplitude mask that is used to filter the dispersed light. The filter was designed so that a real-time amplitude mask could be implemented for those applications that may require a rapid modulation of the coherence properties.

In order to verify the theoretical predictions, the fringe visibility resulting from the interference of the partially coherent source was measured over the wavelength band of interest. To facilitate the coherence measurements, a Coherent 699-01 dye laser (without the Faraday rotator and etalon assembly) was used to scan the dye spectrum. The results of experimental measurements along with the theoretical predictions [see Eq. (3.2.10)] are shown in Fig. 3.5.1.

3.6 References: Chapter 3

1. B. J. Thompson and E. Wolf, "Two-beam interference with partially coherent light," J. Opt. Soc. Am. **47**, 895 (1957).

2. D. Faklis and G. M. Morris, "Spectral shifts produced by source correlations," Opt. Lett. **13**, 4 (1988).

3. W. Martienssen and E. Spiller, Am. J. Phys. **32**, 919 (1964).

4. H. Arsenault and S. Lowenthal, "Partial coherence of an object illuminated with laser light through a moving diffuser," Opt. Commun. **1**, 451 (1970).

5. P. De Santis, F. Gori, G. Guattari, and C. Palma, "An example of a Collett-Wolf source," Opt. Commun. **29**, 256 (1979).

6. F. Scudieri, M. Bertolotti, and R. Bartolino, "Light scattered by a Liquid Crystal: a new quasi-thermal source," Appl. Opt. **13**, 181 (1974).

7. Y. Ohtsuka and Y. Imai, "Partial coherence controlled by a progressive ultrasonic wave," J. Opt. Soc .Am. **69**, 684 (1979).

8. Y. Imai and Y. Ohtsuka, "Optical coherence modulation by ultrasonic waves. 1: dependence of partial coherence on ultrasonic parameters," Appl. Opt. **19**, 542 (1980).

9. Y. Ohtsuka and Y. Nozoe, "Two-dimensional control of optical spatial coherence by acoustooptic interactions," Appl. Opt. **22**, 3630 (1983).

10. Y. Ohtsuka, "Modulation of optical coherence by ultrasonic waves," J. Opt. Soc. Am. **A 3**, 1247 (1986).

11. L. Buthaud, "Partial coherence of light modulated by progressive periodic ultrasonic waves," J. Opt. Soc. Am. **A 3**, 1065 (1986).

12. J. Deschamps, D. Courjon, and J. Bulabois, "Gaussian Schell-model sources: an example and some perspectives," J. Opt. Soc. Am. **73**, 256 (1983).

13. D. Courjon, J. Bulabois, and W. H. Carter, "Use of a holographic filter to modify the coherence of a light field," J. Opt. Soc. Am. **71**, 469 (1981).

14. P. De Santis, F. Gori, G. Guattari, and C. Palma, "Synthesis of partially coherent fields," J. Opt. Soc. Am. **A 3**, 1258 (1986).

15. F. Gori, "Lau effect and coherence theory," Opt. Commun. **31**, 4 (1979).

16. R. Sudol and B. J. Thompson, "Lau effect, theory and experiment" Appl. Opt. **20**, 1107 (1981).

17. D. Courjon and J. Bulabois, "Optical processing using a peculiar extended incoherent source," Opt. Commun. **31**, 270 (1979).

18. D. Courjon and J. Bulabois, "Modifications of the coherence properties of a light beam: applications in otical processing," Proc. Soc. Photo-Opt. Instrum. Eng. **194**, 129 (1979).

19. J. D. Farina, L. M. Narducci, and E. Collett, "Generation of highly directional beams from a globally incoherent source," Opt. Commun. **32**, 203 (1980).

20. G. Indebetouw, "Synthesis of polychromatic light sources with arbitrary degrees of coherence: some experiments," J. Mod. Opt. **36**, 251 (1989).

21. E. Wolf, "Redshifts and blueshifts of spectral lines emitted by two correlated sources," Phys. Rev. Lett. **58**, 2646 (1987).

22. M. F. Bocko, D. H. Douglass, and R. S. Knox, "Observation of frequency shifts of spectral lines due to source correlations," Phys. Rev. Lett. **58**, 2649 (1987).

23. W. H. Knox and R. S. Knox, "Direct observation of the optical Wolf shift using white-light interferometry," abstract of postdeadline paper PD21, Annual Meeting of

the Optical Society of America (Rochester, NY), October, 1987. J. Opt. Soc. Am. A **4** P131 (1987).

24. F. Gori, G. Guattari, C. Palma, and G. Padovani, "Observation of optical redshifts and blueshifts produced by source correlations," Opt. Commun. **67**, 1 (1988).

25. A. Gamliel and E. Wolf, "Spectral modulation by control of source correlations," Opt. Commun. **65**, 91 (1988).

26. W. P. Alford and A. Gold, "Laboratory measurement of the velocity of light," Am. J. Phys. **26**, 481 (1958).

27. M. P. Givens, "Photoelectric detection of interference between two light beams having large path difference," J. Opt. Soc. Am. **51**, 1030 (1961).

28. M. P. Givens, "Noise in wave interaction experiments," J. Opt. Soc. Am. **52**, 225 (1962).

29. D. Faklis and G. M. Morris, "Synthesis of sources with controlled correlation," J. Opt. Soc. Am. A P131 (1989).

30. D. Faklis and G. M. Morris, "Generation of partially coherent sources with controlled correlation," submitted for publication to Opt. Commun., March (1990).

Chapter 4

4. Coherence Properties of Synchrotron Radiation

4.1 Introduction: Synchrotron Radiation and its Applications

It is well known that accelerated charges emit electromagnetic radiation. The theoretical investigation into the radiation by charges in circular motion dates back to the work of Lienard[1] in 1898. Subsequent theoretical research was performed by Schott[2], Kerst[3], and Ivanenko and Pomeranchuk.[4] In the 1940's, Sokolov and colleagues[5] and Schwinger[6-7] reported analytical treatments of the phenomenon, known as synchrotron radiation, including a description of the intensity, spectral and angular distributions, and polarization properties. A review of the fundamental theory describing synchrotron radiation is given by Jackson.[8]

Blewett[9] was one of the first to be concerned with the effects of synchrotron radiation on the operation of electron accelerators and observed its effects on the electron orbit experimentally in 1945-46 at the General Electric Research Laboratories. A detailed history of these developments is given by Lea.[10] Elder and his colleagues,[11] also at General Electric, observed the radiation visually in 1946. During 1947, Elder *et. al.*[12-13] were able to verify Schwinger's predictions of the spectrum and polarization characteristics of the radiation. There are now many excellent reviews of synchrotron radiation and its applications.[14-23]

Synchrotron radiation emitted from electrons in a storage ring has a number of useful properties. The radiation is intense over a broad spectrum and highly polarized in the plane of the electron orbit. The continuous spectrum of the radiation reaches

from the infrared to the gamma-ray region. The general shape of the radiation spectrum of an electron moving in a curved trajectory is shown in Fig. 4.1.1. The radiation can be tuned in frequency and is typically emitted in pulses of duration ranging from 10^{-11} - 10^{-9} seconds; the pulsewidth is a function of the specific accelerator design. The pulse repetition rate ranges from 100 KHz to 500 MHz containing approximately 10^6 - 10^9 photons per pulse. The radiation has a high degree of collimation due to the relatively small effective source area which is of the order of 1 mm^2.

For the case of circularly accelerated electrons, the radiation is confined to a narrow cone tangent to the curved electron orbit (approximately 0.1 mrad). The storage ring as a source of synchrotron radiation also offers a high-vacuum environment necessary for surface physics experiments. Because of the long time constant associated with the decay of the electron beam in the ring, the spectral intensity and many other source properties are quite stable over time periods of several hours. The fact that all these properties are found in radiation from one source makes synchrotron radiation a versatile analytical tool for basic and applied research in a multitude of scientific fields.

Synchrotrons and storage rings usually consist of an evacuated ring-shaped chamber around which two basic types of magnets have been arranged: focussing and bending magnets. The focussing magnet's multiple poles set up a *nonuniform* magnetic field that acts as a lens, confining the electrons in a tight beam as they travel around the chamber. A bending magnet establishes a uniform magnetic field that is at right angles to the direction in which the electrons are moving. Such a field bends the path of the electrons.

The ring-shaped chamber contains one or more cavities in which electromagnetic fields that oscillate at radio frequencies are present. These fields

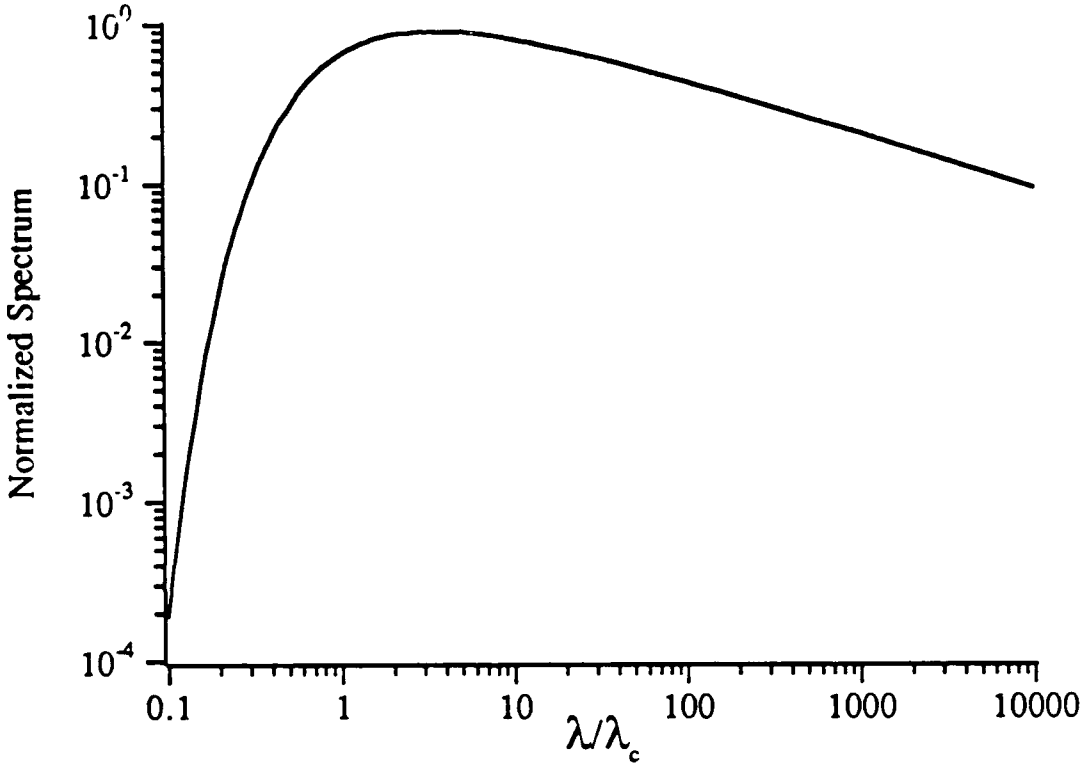

Fig. 4.1.1 The general shape of the radiation spectrum of an electron moving in a curved trajectory. λ_c represents the critical wavelength. The critical wavelength is defined such that half of the power is radiated at wavelengths above λ_c and half below λ_c.

replenish the energy lost by the electrons as they radiate and can even raise the energy of the beam if desired. The rf energy divides the circulating beam into electron "bunches" (this gives rise to the pulsed behavior discussed earlier) which are typically a few centimeters in length. Because storage rings provide a much stabler electron beam as well as a more constant radiation intensity and spectrum than synchrotrons, storage rings have become the predominant source of synchrotron radiation.

The flux and brightness of synchrotron radiation can be increased even more if the charges are made to interact with a periodic magnetic field in the cavity. The magnets that produce these alternating field are commonly called wigglers and undulators. As the electrons progress (accelerate) through the periodic field they emit radiation that is more intense and spectrally bright than a conventional storage ring or synchrotron. Wigglers and undulators are implemented in most synchrotron sources today.

There has been a recent surge of interest in applications of synchrotron radiation. Synchrotron radiation has been mainly used to study electronic excitations by absorption and reflection spectroscopy or by following excited systems via fluorescence, photoelectrons or photons.[17] The intense x-rays produced can be applied to etch integrated-circuit elements that are smaller than the wavelength of visible or ultraviolet light.[17,23] Synchrotron-generated x-rays are currently finding applications in medicine. The tunability of the radiation source makes it possible to image coronary arteries in less time and with a much smaller iodine concentration than is needed with conventional angiography.[23] There is also significant interest in using the synchrotron source to generate holographic medical images in the x-ray region.

The basic properties of synchrotron radiation such as source intensity, spectrum and polarization have been studied extensively. However, there have been very few

investigations into the understanding of the statistical properties of the synchrotron source and the emitted radiation. It is clear that since the effects of coherence can be very important in many synchrotron applications (e.g., propagation through optical systems and x-ray holography), the correlation properties of the source must be known.

Mazmanishvili and Uvarov,[24] in 1971, investigated the spatial coherence of the field of synchrotron radiation resulting from a relativistic electron in circular motion. Their analysis was performed in the space-time domain and it considered only a single relativistic electron emitting randomly at two different times. They determined theoretically, that one should be able to observe coherence phenomena, both spatial and temporal, from synchrotron radiation produced by the single electron. Since it is practically impossible to observe the radiation from a single electron, their analysis is of limited utility. In fact, measurable synchrotron radiation results from many accelerated electrons and the energy distribution and the correlations of these electrons are of crucial importance in understanding the coherence of the emitted field.

Benard and Rousseau[25] in 1974 reported an investigation into the statistical properties of synchrotron radiation. They restricted their study to a classical procedure and introduced quantum fluctuations (in the emission of light and in the movement of the electrons) as stochastic quantities. They assumed that the electrons in a given bunch were independent of one another and they neglected the radial and vertical spread of the electron bunch distribution. More importantly, the model neglected the inherent random velocity distribution within the electron bunch.

In their paper, Benard and Rousseau attempted to calculate the second-order spatial coherence of the synchrotron field as a function of frequency. However, they incorrectly computed the spectral amplitude of the field. Their expression for the

spectrum (in the frequency domain) is a function of time and it illustrates how they neglected to integrate fully over the time variable. Relying on their Eq. (44) which is the expression for the spatial coherence as a function of frequency (and time), they concluded that correlations in the field cannot be seen with synchrotron radiation resulting from a bunch of uncorrelated electrons for visible or shorter wavelengths. Experiments were not performed to verify this result.

Korkhmazyan[26] *et. al.* investigated the effects of the electron distribution on the radiation from an electron bunch. Their analysis was performed at the same level of approximation as Mazmanishvili and Uvarov although they allowed for an extended N-electron bunch. They do not derive any statistical properties of the emitted radiation rather they consider the influence on the intensity from electron distributions of different profiles. The main feature of their investigation is that it allows for the calculation of some *intensity distributions* resulting from electron propagation in certain media.

Akmanov[27] *et. al.* furthered the research of Benard and Rousseau and allowed for a radial spread in the relativistic electron bunch. In their scalar approach, the radial spread had the effect of including an additional random phase term in the radiation field. They did not, however, include any insight or detail as to the statistics describing this new phase term. A statistical model for the electron bunch is needed in order to correctly evaluate the spectrum. Their result is left in the form of an integral over time since their main result lacks the necessary statistical model for the bunch dynamics. Unfortunately, additional assumptions must be utilized to obtain a viable result.

In this Chapter, the second-order statistical properties of synchrotron radiation resulting from a three-dimensional relativistic electron bunch (N-electrons) in a storage ring are calculated for the first time. The theory extends previous work to allow the

electrons in a 3-D bunch to have an appropriate distribution of velocities (e.g., variance in the energy of the charges). The new formalism is generated in the space-frequency domain to facilitate experimental demonstrations. In accord with previous attempts, a classical approach is used. For the range of electron energies that are present in storage rings and synchrotrons, this approximation has been justified by many authors.[5,6,31]

In Section 4.2, the spectral amplitude produced by an N-electron bunch in a storage ring is reviewed. This calculation, along with all others in this Chapter, will be valid on a time scale much smaller than the rotation period of the electrons in the ring. The reason for this is that we are interested in the field correlations that are present for one electron bunch and a given observation location.

In Section 4.3, a model for the statistical behavior of the N-electron bunch and its associated classical field will be investigated. Using a Gaussian distribution for the spatial characteristics of the bunch and a Gaussian velocity distribution, the mean value of the field and the second-order coherence are calculated.

For this analysis, it is assumed that the electrons in the ring are independent of one another. Although this assumption has been justified in the literature for the case of synchrotrons and storage rings, electron correlations are present and will play an important role in understanding the field correlations in systems that use wigglers and undulators. The present research will generate a framework that will permit future work on systems that utilize wigglers and undulators (e.g., the free-electron laser).

4.2 Spectral Amplitude Generated by N Electrons in a Storage Ring

In this Section, the electrodynamics of a group of single point charges subject to relativistic uniform circular motion is reported. The derivation begins with the calculation of the radiated field for a single relativistic electron. The result for the field of a single electron is well known [see Jackson, Ref. 8] and is presented here to introduce the formalism. The framework for all of the calculations is this Chapter is given in the space-frequency domain. It is important to remember that the frequencies that are of interest to us are those appropriately transformed to the observers frame.

4.2.1 Classical Treatment for the Field of a Single Relativistic Electron

The electromagnetic field generated by a circulating, relativistic electron is calculated using the Lienard-Wiechert potentials. To obtain these potentials and to illustrate the notation, consider Fig. 4.2.1. An element of charge is located at a distance $\mathbf{r}'$ from the origin and at a distance $\mathbf{r}-\mathbf{r}'$ from an observation point, P. In the Lorentz gauge and using Gaussian units throughout, the wave equations describing the scalar and vector potentials are given by

$$\nabla^2\Phi - \frac{1}{c^2}\ddot{\Phi} = -4\pi\rho \quad , \tag{4.2.1}$$

$$\nabla^2\mathbf{A} - \frac{1}{c^2}\ddot{\mathbf{A}} = \frac{-4\pi}{c}\mathbf{J} \quad , \tag{4.2.2}$$

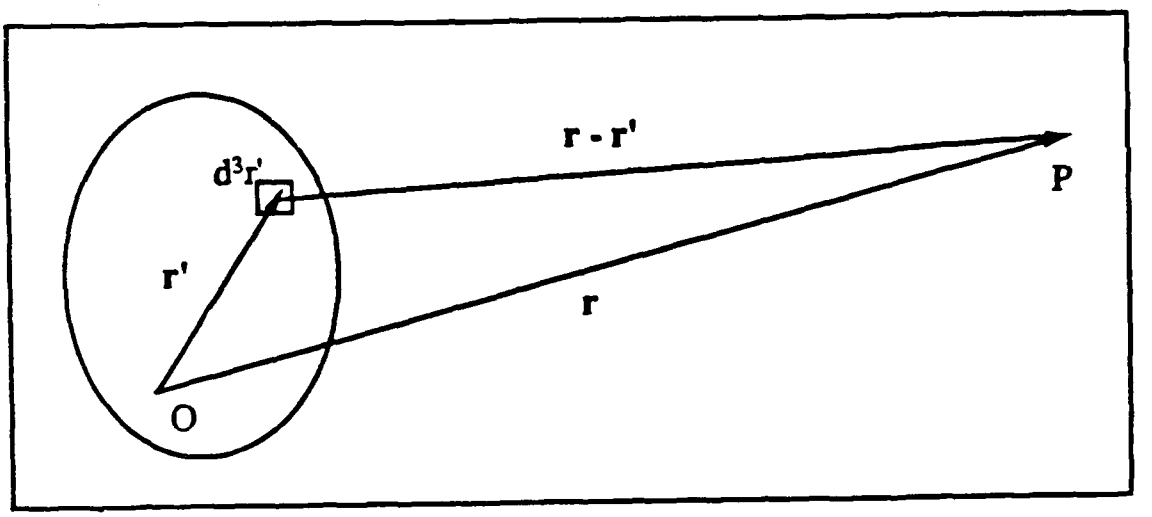

Fig. 4.2.1 Illustrating the notation. The element of volume within the source domain, d^3r', is located a distance r' from the origin and a distance r-r' from the observation point, P.

where $\rho=\rho(\mathbf{r},t)$ and $\mathbf{J}=\mathbf{J}(\mathbf{r},t)$ represent the free charge density and current density respectively, and for this calculation, c is the speed of light *in vacuo*. These wave equations [Eqs. (4.2.1) and (4.2.2)] are solved using the retarded Green's function for outgoing waves to give

$$\Phi(\mathbf{r},t) = \int \frac{\rho(\mathbf{r}',t')}{|\mathbf{r}-\mathbf{r}'|}\,\delta\left(t'-t+\frac{|\mathbf{r}-\mathbf{r}'|}{c}\right) d^3r'dt' \quad , \tag{4.2.3}$$

$$\mathbf{A}(\mathbf{r},t) = \frac{1}{c}\int \frac{\mathbf{J}(\mathbf{r}',t')}{|\mathbf{r}-\mathbf{r}'|}\,\delta\left(t'-t+\frac{|\mathbf{r}-\mathbf{r}'|}{c}\right) d^3r'dt' \quad . \tag{4.2.4}$$

At this point, it is convenient to introduce a notation using square brackets. Functions enclosed by square brackets are to be evaluated at the retarded time, t', given by

$$t' = t - \frac{|\mathbf{R}|}{c} \quad , \tag{4.2.5}$$

where

$$|\mathbf{R}| = |\mathbf{r}-\mathbf{r}'| \quad . \tag{4.2.6}$$

Using the square bracket notation, Eqs (4.2.3) and (4.2.4) simplify to

$$\Phi(\mathbf{r},t) = \int \frac{[\rho(\mathbf{r}')]}{|\mathbf{r}-\mathbf{r}'|}\, d^3r' \quad , \tag{4.2.7}$$

$$\mathbf{A}(\mathbf{r},t) = \frac{1}{c}\int \frac{[\mathbf{J}(\mathbf{r}')]}{|\mathbf{r}-\mathbf{r}'|}\, d^3r' \quad . \tag{4.2.8}$$

At this point in the calculation, no assumptions have been made regarding the form of the source distribution. Since our goal is to understand the radiation from a

bunch of independent electrons, we now consider a free charge, e (a point particle), in motion in free space with velocity, **u**. Figure 4.2.2 illustrates the geometry of the charge's motion. The charge density for this case is given by

$$\rho(\mathbf{r}') = e\,\delta^3(\mathbf{r}' - \mathbf{r}_e) \quad , \tag{4.2.9}$$

where δ^3 is the three-dimensional Dirac delta function and $\mathbf{r}_e$ locates the charge at the retarded time. Also, note that the current density in this case is given by $\mathbf{J} = \mathbf{u}\rho$. Substitution of Eq. (4.2.9) into Eq. (4.2.7) gives, after some manipulation,

$$\Phi(\mathbf{r},t) = \frac{e}{[|\mathbf{R}| - \beta \bullet \mathbf{R}]} \quad , \tag{4.2.10}$$

where $\beta = \mathbf{u}/c$ represents the normalized velocity vector and the brackets again imply evaluation at the retarded time. Similarly, the expression for the current density becomes

$$\mathbf{A}(\mathbf{r},t) = \frac{e\,[\beta]}{[|\mathbf{R}| - \beta \bullet \mathbf{R}]} \quad . \tag{4.2.11}$$

Equations (4.2.10) and (4.2.11) are written in a more compact form as follows:

$$\Phi(\mathbf{r},t) = \frac{e}{[K]} \quad , \tag{4.2.12}$$

$$\mathbf{A}(\mathbf{r},t) = e\left[\frac{\beta}{K}\right] \quad , \tag{4.2.13}$$

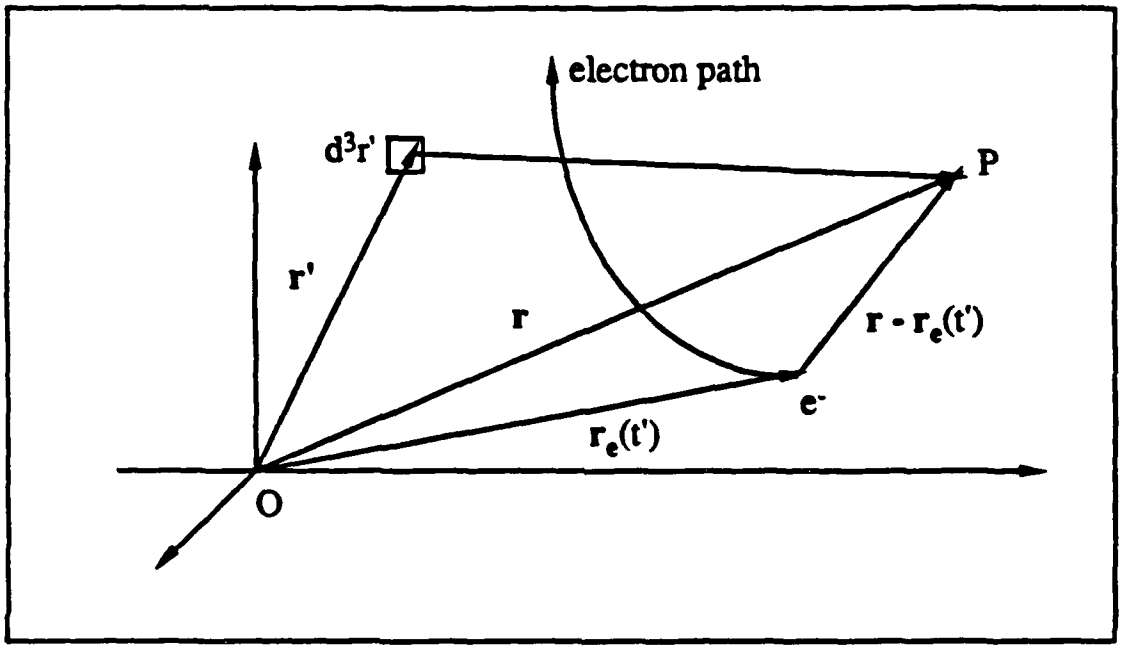

Fig. 4.2.2 Illustrating the electron motion. The electron is located at a distance $r_e(t')$ from the origin and a distance $r-r_e(t')$ from the observation point, P.

where

$$K = |R| - \beta \bullet R \quad . \tag{4.2.14}$$

Equations (4.2.12) and (4.2.13) are known as the Lienard-Wiechert potentials. Again, most importantly, the brackets indicate that the functions are to be evaluated at the retarded time, t'. The fields, $\mathbf{E}(\mathbf{r},t)$ and $\mathbf{B}(\mathbf{r},t)$, associated with the motion of the charged particle are now calculated using the following (Lorentz gauge):

$$\mathbf{E} = -(\nabla\Phi + \frac{1}{c}\dot{\mathbf{A}}) \quad , \tag{4.2.15}$$

$$\mathbf{B} = \nabla \otimes \mathbf{A} \quad . \tag{4.2.16}$$

The calculation of the fields **E** and **B** from Eqs. (4.2.12)-(4.2.16) is somewhat lengthy and is very well known so only the results will be stated. The electromagnetic field for a charged (point) particle in motion is given by

$$\mathbf{E}(\mathbf{r},t) = \left[\frac{e}{K^3}(\mathbf{R}-|\mathbf{R}|\beta)(1-\beta^2)+\frac{e}{cK^3}(\mathbf{R}\bullet\dot{\beta})(\mathbf{R}-|\mathbf{R}|\beta)-\frac{e}{cK^2}|\mathbf{R}|\dot{\beta}\right] \quad , \tag{4.2.17}$$

$$\mathbf{B}(\mathbf{r},t) = \left[\frac{e}{K^3}(\beta\otimes\mathbf{R})(1-\beta^2)+\frac{e}{cK^3}(\mathbf{R}\bullet\dot{\beta})(\beta\otimes\mathbf{R})+\frac{e}{cK^2}\dot{\beta}\otimes\mathbf{R}\right] \quad . \tag{4.2.18}$$

Since all quantities are to be evaluated at the retarded time, the square brackets will now be suppressed. The fields each consist of two distinct components. One component is due to the velocity of the particle and the other is due to its acceleration. It is easily

shown that the velocity components cause no net radiated energy. Therefore, in the following, only the contributions that result because of the acceleration will be considered. The electromagnetic field can be rewritten as

$$\mathbf{E}(\mathbf{r},t) = \mathbf{E}_a(\mathbf{r},t) \quad , \tag{4.2.19}$$

$$\mathbf{B}(\mathbf{r},t) = \mathbf{B}_a(\mathbf{r},t) \quad , \tag{4.2.20}$$

where

$$\mathbf{E}_a(\mathbf{r},t) = \left[\frac{e}{cK^3}(\mathbf{R}\bullet\dot{\beta})(\mathbf{R}-|\mathbf{R}|\beta) - \frac{e}{cK^2}|\mathbf{R}|\dot{\beta}\right] \quad , \tag{4.2.21}$$

$$\mathbf{B}_a(\mathbf{r},t) = \left[\frac{e}{cK^3}(\mathbf{R}\bullet\dot{\beta})(\beta\otimes\mathbf{R}) + \frac{e}{cK^2}\dot{\beta}\otimes\mathbf{R}\right] \quad . \tag{4.2.22}$$

An interesting property of the acceleration fields is that $\mathbf{E}_a(\mathbf{r},t)$ and $\mathbf{B}_a(\mathbf{r},t)$ are orthogonal, i.e.,

$$\mathbf{E}_a(\mathbf{r},t) \bullet \mathbf{B}_a(\mathbf{r},t) = 0 \quad . \tag{4.2.23}$$

Poynting's vector, which represents an energy flow per unit area per unit time is defined, for the present discussion, as

$$\mathbf{S}_a = \frac{c}{4\pi}\,\mathbf{E}_a \otimes \mathbf{B}_a \quad . \tag{4.2.24}$$

Using Eqs. (4.2.21) and (4.2.22), Poynting's vector is computed to give

$$\mathbf{S_a} = \left(\frac{e^2}{4\pi c K^6}\right)\left[\mathbf{R}\left\{|\mathbf{R}||\dot{\beta}|^2 K^2 + 2|\mathbf{R}|(\dot{\beta}\bullet\beta)(\dot{\beta}\bullet\mathbf{R})K - |\mathbf{R}|(1-|\beta|^2)(\dot{\beta}\bullet\mathbf{R})^2\right\}\right] . \quad (4.2.25)$$

Equation (4.2.25) is a quite general representation of the radiated energy for an accelerated electron. It is interesting to examine the radiation pattern of the accelerated electron under certain different conditions.

It is easily determined from Eq. (4.2.25) that if the charge is in uniform motion (i.e., the acceleration is zero and obviously the velocity is constant) that no net energy is radiated. For the case when the charge is accelerated at low velocities, the classic Larmor formula for the radiated power results. Figure 4.2.3 illustrates the case of colinear acceleration and velocity for three different velocities. For the case of low velocities [Fig. 4.2.3a, $\beta=3.33\times10^{-5}$], the Larmor formula holds and the familiar dipole pattern results in the far zone. As the velocity of the particle increases [Figs. 4.2.3b and 4.2.3c, $\beta=0.66$ and $=0.934$], the radiation pattern becomes modified with most of the energy radiated in the direction of motion. Figure 4.2.4 illustrates the case of uniform circular motion for three different velocities. Again, as the velocity increases, the radiation pattern becomes concentrated in the forward direction. Synchrotron radiation results from electrons accelerated to extremely relativistic velocities in uniform circular motion. The radiation pattern illustrated in Fig. 4.2.4c is characteristic of synchrotron radiation produced by synchrotrons and storage rings.

Using Eqs. (4.2.21)-(4.2.24), Eq. (4.2.25) can be written as

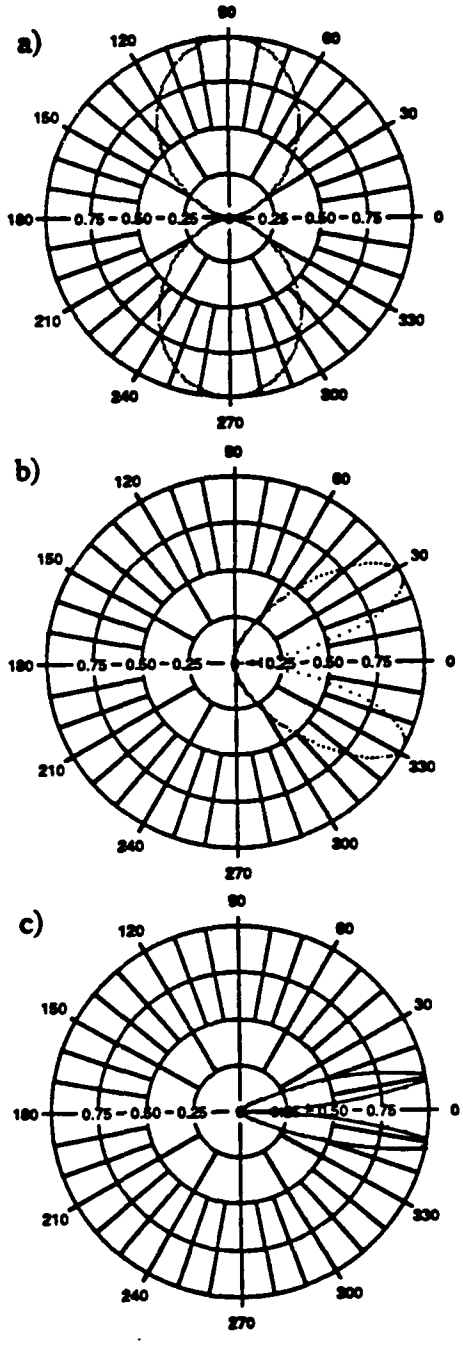

$\beta = 3.33 \times 10^{-5}$

$\beta = 0.66$

$\beta = 0.934$

Fig. 4.2.3 Radiation patterns associated with an accelerated electron: colinear acceleration and velocity. For relatively low velocities, a) illustrates the validity of the Larmor formula. In b) and c), as the velocity increases, most of the energy is radiated in the forward direction.

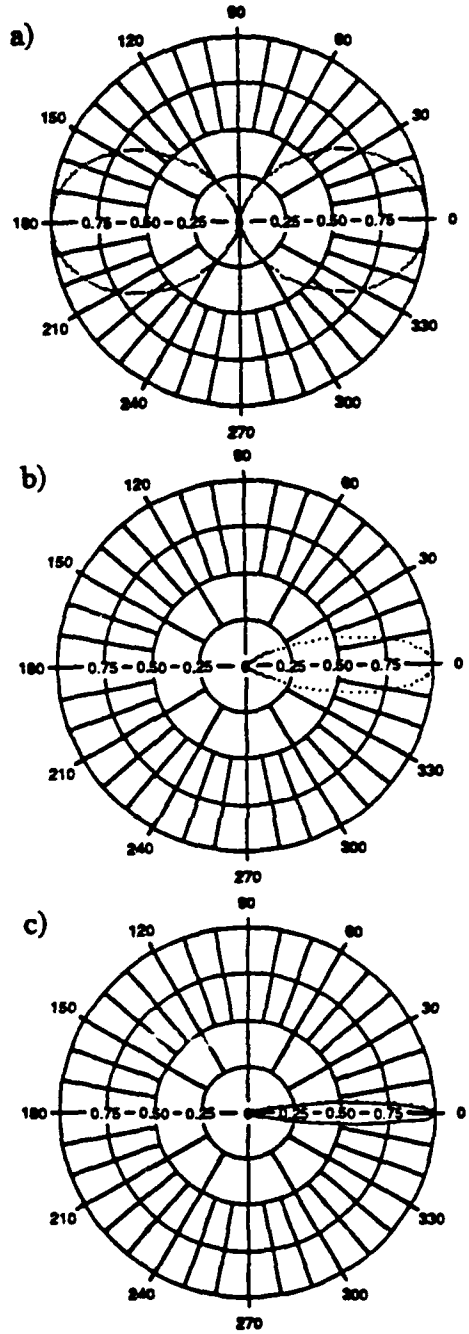

$\beta = 3.33 \times 10^{-5}$

$\beta = 0.66$

$\beta = 0.934$

Fig. 4.2.4 Radiation patterns associated with an accelerated electron: uniform circular motion. Note in b) and c) that the radiation is again concentrated in the forward direction as the velocity increases.

$$\mathbf{S_a} = \frac{c}{4\pi} |\mathbf{E_a}|^2 \mathbf{n} \quad , \tag{4.2.26}$$

where $\mathbf{n}=\mathbf{R}/|\mathbf{R}|$, is the unit vector pointing in the direction of the observation point. Now, using the energy radiated per unit solid angle and Parseval's theorem,

$$\int_{-\infty}^{\infty} \left(\frac{c}{4\pi} |\mathbf{E_a}|^2 |\mathbf{R}|^2 \right) dt = \int_{-\infty}^{\infty} |U(\nu)|^2 \, d\nu \quad , \tag{4.2.27}$$

the spectral amplitude of the radiated field is given by

$$\mathbf{U}(\nu) = \left(\frac{c}{4\pi}\right)^{1/2} \int_{-\infty}^{\infty} \left[|\mathbf{R}| \, \mathbf{E_a} \right] \exp(i2\pi\nu t) \, dt \quad , \tag{4.2.28}$$

where ν denotes the spectral frequency. Note that the Fourier transformation exists since the acceleration occurs effectively for a finite time which gives rise to finite radiated energy.

Substitution of Eq. (4.2.21) into Eq. (4.2.28) gives

$$\mathbf{U}(\nu) = \left(\frac{e^2}{4\pi c}\right)^{1/2} \int_{-\infty}^{\infty} \left[\frac{\mathbf{n} \otimes \{(\mathbf{n} - \boldsymbol{\beta}) \otimes \dot{\boldsymbol{\beta}}\}}{(1 - \boldsymbol{\beta} \bullet \mathbf{n})^3} \right] \exp(i2\pi\nu t) \, dt \quad , \tag{4.2.29}$$

where the function in square brackets is evaluated at the retarded time to give

$$U(\nu) = \left(\frac{e^2}{4\pi c}\right)^{1/2} \int_{-\infty}^{\infty} \frac{\mathbf{n} \otimes \{(\mathbf{n} - \boldsymbol{\beta}) \otimes \dot{\boldsymbol{\beta}}\}}{(1 - \boldsymbol{\beta} \bullet \mathbf{n})^2} \exp[i2\pi\nu(t + |\mathbf{R}|/c)]\, dt \quad . \quad (4.2.30)$$

Equation (4.2.30) represents the spectral amplitude in the observers frequencies for a single deterministic electron undergoing uniform circular motion at relativistic velocities.

4.2.2 Generalization to N Electrons

Given the results of the previous calculation, it is now possible to describe the spectral amplitude produced by a bunch of N circulating electrons. The field at the observation point can be written as a sum of the fields contributed by each electron and is given by

$$U(\nu) = \sum_{j=1}^{N} {}^{j}U(\nu) \quad . \quad (4.2.31)$$

Substituting Eq. (4.2.30) into Eq. (4.2.31) gives

$$U(\nu) = \left(\frac{e^2}{4\pi c}\right)^{1/2} \sum_{j=1}^{N} \int_{-\infty}^{\infty} {}^{j}f(t) \exp[i2\pi\nu(t + |{}^{j}\mathbf{R}|/c)]\, dt \quad , \quad (4.2.32)$$

where

$$ {}^{j}\mathbf{f}(t) = \frac{{}^{j}\mathbf{n} \otimes \{ ({}^{j}\mathbf{n} - {}^{j}\boldsymbol{\beta}) \otimes {}^{j}\dot{\boldsymbol{\beta}} \}}{(1 - {}^{j}\boldsymbol{\beta} \bullet {}^{j}\mathbf{n})^2} \quad . \tag{4.2.33} $$

The superscript, j, identifies one particular electron in the total population, N. It is now assumed that the observation point is far away from the region of space where the acceleration takes place; the unit vector $\mathbf{n}$, is sensibly constant in time. Also, it is assumed that over the short time τ, the form factor given by Eq. (4.2.33) is slowly varying and the approximation

$$ {}^{j}\mathbf{f}(t) = {}^{1}\mathbf{f}(t) \quad , \tag{4.2.34} $$

is justified.[25] For this calculation, the effects resulting from fluctuations of the slowly varying form factor are not investigated. The fluctuations in the phase term will have the larger effect and the consequences of these fluctuations will be studied. The factor $\exp[i2\pi\nu|\mathbf{R}|/c]$ oscillates rapidly over the domain of integration while the form factor is slowly varying. Exchanging the orders of summation and integration in Eq. (4.2.32) gives

$$ \mathbf{U}(\nu) = \left(\frac{e^2}{4\pi c}\right)^{1/2} \int_{-\infty}^{\infty} {}^{1}\mathbf{f}(t) \exp[i2\pi\nu t] \sum_{j=1}^{N} \exp[i2\pi\nu\, {}^{j}|\mathbf{R}|/c]\, dt \quad . \tag{4.2.35} $$

Equation (4.2.35) represents, to within the present level of approximation, the spectral amplitude generated by an N-electron bunch.

4.3 Statistics of the N-Electron Field

The central orbit of a storage ring is that orbit which will be repetitively traced by a particle of design energy launched precisely on that orbit. In order to ensure that particles will remain indefinitely in the neighborhood of the central orbit when subjected to disturbances and imperfections, strong restoring forces are applied. The circulating beam in the storage ring is preserved by continuously restoring energy lost to synchrotron radiation with radio frequency power. The rf field focuses the beam and thus causes the electrons to travel in bunches. A storage ring can contain any number of electron bunches from one to a maximum number defined by the ratio of ring circulation period to the period of the accelerating rf field. The bunch length is set primarily by the frequency of the accelerating field.

In any real storage ring there will be imperfections (small perturbations from photon emission and nonuniformities in the confinement fields) and the electrons will oscillate about the central orbit. These oscillations cause a statistical spread in the position and velocity of the electrons in the bunch. The effects of randomness in the electron dynamics on the emitted field are investigated in this Section using an appropriate model for the bunch profile and velocity distribution. The mean value and second-order correlation function of the field are calculated and analyzed in the space-frequency domain.

4.3.1 Density Function for Electron Distances

As explained above, the electrons travel around the ring in bunches as a consequence of the radio frequency amplifier in the chamber. A typical bunch consists of 10^8 to 10^{12} electrons and is 0.1-10 cm in length. The distribution of the electrons in the bunch is a function of the storage ring design and the intensity of the rf field and, in the case of synchrotrons, the circumferential position. The electron distribution also depends on the effects due to photon emission. Experiment shows that the density distribution of the electrons in bunches produced by ordinary methods can be approximated by a Gaussian distribution at moderate bunch currents.[25] For these studies, a Gaussian electron-bunch distribution will be assumed. It is important to note that other distributions are possible and can give rise to modifications in the far zone intensity.[26]

An illustration of the storage ring geometry[32] and the notation is shown in Fig. 4.3.1. The probability density function of the electron bunch is represented by

$$p(x,y,z;t) = \frac{1}{(2\pi)^{3/2}\sigma_x\sigma_y\sigma_z}\exp\left[-\left\{\frac{(x-\bar{x})^2}{2\sigma_x^2}+\frac{(y-\bar{y})^2}{2\sigma_y^2}+\frac{(z-\bar{z})^2}{2\sigma_z^2}\right\}\right], \qquad (4.3.1)$$

where the barred quantities locate, at the time t, the mean electron position and $\sigma_x,\sigma_y,\sigma_z$ represent the variance in the electron position. The means and variances are definite functions of time; they evolve in a deterministic manner. For the present calculation, a term describing electron correlations has been purposely omitted in Eq.

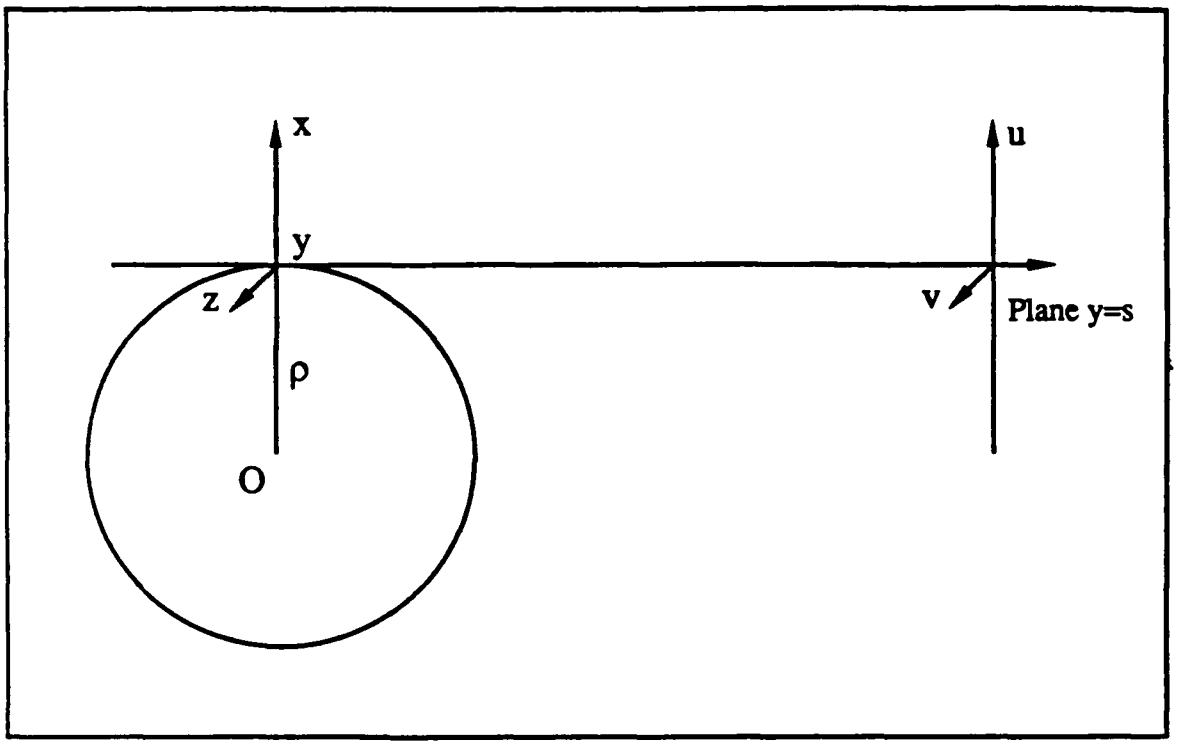

Fig. 4.3.1 An illustration of the notation and geometry for the computation of the electron distances.

(4.3.1). It is assumed that the electrons are independent of one another. This assumption has been justified in the literature for electron densities and energies found in typical storage rings and synchrotrons.[5]

It is clear that from Eq. (4.2.35) that to investigate the fluctuations in the spectral amplitude, the statistics of $|\mathbf{R}(t)|$ are needed. This implies that the electron statistics must be appropriately transformed to obtain the statistics in $|\mathbf{R}(t)|$. It is important to note that the distribution of $|\mathbf{R}(t)|$ is strictly *not* Gaussian. The functional form of the distribution is certainly dependent on the vectorial distance to the observation region. So that the calculation remains general, no assumption is made about the observation point and the density function of $|\mathbf{R}(t)|$ is computed from the density of electrons in the bunch.

The distance from any given electron in the bunch to the observation point is given by

$$|\mathbf{R}(t)| = \left[(u-x)^2 + (s-y)^2 + (v-z)^2\right]^{1/2} \quad . \tag{4.3.2}$$

Now we let $\alpha=(u-x)$, $\delta=(s-y)$, $\gamma=(v-z)$. Substituting these new variables in Eq. (4.3.1) gives

$$p(\alpha,\delta,\gamma) = \frac{1}{(2\pi)^{3/2}\sigma_x\sigma_y\sigma_z}\exp\left[-\left\{\frac{(u-\alpha-\bar{x})^2}{2\sigma_x^2} + \frac{(s-\delta-\bar{y})^2}{2\sigma_y^2} + \frac{(v-\gamma-\bar{z})^2}{2\sigma_z^2}\right\}\right] \quad , \tag{4.3.3}$$

where the Jacobian for this change of variables is unity. Using spherical coordinates, $\alpha=|\mathbf{R}(t)|\sin\phi\cos\theta$, $\delta=|\mathbf{R}(t)|\sin\phi\sin\theta$, $\gamma=|\mathbf{R}(t)|\cos\phi$ and $|\mathbf{R}(t)|=[\alpha^2+\delta^2+\gamma^2]^{1/2}$. The Jacobian, for this change of variables, is well known and is given by

$$\|J\| = |R|^2 \sin\phi \quad , \qquad 0 \le \phi \le \pi \quad . \tag{4.3.4}$$

Substitution of Eq. (4.3.4) in Eq. (4.3.3) gives the following:

$$p(|R|,\theta,\phi) = \frac{|R|^2 \sin\phi}{(2\pi)^{3/2}\sigma_x\sigma_y\sigma_z} \exp\left[-\left\{\frac{(a-|R|\sin\phi\cos\theta)^2}{2\sigma_x^2} + \frac{(b-|R|\sin\phi\sin\theta)^2}{2\sigma_y^2} + \frac{(c-|R|\cos\phi)^2}{2\sigma_z^2}\right\}\right] , \tag{4.3.5}$$

in which

$$a = (u - \bar{x}) \quad , \tag{4.3.6}$$

$$b = (s - \bar{y}) \quad , \tag{4.3.7}$$

$$c = (v - \bar{z}) \quad . \tag{4.3.8}$$

The probability density function of the electron distances is obtained by integrating Eq. (4.3.5) over all of the possible combinations of the variables θ and ϕ. This marginal density function is needed in order to compute the mean and higher-order moments of the spectral amplitude [see Eq. (4.2.35)]. Unfortunately, a general analytic solution for the marginal density (integrating the variables θ and ϕ) of Eq. (4.3.5) does not exist.

It is possible, however, to calculate in closed form, the density function for a special case and to compute the integral numerically for other cases to investigate the mathematical form of the density function for the electron distances. The following is a calculation of the electron-distance density function for a specific electron bunch distribution and specific observation region. The result will then be verified and

extended numerically in order to quantitatively describe the density function for other cases.

A particularly interesting special case is chosen at this point so that a closed form solution for the electron-distance density function is possible. First, assume that the variances of the bunch (σ_x,σ_y,σ_z) in all three dimensions are the same (note that experiments have shown that this is strictly *not* true in practice; $\sigma_x > \sigma_z$ and $\sigma_x \approx \sigma_y$,) and equal to σ. Substituting this assumption into Eq. (4.3.5) gives

$$p(|R|,\theta,\phi) = \frac{|R|^2 \sin\phi}{(2\pi)^{3/2}\sigma^3} \exp\left[-\left\{\frac{|R|^2 + a^2 + b^2 + c^2}{2\sigma^2} - \frac{|R| \sin\phi\,(a\cos\theta + b\sin\theta)}{\sigma^2} - \frac{|R|\, c\cos\phi}{\sigma^2}\right\}\right] \quad . \tag{4.3.9}$$

Recall that the integral that we are trying to compute is given by

$$p(|R|) = \int_0^{\pi}\int_0^{2\pi} (p(|R|,\theta,\phi)\, d\theta\, d\phi \quad . \tag{4.3.10}$$

Using Eq. (4.3.9) and Eq. (4.3.10), we can now perform the integration over the variable, θ. The two-dimensional marginal density is now given by

$$p(|R|,\phi) = \int_0^{2\pi} m \sin\phi \exp\left[\frac{|R|}{\sigma^2}\left\{\sin\phi\,(a\cos\theta + b\sin\theta) + c\cos\phi\right\}\right] d\theta \quad , \tag{4.3.11}$$

in which

$$m = \frac{|R|^2}{(2\pi)^{3/2}\sigma^3}\exp\left[-\frac{(|R|^2+a^2+b^2+c^2)}{2\sigma^2}\right] \quad . \qquad (4.3.12)$$

Further simplification of Eq. (4.3.11) gives

$$p(|R|,\phi) = m'\int_0^{2\pi}\exp\left[\xi(a\cos\theta + b\sin\theta)\right]d\theta \quad , \qquad (4.3.13)$$

where

$$\xi = \frac{|R|\sin\phi}{\sigma^2} \quad , \qquad (4.3.14)$$

and

$$m' = m\sin\phi\exp\left[\frac{|R|\,c\cos\phi}{\sigma^2}\right] \quad . \qquad (4.3.15)$$

The integral in Eq. (4.3.13) can be computed using the similar integral 3.937.2 in Reference 33. Performing the integration over θ, Eq. (4.3.13) reduces to

$$p(|R|) = 2\pi m\int_0^{\pi}\sin\phi\exp\left[\frac{|R|\,c\cos\phi}{\sigma^2}\right] I_0\left\{\frac{|R|}{\sigma^2}\sin\phi\sqrt{a^2+b^2}\right\}d\phi \quad , \qquad (4.3.16)$$

where I_0 is the modified Bessel function of the first kind and of order zero. The following relationship exists between the ordinary Bessel function and the modified Bessel function:

$$I_n(x) = (-1)^n J_n(ix) \quad . \tag{4.3.17}$$

Substituting Eq. (4.3.17) into Eq. (4.3.16) gives

$$p(|R|) = 2\pi m \int_0^{\pi} \sin\phi \exp\left[\frac{|R|\, c \cos\phi}{\sigma^2}\right] J_0\left\{\frac{i|R|}{\sigma^2}\sin\phi \sqrt{a^2 + b^2}\right\} d\phi \quad . \tag{4.3.18}$$

Unfortunately, the integral in Eq. (4.3.18) has no closed form solution. However, an attempt was made to approximate the integral in Eq. (4.3.18) using the series expansion for $\exp[\zeta\cos\phi]$ and integrating term by term. After a lengthy calculation, it was shown that the integrand vanishes exactly for odd terms in $\cos\phi$. In fact, for the case of storage ring-generated synchrotron radiation, the range of values of ϕ that contribute to the density function is extremely *narrow* and centered around $\pi/2$. It was also shown that the contribution to the integral by the first term in the series was by far the largest. We next assume for the present case that c is small; the result will be strictly valid for near axis points. For the special case at hand and with reference to Eq. (4.3.18), we assume that the density can be approximated by

$$p(|R|) = 2\pi m \int_0^{\pi} \sin\phi\, J_0\left\{\frac{i|R|}{\sigma^2}\sin\phi \sqrt{a^2 + b^2}\right\} d\phi \quad . \tag{4.3.19}$$

The resulting integral in Eq. (4.3.19) has the form of integral 6.681.8 in Reference 33. After a lengthy mathematical manipulation [see Appendix B], the density function for electron distances within our level of approximation becomes

$$p(|\mathbf{R}|) = \frac{|\mathbf{R}|}{\sqrt{(2\pi)(a^2+b^2)}\sigma} \exp\left[\frac{-(|\mathbf{R}|-\sqrt{a^2+b^2})^2}{2\sigma^2}\right] \quad . \qquad (4.3.20)$$

Note that $(a^2+b^2)^{1/2}$ is proportional to the mean value of the electron distance, $|^1\mathbf{R}|$.

Using typical parameters, curves of the density function represented by Eq. (4.3.20) are shown in Fig. 4.3.2. The axial distance to the observation plane is taken to be one meter and σ is chosen to be 1 mm. Fig. 4.3.2 shows how the profile remains constant as the observation point is moved out into the field.

In order to confirm the steps used in simplifying the calculation to arrive at Eq. (4.3.20), the integral in Eq. (4.3.10) was computed numerically using a customized Gaussian quadrature method. The parameter set used in the numerical calculations were the same as that used in the calculation leading to Eq. (4.3.20). Figure 4.3.3 illustrates the error associated with using the simplified form given by Eq. (4.3.20). Figure 4.3.3a illustrates the actual density function resulting from direct numerical integration of Eq. (4.3.10) for an off-axis point. Figure 4.3.3b shows the probability density function that results from application of Eq. (4.3.20) for the same off-axis point. Figure 4.3.3c shows simply the difference of the curves in Fig. 4.3.3a and Fig. 4.3.3b. Note that although there is evidence of a slight shift of the peak the error is quite small. For typical observation distances used in synchrotron radiation experiments, the density function for electron distances is approximately, *but strictly not*, Gaussian.

It is important to recall that in this special case, that the variances in all three dimensions were set equal in computing Eq. (4.3.20). The integral in Eq. (4.3.10) was studied numerically for cases when the variances were not equal. For the parameters present in typical synchrotrons and storage rings and at typical observation

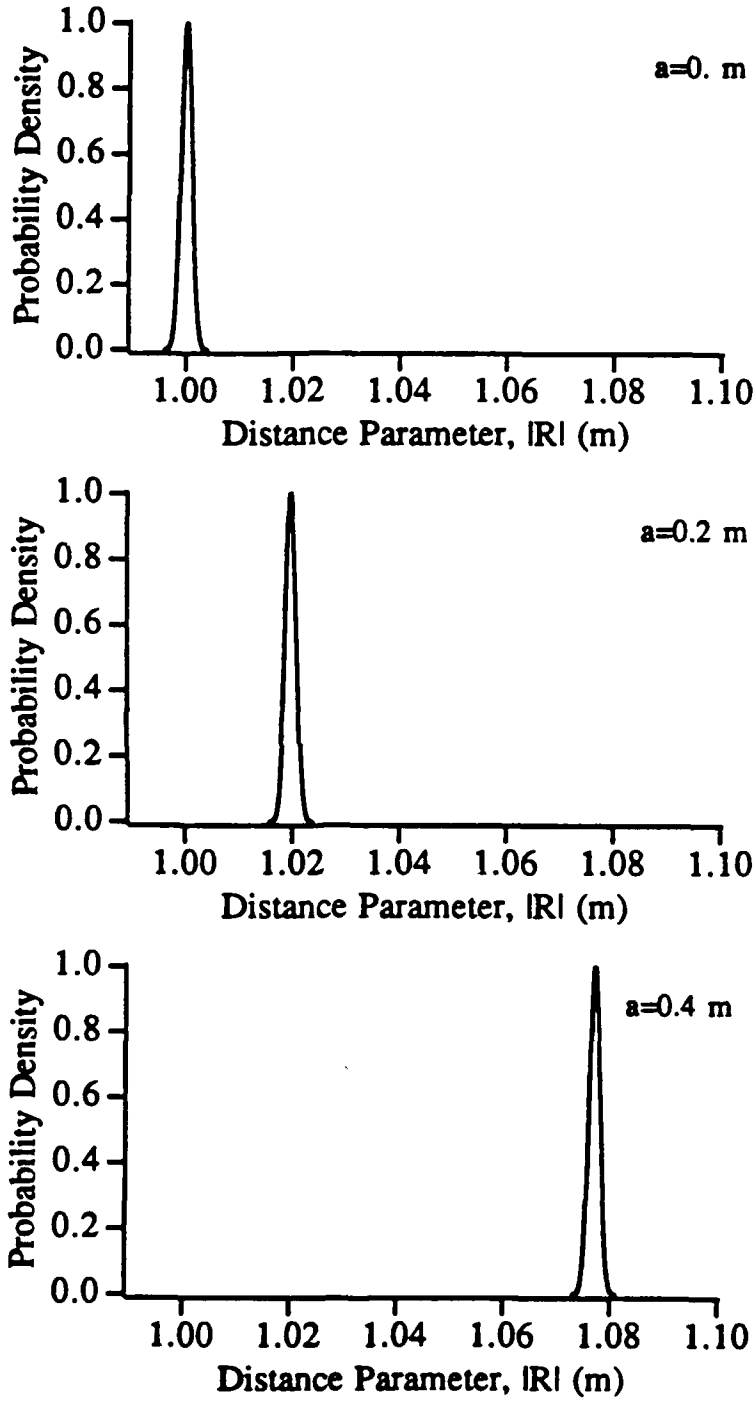

Fig. 4.3.2 The density function for electron distances given by Eq. (4.3.20). The axial distance is taken to be one meter and σ=1mm. The magnitude of the parameter, a, is a measure of the distance from the origin in the observation plane. This figure shows how the profile remains constant as the observation point is moved out into the field.

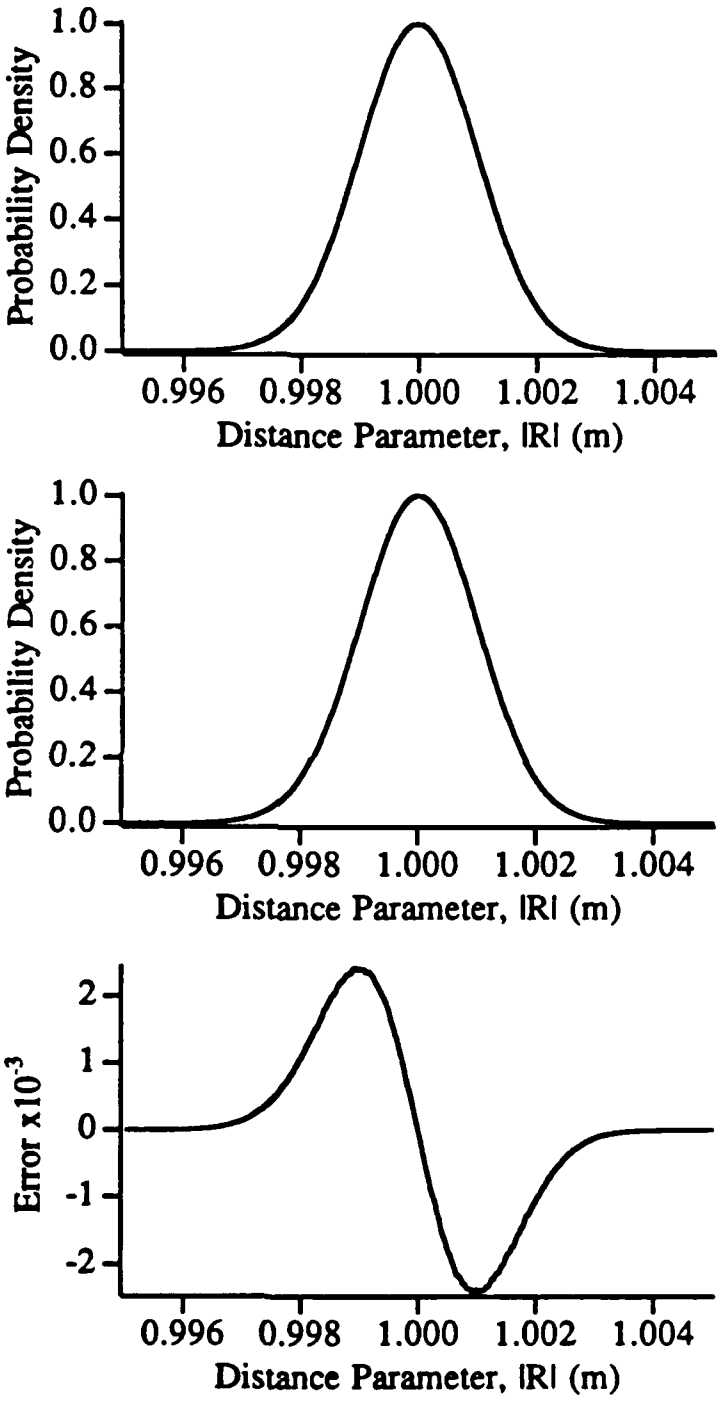

Fig. 4.3.3 Numerical verification of Eq. (4.3.20). Results of numerical integration of Eq. (4.3.10) for an off-axis point are illustrated in a) with the curve generated using Eq. (4.3.20) shown in b). The difference between the two curves is illustrated in c).

distances, the density function for electron distances remained approximately Gaussian. The result of this rather lengthy calculation provides confidence to know under what circumstances when to assume that the density function for electron distances approaches a Gaussian function. Cases of practical interest may exist where full integration of Eq. (4.3.10) is required.

Using the results of the previous calculation, we will assume that the conditions are satisfied to allow us to represent the density function for electron distances by

$$p(|\mathbf{R}|) = \frac{1}{\sqrt{2\pi}\,\sigma} \exp\left[\frac{-(|\mathbf{R}| - |{}^{1}\mathbf{R}|)^2}{2\sigma^2}\right] \quad . \qquad (4.3.21)$$

Equation (4.3.21) will be used in the computation of the mean and second-order coherence of the synchrotron field.

4.3.2 Mean Value of the Field

Since only the fluctuations in the electron-distance parameter are of interest here [see Eq. (4.2.35)], finding the mean value of the synchrotron field includes calculating the characteristic function of the electron distance random process. Using Eq. (4.2.35), the mean value of the N-electron field is given by

$$< \mathbf{U}(\nu) > \; = \; \left(\frac{e^2}{4\pi c}\right)^{1/2} \int_{-\infty}^{\infty} {}^{1}f(t) \exp[i2\pi\nu t] < \sum_{j=1}^{N} \exp[i2\pi\nu\, {}^{j}\mathbf{R}|/c] > dt \quad . \qquad (4.3.22)$$

In order to determine the mean, the characteristic function of the process **R** must be evaluated. Recall that the electrons are assumed to be uncorrelated with respect to

one another. Exchanging the order of summation and the averaging procedure and using the results of the previous discussion in Section 4.3.1, the characteristic function of the electron distances is given by[34]

$$< \exp[ik|\mathbf{R}|] > \;=\; \exp\Big[ik\,|^1\mathbf{R}| \;-\frac{k^2\sigma^2}{2}\Big] \quad . \tag{4.3.23}$$

Using Eq. (4.3.23), the mean value of the field given by Eq. (4.3.22), can be simplified to give

$$< \mathbf{U}(\nu) > \;=\; N\,{}^1\mathbf{U}(\nu)\,\exp[-\frac{k^2\sigma^2}{2}] \quad , \tag{4.3.24}$$

where, as before, N is the total number of electrons in the bunch and ${}^1\mathbf{U}(\nu)$ is the spectral amplitude produced by the nominal electron. Note that for infrared and higher frequencies (large k) the mean value tends towards zero very rapidly.

4.3.3 Correlations in the Space-Frequency Domain

In this section, the second-order correlation in the field is calculated based on a statistical model for the electron dynamics. The calculation is performed in terms of the observer's frequencies. Recall that the relationship for the spectral amplitude of the synchrotron field is given by

$$\mathbf{U}(\nu) \;=\; \Big(\frac{e^2}{4\pi c}\Big)^{1/2} \int_{-\infty}^{\infty} {}^1\mathbf{f}(t)\,\exp[i2\pi\nu t] \sum_{j=1}^{N} \exp[i2\pi\nu\,|^j\mathbf{R}|/c]\,dt \quad . \tag{4.3.25}$$

The object of the present calculation is to compute the second-order coherence function given by

$$< U_1(\nu)\, U_2^*(\nu) > \;=\; \left(\frac{e^2}{4\pi c}\right) \int_{-\infty}^{\infty} \int_{-\infty}^{\infty} {}^1f_1(t)\, {}^1f_2(t') \exp[i\omega(t-t')]$$

$$< \sum_{j=1}^{N} \exp[ik\, |{}^jR_1(t)|] \sum_{l=1}^{N} \exp[-ik\, |{}^lR_2'(t')|] > dt\, dt' \quad . \qquad (4.3.26)$$

Equation (4.3.26) is general in that it is not based on any particular model for electron statistics or electron-bunch profile. Since we have already assumed that the electrons in the bunch are independent, Eq. (4.3.26) can be simplified to give

$$< U_1(\nu)\, U_2^*(\nu) > \;=\; \left(\frac{e^2}{4\pi c}\right) \int_{-\infty}^{\infty} \int_{-\infty}^{\infty} {}^1f_1(t)\, {}^1f_2(t') \exp[i\omega(t-t')]$$

$$\times \quad \{N < \exp[ik\{|{}^jR_1(t)| - |{}^jR_2'(t')|\}] > \; +$$

$$(N^2 - N) < \exp[ik\, |R_1(t)|] >< \exp[-ik\, |R_2'(t')|] > \} dt dt' \quad . \qquad (4.3.27)$$

Using the results of the previous section, we will now restrict our attention to infrared and optical frequencies and assume that the mean value of the field is approximately zero. Note however that for longer wavelengths the mean value must be included in the analysis. Using these approximations, Eq. (4.3.27) can be rewritten as

$$< U_1(\nu)\, U_2^*(\nu) > \;=\; \left(\frac{e^2}{4\pi c}\right) \int_{-\infty}^{\infty} \int_{-\infty}^{\infty} {}^1f_1(t)\, {}^1f_2(t') \exp[i\omega(t-t')]$$

$$\times \quad N < \exp[ik\{|{}^jR_1(t)| - |{}^jR_2'(t')|\}] > \; dt dt' \quad . \qquad (4.3.28)$$

The next step in the calculation is to evaluate the characteristic function of the electron distance difference parameter. The electron bunch profile and a statistical model describing the electron dynamics are now required. We will assume as before that the electron bunch is described by a Gaussian profile [see Eq. (4.3.1)].

The proposed statistical model can be understood using the following assumptions. Let $(|\mathbf{R}_1(t)|,t)$ locate a given charge with respect to a particular observation point at time, t. Let $(|\mathbf{R}_2'(t')|,t')$ locate the same charge with respect to a second observation point at time, t'. We assume that the observer performs his measurements in a plane located at some fixed distance from the storage ring. Since we are only concerned with a single individual electron bunch, assume that $\tau=t'-t$ is small, i.e., $1/\tau$ is large compared to the cavity frequency, and that the form factor represented by Eq. (4.2.33) is slowly varying and obeys the condition in Eq. (4.2.34) for small τ (for a given observation point). It is known experimentally that during the emission time interval, (e.g., $\Delta t=10^{-11}$ s at $\lambda = 0.5$ μm) the mean number of emitted photons is of the order of 0.01; it can be assumed that the electron is unperturbed during the emission time interval. The assumption is equivalent to stating that the electron's velocity is unchanged during times of the order of an emission time. During the short time interval, τ, it is also assumed that the electron motion is nearly rectilinear.

It is clear from Eq. (4.3.28) that the relationship between the distances, $|\mathbf{R}_1(t)|$ and $|\mathbf{R}_2'(t')|$, for the same electron is required. This relationship is calculated using geometrical considerations that relate the source volume coordinates and the observation plane coordinates. Since the observation region is typically in the far zone of the source bunch, the first term in the power series (for all variables including τ) is assumed to correctly describe the electron distance. Using these assumptions along with Fig. 4.3.1, the motion of a given electron can be described by the following model:

$$|^{j}\mathbf{R}_1(t)| - |^{j}\mathbf{R}_2'(t')| \cong {}^{j}V|\tau + \frac{1}{s}[\Delta u(\bar{u} - {}^{j}x) + \Delta v(\bar{v} - {}^{j}z)] \quad . \qquad (4.3.29)$$

The random variable that describes the electron population's velocity is denoted by V. It is assumed that the distribution of velocities is represented by a Gaussian function with a mean value of ${}^{1}V$ and a variance equal to σ_v^2. As stated before, during a time τ, the velocity is assumed to be constant for each electron. Also note that for short times, ${}^{j}x$ and ${}^{j}z$ are independent of time. In Equation (4.3.29),

$$\Delta u = u_1 - u_2 \quad , \quad \Delta v = v_1 - v_2 \quad , \qquad (4.3.30)$$

and

$$\bar{u} = \frac{u_1 + u_2}{2} \quad , \quad \bar{v} = \frac{v_1 + v_2}{2} \quad . \qquad (4.3.31)$$

The first term on the right hand side of Eq. (4.3.29) represents the difference in the electron distance due to motion during a time τ. The second term represents a geometric factor that depends primarily on the observation location.

Equation (4.3.29) is used to characterize the position of a particular electron at a time, t' resulting from a random starting position at time t and undergoing motion with a randomly chosen velocity for a time τ=t'-t. Again, it is assumed that the distribution of the electron velocities does not change (uniform circular motion) during the time interval, τ. It is also assumed that the random variables describing the initial position and velocity are independent.

The characteristic function in Eq. (4.3.28) can now be evaluated. For the Gaussian processes,[34] the following terms result:

$$< \exp\left[ik\{{}^{j}\mathbf{R}_1(t)| - {}^{j}\mathbf{R}_2'(t')|\}\right] > \;=\; \exp\left[ik|{}^{1}\mathbf{V}|\tau \;-\; \frac{k^2\sigma_V^2\tau^2}{2}\right]$$

$$\mathrm{x} \quad \exp\left\{\frac{ik}{s}[\Delta u(\bar{u}\text{-}^{1}x) + \Delta v(\bar{v}\text{-}^{1}z)] \;-\; \frac{k^2\sigma^2}{2s^2}[(\Delta u)^2 + (\Delta v)^2]\right\} \;. \qquad (4.3.32)$$

Substitution of Eqs. (4.3.32) into Eq. (4.3.28) gives

$$< \mathbf{U}_1(\nu)\,\mathbf{U}_2^{*}(\nu) > \;=\; \mathrm{N}\left(\frac{e^2}{4\pi c}\right)\int_{-\infty}^{\infty}\int_{-\infty}^{\infty} {}^{1}\mathbf{f}_1(t)\,{}^{1}\mathbf{f}_2(t')\exp[i\omega(t-t')]$$

$$\mathrm{x} \quad \exp\left[ik|{}^{1}\mathbf{V}|\tau \;-\; \frac{k^2\sigma_V^2\tau^2}{2}\right]$$

$$\mathrm{x} \quad \exp\left\{\frac{ik}{s}[\Delta u(\bar{u}\text{-}^{1}x) + \Delta v(\bar{v}\text{-}^{1}z)] \;-\; \frac{k^2\sigma^2}{2s^2}[(\Delta u)^2 + (\Delta v)^2]\right\} dtdt' \;. \qquad (4.3.33)$$

At this point it is useful to introduce the following change of variables in the time domain:

$$\tau \;=\; t' - t \qquad , \qquad (4.3.34)$$

$$\bar{t} \;=\; \frac{t' + t}{2} \qquad . \qquad (4.3.35)$$

Using Eq. (4.3.34) - (4.3.35), Eq. (4.3.33) can be rewritten as

$$< U_1(\nu)\, U_2^*(\nu) > \;=\; N \exp\left\{\frac{ik}{s}[\Delta u(\bar{u}^{-1}x) + \Delta v(\bar{v}^{-1}z)] \;-\; \frac{k^2\sigma^2}{2s^2}[(\Delta u)^2 + (\Delta v)^2]\right\}$$

$$\times \quad \left(\frac{e^2}{4\pi c}\right) \int_{-\infty}^{\infty} \int_{-\infty}^{\infty} {}^1f_1\left(\bar{t} - \frac{\tau}{2}\right) {}^1f_2\left(\bar{t} + \frac{\tau}{2}\right) \exp[i\omega\tau]$$

$$\times \quad \exp\left[ik|^1V|\tau \;-\; \frac{k^2\sigma_V^2\tau^2}{2}\right] d\bar{t}\, d\tau \qquad . \qquad (4.3.36)$$

Simplification of Eq. (4.3.36) using the fact that the form factor is slowly varying gives

$$< U_1(\nu)\, U_2^*(\nu) > \;=\; N \exp\left\{\frac{ik}{s}[\Delta u(\bar{u}^{-1}x) + \Delta v(\bar{v}^{-1}z)] \;-\; \frac{k^2\sigma^2}{2s^2}[(\Delta u)^2 + (\Delta v)^2]\right\}$$

$$\times \quad \left(\frac{e^2}{4\pi c}\right) \int_{-\infty}^{\infty} {}^1f_1(\bar{t})\, {}^1f_2(\bar{t})\, d\bar{t} \int_{-\infty}^{\infty} \exp\left[-\frac{k^2\sigma_V^2\tau^2}{2}\right] \exp[-i\omega'\tau]\, d\tau \quad , \qquad (4.3.37)$$

where

$$\omega' \;=\; \omega\left(1 - \frac{|^1V|}{c}\right) \qquad . \qquad (4.3.38)$$

Equation (4.3.37) can be evaluated to give

$$< U_1(\nu)\, U_2^*(\nu) > \;=\; NKF_{12} \exp\left\{\frac{ik}{s}[\Delta u(\bar{u}^{-1}x) + \Delta v(\bar{v}^{-1}z)] \;-\; \frac{k^2\sigma^2}{2s^2}[(\Delta u)^2 + (\Delta v)^2]\right\}$$

$$\times \quad \frac{\exp\left[-\frac{c^2}{2\sigma_V^2}\left(\frac{\nu'}{\nu}\right)^2\right]}{\nu} \quad , \qquad (4.3.39)$$

where

$$F_{12} = \int_{-\infty}^{\infty} {}^{1}f_1(\bar{t})\,{}^{1}f_2(\bar{t})\,d\bar{t} \quad , \tag{4.3.40}$$

$$K = \left(\frac{e^2}{\sqrt{32\pi^3}\,\sigma_V}\right) \quad , \tag{4.3.41}$$

and

$$\nu = \frac{\omega}{2\pi} \quad . \tag{4.3.42}$$

Equation (4.3.39) represents the second-order coherence of the synchrotron field. Using Eq. (4.3.39), the complex degree of spatial coherence is given by

$$\mu_{12}(\nu) = \frac{F_{12}\exp\left\{\frac{ik}{s}[\Delta u(\bar{u}\text{-}^{1}x) + \Delta v(\bar{v}\text{-}^{1}z)] - \frac{k^2\sigma^2}{2s^2}[(\Delta u)^2 + (\Delta v)^2]\right\}}{[F_{11}F_{22}]^{1/2}} \quad . \tag{4.3.43}$$

The intent of the derivation presented in this section was to predict the degree of partial coherence in the synchrotron field due to the random motion of a three-dimensional electron bunch in a storage ring. Notice that, within our level of approximation, Eq. (4.3.43) has the form similar to that resulting from application of the generalized Van Cittert-Zernike theorem. Recall that during the calculation we evaluated the characteristic function of the electron source distribution. Experiments suggest that the electron-position probability density can be approximated by a Gaussian function. Fourier transformation of this distribution gives a Gaussian function of the difference variables in the observation plane [see Eq. (4.3.43)]. A

three-dimensional plot of the magnitude of Eq. (4.3.43) is shown in Fig. 4.3.4. The parameters used for Fig. 4.3.4 are σ=1 mm, s=1 m and λ=0.5 μm. The coherence interval (to the 1/e point) at this wavelength is approximately 120 μm. An important note here is that the field correlation obeys a scaling condition. That is to say, the correlation function is proportional to $k(\rho_1-\rho_2)$. Note that for the case considered here of independent electrons in the bunch, the spectrum detected at a distant point will not be modified as a result of any source correlations.

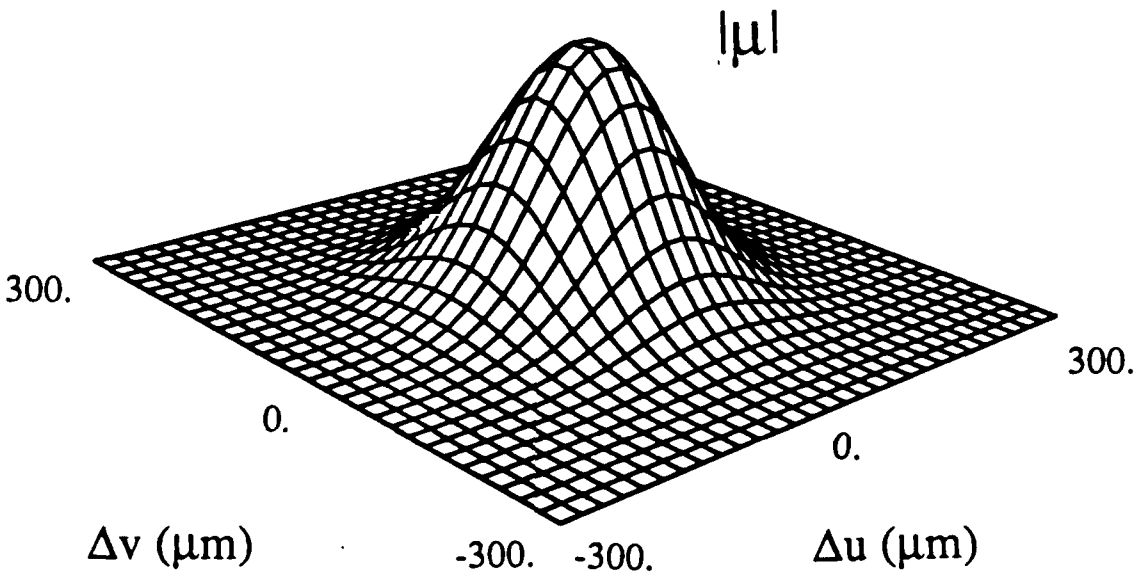

Fig. 4.3.4 Illustrating the magnitude of the degree of spatial coherence given by Eq. (4.3.43). The parameters used are σ=1 mm, s=1 m and λ=0.5 μm. The coherence interval at this wavelength is approximately 120 μm. An important note is that the field correlation obeys a scaling condition.

4.4 Suggestions for Experimental Verification

Reports of careful measurements of the magnitude of the degree of spatial coherence of synchrotron radiation do not appear to have been presented. However, due to recent developments in synchrotron source technology, there have been many investigations into holography and interferometry using synchrotron radiation. Bonse and Hart[35] and Kikuta *et. al*[36] reported some of the first experiments on x-ray holography using C Kα (4.48 nm) radiation from a conventional x-ray source. The recording of Kikuta *et. al* took approximately one hour using Fuji Softex x-ray film FG. Aoki and Kikuta[37] later performed interference experiments using the synchrotron source at the University of Tsukuba in Japan. They produced Young's interference fringes using undulator radiation and small slits cut in carbon foil. The illumination wavelength was 2 nm at 5% bandwidth. The recording material was AGFA 10E56 film. The required dose was approximately 10^{14} photons in the bandwidth of interest giving an exposure time of less than one second.

Given these previous experimental results concerning interferometry using synchrotron radiation, it appears promising that similar techniques based on Young's experiment might be used to measure the magnitude of the degree of spatial coherence. Of course, for our present case of synchrotron radiation that is not influenced by wigglers and undulators, an intermediate step to spectrally filter the otherwise broadband illumination must be taken. Grazing-incidence optics and monochromators are currently used to narrow the radiation spectrum and to provide a mechanism to scan the wavelength range of interest.

Several pairs of apertures (with varying separation) for use in the measurement of the visibility function can be fabricated out of sheets of nickel or carbon foil. Kikuta *et. al.*[36] used an electroforming method with nickel to fabricate their diffracting apertures. The visibility of fringes could therefore be sampled as a function of the wavelength and slit separation in a Young's interferometer. Within the limits of current technology, exposure times are typically of the order of seconds per interferogram. The processed recording material (typically a light-sensitive film) could be scanned in a calibrated microdensitometer to obtain the visibility. The measurements could extend from the infrared[38] to the soft x-ray region given the available photosensitive materials.

4.5 Summary of Chapter 4

In this Chapter, the second-order correlation properties of synchrotron radiation resulting from a three-dimensional relativistic electron bunch in a storage ring were calculated. The theory extended previous research to allow a three-dimensional electron bunch with a distribution of electron velocities (e.g., variance in the energy of the charges). The new formalism was generated in the space-frequency domain and suggestions for experimental investigations were discussed.

In Section 4.2, the spectral amplitude produced by an N-electron bunch in a storage ring was calculated [see Eq. (4.2.35)]. In Section 4.3, a model for the statistical behavior of the N-electron bunch and its associated classical field was investigated. Using a Gaussian distribution for the spatial characteristics of the bunch and a Gaussian velocity distribution, the mean value of the field and the second-order coherence were calculated [see Eqs. (4.3.24) and (4.3.43) and Fig. 4.3.4].

For this analysis, it was assumed that the electrons in the ring were statistically independent of one another. Although this assumption has been justified in the literature for the case of synchrotrons and storage rings, electron correlations will play an important role in understanding the field correlations in systems that use wigglers and undulators. This research has generated a framework in the space-frequency domain that will support future investigations on systems that utilize wigglers and undulators (e.g., the free-electron laser).

4.6 References: Chapter 4

1. A. Lienard, L'Eclairage Elect. **16**, 5 (1898).

2. G. A. Schott, *Electromagnetic Radiation*, Cambridge University Press, London (1912), Chapters 7 and 8.

3. D. Kerst, Phys. Rev. **60**, 47 (1941).

4. D. Ivanenko and I. Pomeranchuk, Phys. Rev. **65**, 343 (1944).

5. A. A. Sokolov and I. M. Ternov, *Synchrotron Radiation*, (Pergamon Press, New York, 1968); I. M. Ternov, V.. V. Mikhailin, and V. R. Khalilov, *Synchrotron Radiation and its Applications*, (Harwood Academic Publishers, New York, 1985).

6. J. Schwinger, Phys. Rev. **70**, 798 (1946); E. M. McMillan, "Radiation from a group of electrons moving in a circular orbit," Phys. Rev. **68**, 144 (1945).

7. J. Schwinger, "On the classical radiation of accelerated electrons," Phys. Rev. **75**, 1912 (1949).

8. J. D. Jackson, *Classical Electrodynamics*, Wiley, New York (1962, 1975) Chapter 14.

9. J. P. Blewett, Phys. Rev. **69**, 87 (1946).

10. K. R. Lea, Phys. Rep. (Section C of Physics Letters) **43**, 337 (1978).

11. F.R. Elder, A. M. Gurewitsch, R. V. Langmuir, and H. D. Pollack, Phys Rev. **71**, 829 (1947).

12. F.R. Elder, A. M. Gurewitsch, R. V. Langmuir, and H. D. Pollack, J. Appl. Phys. **18**, 810 (1947).

13. F.R. Elder, R. V. Langmuir, and H. D. Pollack, Phys. Rev. **74**, 52 (1948).

14. N. G. Basov (ed.), *Synchrotron Radiation*, Plenum Press New York and London (1976).

15. G. K. Green, "Spectra and Optics of Synchrotron Radiation", Brookhaven National Laboratory Report BNL 50522 (1976) (NTIS, Springfield, VA.).

16. C. Kunz (ed.), *Topics in Current Physics -- Synchrotron Radiation; Techniques and Applications*, Springer-Verlag (1979).

17. H. Winick and S. Doniach (eds.), *Synchrotron Radiation Research*, Plenum Press New York and London (1980).

18. E.E. Koch (ed.), *Handbook on Synchrotron Radiation*, North-Holland, Amsterdam (1983).

19. G. V. Marr, *Handbook on Synchrotron Radiation, Volume 2*, North-Holland, New York (1987).

20. E. M. Rowe, "Synchrotron radiation facilities in the United States," Physics Today p. 28, May (1981).

21. H. Winick, G. Brown, K. Halbach, and J. Harris, "Synchrotron radiation: Wiggler and undulator magnets," Physics Today p. 50, May (1981).

22. D. Attwood, K. Halbach, and K. Kim, "Tunable coherent X-rays," Science **228**, 1265 (1985).

23. H. Winick, "Synchrotron radiation," Scientific American p. 88, November (1987).

24. A. S. Mazmanishvili and V. L. Uvarov, "Spatial coherence of the field of synchrotron radiation of relativistic electrons," Opt. and Spect. **33**, 283 (1972).

25. C. Benard and M. Rousseau, "Statistical properties of synchrotron radiation," J. Opt. Soc. Am. **64**, 1433 (1974).

26. N. A. Korkhmazyan, L. A. Gevorgyan, and M. L. Petrosyan, "Effect of electron distribution on the coherent radiation from an electron bunch," Sov. Phys. Tech. Phys. **22**, 917 (1977).

27. S. A. Akhmanov, B. A. Grishanin, G. A. Lyakhov, and Yu. V. Ponomarov, "Coherence properties of X-ray sources and coherence effects in X-ray optics. I. Spatial coherence of synchrotron radiation," Moscow University Physics Bulletin, Allerton Press, USA, p. 32 (1980).

28. S. A. Akhmanov, B. A. Grishanin, G. A. Lyakhov, and Yu. V. Ponomarov, "Coherence properties of X-ray sources and coherence effects in X-ray optics. II. Dynamic scattering pf partially coherent X-radiation in crystals," Moscow University Physics Bulletin, Allerton Press, USA, p. 39 (1980).

29. M. M. Nikitin, "Coherent phase oscillations of electrons in a synchrotron," Sov. Phys. Tech. Phys. **19**, 1633 (1975).

30. I. S. Guk, N. N. Naugolnyi, and A. S. Tarasenko, "Photon statistics for the synchrotron radiation from electrons in a storage ring," Sov. Phys.-JETP **43**, 263 (1976).

31. M. Sands, "Synchrotron oscillations induced by radiation fluctuations," Phys. Rev. **97**, 470 (1955).

32. A. P. Sabersky, "The geometry and optics of synchrotron radiation," Particle Accelerators **5**, 199 (1973).

33. I. S. Gradshteyn and I. M. Ryzhik, *Table of Integrals, Series and Products*, Fourth edition, (Academic Press, New York, 1980).

34. J. W. Goodman, *Statistical Optics*, (Wiley, NewYork, 1985).

35. U. Bonse and M. Hart, "An x-ray interferometer," Appl. Phys. Lett. **6**, 155 (1965).

36. S. Kikuta, S. Aoki, S. Kosaki, and K. Kohra, "X-ray holography of lensless Fourier-transform type," Opt. Commun. **5**, 86 (1972).

37. S. Aoki and S. Kikuta, "Soft x-ray interferometry and holography," in Short Wavelength Coherent Radiation: Generation and Applications, D. T. Attwood and J. Bokor eds., (American Institute of Physics Proceedings 147, New York, 1986).

38. W. D. Duncan and Gwyn P. Williams, "Infrared synchrotron radiation from electron storage rings," Appl. Opt. **22**, 2914 (1983).

Chapter 5

5. Concluding Remarks

In each chapter of this Thesis, an investigation of a topic concerning the influence and control of optical coherence in the space-frequency domain is reported. In Chapter 2, the first experiments that illustrate the effects of source correlations on the spectrum of light are described. As observed in the experiments and consistent with Wolf's theoretical predictions, the spectrum of light in the far field is dependent on the correlation properties of the light at the source. If the optical field at the source obeys the scaling law, the spectrum of light on propagation is invariant. Departures from the scaling law produce changes in the spectrum that depend on the spectrum at the source, the degree of spatial coherence at the source, and the location of the observation point.

It is also demonstrated experimentally that source correlations can produce frequency shifts in the spectrum observed in the far field of an optical source if the correlation function of the emitted radiation does not obey Wolf's scaling condition. A Fourier achromat is used to generate the non-scaling-law secondary source. The spectrum detected in the far zone of the secondary source was found to be displaced in frequency and distorted relative to the spectrum measured at the secondary source. The displacement was toward both the higher frequencies and the lower frequencies depending on the direction of observation.

Since Wolf's original paper in 1986, the subject of correlation-induced changes in the spectrum of light has received great attention both theoretically and experimentally. There are already some twenty five manuscripts published in the literature along with an equal number of papers given at technical meetings. A

mathematical framework now exists to describe the influence of source correlations on the optical spectrum for both static sources and dynamic scatterers. Exciting new developments in the theory have predicted frequency shifts of spectral lines that actually imitate the Doppler effect. Wolf is investigating the relevance of these new correlation effects to the origin of discrepancies observed in some quasar spectra. In future research it would be useful to verify experimentally the theory describing changes in the spectrum resulting from interactions with random scatterers. These experiments might make use of electronically-addressable liquid-crystal spatial light modulators to generate the prescribed correlations. It is likely that the importance of all of these investigations to new applications will be clearly understood as more information is made available concerning the correlation properties of certain plasmas and other random media.

The generation of sources with controlled coherence is important for the verification of new concepts in optical coherence theory. In Chapter 3, experiments are described in which a new method is employed to generate an optical secondary source with a controlled degree of spatial coherence. The technique consists of mixing controllable amounts of two uncorrelated sources in an interferometer. The correlations are produced using a general spectral filter. The spectral filter employs dispersive optics that are used to spatially separate (and recombine) the wavelength components of a broadband primary source, and an amplitude mask that is used to filter the dispersed light. The degree of coherence is shown to be related to the passband of the filter. This new method of source synthesis should provide researchers with a valuable tool for analysis of spectral modulation experiments.

With the increased use of unconventional light sources for a variety of innovative applications in spectroscopy and imaging, models describing their source correlations should be investigated so that experiments that utilize these sources can be

correctly explained. Because of the importance of synchrotron radiation in industry, medicine, and research and its potential applications in astrophysics, Chapter 4 contains an investigation into the statistical properties of synchrotron radiation produced by bunch of circulating charges.

In Chapter 4, the second-order statistical properties of synchrotron radiation resulting from a three-dimensional relativistic electron bunch (N-electrons) in a storage ring are calculated. The new theory in the space frequency domain extends previous research to allow the electrons in a 3-D bunch to have an appropriate distribution of velocities (e.g., variance in the energy of the charges).

In Section 4.3, a model for the statistical behavior of the N-electron bunch and its associated classical field is investigated. Using a Gaussian distribution for the spatial characteristics of the bunch and a Gaussian velocity distribution, the mean value of the field and the second-order coherence are calculated. Experiments based on Young's experiment are suggested for future research to verify the theory. The analysis presented generates a framework that will permit future work on systems that utilize wigglers and undulators.

The applications of synchrotron radiation are expanding very rapidly and it appears in the literature that the coherence properties of the radiation are the least understood. Many researchers in the field simply assume that the radiation from storage rings is completely spatially incoherent. In many applications, the radiation is propagated through optical systems where the coherence properties will definitly play a role. The opportunity for future theoretical and experimental work on the statistical properties of synchrotron radiation is great and the benefits to medicine and the commercial sector should be significant.

Appendix A

Appendix A: Calculation of the Spectrum for the Direct-vision Spectroscope.

```
C*********************************************************************
C     Author:     Dean Faklis
C                 The Institute of Optics
C                 University of Rochester
C                 Rochester, New York  14627
C
C
C                 Date:  10/12/88
C*********************************************************************
C               Theoretical spectrum of output angles for the Spindler & Hoyer Amici
C               prism triplet used in the experiments [Chapter 3]. Three prisms; two
C               crowns sandwiching a flint. The glasses are user selectable for other
C               configurations. The coefficients are stored in an input file. These
C               coefficients are available in the Schott glass catalog. These coefficients
C               define the index polynomial. Theta8 is the output angle as a function of
C               wavelength.
C*********************************************************************

      PROGRAM AMICI
      IMPLICIT NONE
      CHARACTER*30 FNAME(2)
       INTEGER I,NPTS,P
       REAL N(2,512),INCREMENT,L(2,512),MIN,MAX,DELT
      REAL A0(2),A1(2),A2(2),A3(2),A4(2),A5(2),THETA8(1,512)
      REAL PIH,STHETA1,THETA4,LAM(1,512)

      WRITE(6,'("Enter the CROWN.COEF filename: _")')
      READ(5,'(A)') FNAME(1)

      WRITE(6,'("Enter the FLINT.COEF filename: _")')
      READ(5,'(A)') FNAME(2)

      MAX=.64
      MIN=.52
      DELT=MAX-MIN

       OPEN(10,FILE=FNAME(1),STATUS='OLD')
       READ(10,'(E14.8)') A0(1),A1(1),A2(1),A3(1),A4(1),A5(1)
      CLOSE(10)
```

```
      OPEN(10,FILE=FNAME(2),STATUS='OLD')
      READ(10,'(E14.8)') A0(2),A1(2),A2(2),A3(2),A4(2),A5(2)
      CLOSE(10)

      NPTS=512
      INCREMENT=DELT/NPTS

C     Index Polynomial

      DO P=1,2
      DO I=1,NPTS
        L(P,I)=I*INCREMENT+MIN
        LAM(1,I)=L(1,I)
            N(P,I)=A0(P)+A1(P)*L(P,I)**2+A2(P)*L(P,I)**(-2)
     >           +A3(P)*L(P,I)**(-4)+A4(P)*L(P,I)**(-6)+A5(P)*L(P,I)**(-8)
            N(P,I)=SQRT(N(P,I))
      END DO
      END DO

C     The Amici apex angle is 51.83 degrees.

      PIH=2.*ATAN(1.)
      STHETA1=SIN((90.-51.83)/57.29)
      DO I=1,NPTS
        THETA4=ASIN(SQRT(N(1,I)**2-STHETA1**2)/N(2,I))
        THETA4=THETA4-103.66/57.29
        THETA8(1,I)=ASIN(SQRT(N(1,I)**2-N(2,I)**2*SIN(THETA4)**2))
      END DO

      OPEN(10,FILE="DISPERSION.DAT")
      DO I=1,NPTS
         WRITE(10,*) LAM(1,I),THETA8(1,I)
      END DO
      CLOSE(10)
      STOP
      END
```

Appendix B

Appendix B: Evaluation of Eq. (4.3.19) Leading to Eq. (4.3.20)

This appendix contains the derivation of Eq. (4.3.20) by integration of Eq. (4.3.19). Recall from Chapter 4 that Eq. (4.3.19) is written as

$$p(|\mathbf{R}|) = 2\pi m \int_0^{\pi} \sin\phi \, J_0\left\{\frac{i|\mathbf{R}|}{\sigma^2}\sin\phi \sqrt{a^2+b^2}\right\} d\phi \ . \qquad \text{(B.1)}$$

The integral in Eq. (B.1) has the form of integral 6.681.8 in Reference 33 of Chapter 4 which is given by

$$\Psi = \int_0^{\pi} \sin(2\mu x) \, J_{2\nu}\{2a'\sin(x)\} \, dx$$
$$= \pi \sin(\mu\pi) \, J_{\nu-\mu}(a')J_{\nu+\mu}(a'); \quad \mathrm{Re}\,\nu > -1 \ . \qquad \text{(B.2)}$$

For the present calculation [compare Eq. (B.1) and (B.2)], $\mu=1/2$, $\nu=0$, $a'=i|\mathbf{R}|(a^2+b^2)^{1/2}/(2\sigma^2)$. Substitution of these parameters into Eq. (B.2) gives

$$\Psi = \pi \, J_{-1/2}\left(\frac{i|\mathbf{R}|}{2\sigma^2}\sqrt{a^2+b^2}\right) J_{1/2}\left(\frac{i|\mathbf{R}|}{2\sigma^2}\sqrt{a^2+b^2}\right) . \qquad \text{(B.3)}$$

Equation (B.3) can be simplified using the following definition:[1]

$$j_n(z) = \sqrt{\frac{\pi}{2z}}\, J_{n+1/2}(z) \quad . \qquad (B.4)$$

The lowercase functions j_n are the spherical Bessel functions. Using Eq. (B.4) along with the fact that $j_0(z)=\sin(z)/z$ and $j_{-1}(z)=\cos(z)/z$, Eq. (B.3) can be written as

$$\Psi = \frac{4\sigma^2}{i|R|} \frac{\sin\left[\frac{i|R|}{2\sigma^2}\sqrt{a^2+b^2}\right]\cos\left[\frac{i|R|}{2\sigma^2}\sqrt{a^2+b^2}\right]}{\sqrt{a^2+b^2}} \quad . \qquad (B.5)$$

Using hyperbolic functions, Eq. (B.5) can be simplified to give

$$\Psi = \frac{4\sigma^2}{|R|\sqrt{a^2+b^2}} \sinh\left[\frac{|R|}{2\sigma^2}\sqrt{a^2+b^2}\right]\cosh\left[\frac{|R|}{2\sigma^2}\sqrt{a^2+b^2}\right] \quad . \qquad (B.6)$$

Comparison of Eq. (B.6) and Eq. (B.1) gives

$$p(|R|) = \frac{4|R|}{\sqrt{2\pi}\sigma} \frac{\exp\left[-\left(|R|^2+a^2+b^2\right)/(2\sigma^2)\right]}{\sqrt{a^2+b^2}} \times \sinh\left[\frac{|R|}{2\sigma^2}\sqrt{a^2+b^2}\right]\cosh\left[\frac{|R|}{2\sigma^2}\sqrt{a^2+b^2}\right] \quad . \qquad (B.7)$$

Equation (B.7) can be simplified to give

$$p(|R|) = \frac{2|R|}{\sqrt{2\pi}\sigma} \frac{\exp\left[-\left(|R|^2+a^2+b^2\right)/(2\sigma^2)\right]}{\sqrt{a^2+b^2}} \sinh\left[\frac{|R|}{\sigma^2}\sqrt{a^2+b^2}\right] \quad . \qquad (B.8)$$

Using the exponential form for sinh gives the following:

$$p(|R|) = \frac{|R|}{\sqrt{2\pi}\sigma} \frac{\exp[-(|R|^2 + a^2 + b^2)/(2\sigma^2)]}{\sqrt{a^2 + b^2}}$$

$$X \quad \{\exp[\frac{|R|}{\sigma^2}\sqrt{a^2 + b^2}] - \exp[\frac{|R|}{\sigma^2}\sqrt{a^2 + b^2}]\} \quad . \qquad (B.9)$$

Simplification of Eq. (B.9) by completing the square in the distance parameter gives

$$p(|R|) = \frac{|R|}{\sqrt{2\pi}\sigma\sqrt{a^2 + b^2}} \{\exp[-\frac{\{|R| - \sqrt{a^2 + b^2}\}^2}{2\sigma^2}] - \exp[-\frac{\{|R| + \sqrt{a^2 + b^2}\}^2}{2\sigma^2}]\} \quad . \qquad (B.10)$$

Note that for the case of interest, the magnitude of the second exponential term on the right hand side is negligable compared to the first exponential term since it is proportional to the sum instead of the difference from the mean value. Equation (B.10) can now be written as

$$p(|R|) = \frac{|R|}{\sqrt{(2\pi)(a^2 + b^2)}\sigma} \exp[\frac{-(|R| - \sqrt{a^2 + b^2})^2}{2\sigma^2}] \quad . \qquad (B.11)$$

which is the density function for electron distances represented by Eq. (4.3.20).

References:

1. M. Abramowitz and I. A. Stegun, eds., *Handbook of Mathematical Functions*, Dover, New York, (1972).